Optimization of Mechanical Properties of Polypropylene-based Composite

by

Youssef Al Herz

A thesis
presented to the University of Waterloo
in fulfillment of the
thesis requirement for the degree of
Master of Applied Science
in
Chemical Engineering

Waterloo, Ontario, Canada, 2012

AUTHOR'S DECLARATION

I hereby declare that I am the sole author of this thesis. This is a true copy of the thesis, including any required final revisions, as accepted by my examiners.

I understand that my thesis may be made electronically available to the public.

Youssef Al Herz

Abstract

Polypropylene-based composites are widely used in the industrial field, especially in automotive applications, due to their excellent mechanical properties and low cost. This research is directed towards obtaining the optimal values of mechanical properties of long glass fiber-reinforced polypropylene composite (LGFPP) and polymer-layered silicate nanocomposites (PP-OMMT) for different objectives. Though the primary objective was to minimize the cost of the composite, simulations were also performed to obtain specific desired properties of the composite (irrespective of the composite cost). The latter simulation results are useful in designing products where quality of the composite cannot be compromised (while the cost of the composite is secondary).

In this study, the properties that were optimized include tensile Young's modulus, flexural Young's modulus, notched I-zod impact, and permeation. Regression models were obtained and used to predict these properties as functions of corresponding compositions of the composites. Further, optimization procedures were simulated using these models along with other constraints and objective functions. All simulations are programmed using MATLAB version 7.10.0 (R2010a).

Acknowledgements

I would like first to express my deep thanks to ALLAH Almighty for the grace he blessed me with throughout my life.

Special thanks to my supervisor Professor. Ali Elkamel for his efforts in guiding me throughout this project, with his encouragement and help he made it possible for me to finish my thesis.

Many thanks too, to my co-supervisor Dr. Chandramouli R. Madhuranthakam for his amazing help in clarifying the project, and the good ideas all through my thesis-work period. Your time and efforts are greatly appreciated.

I am very countlessly grateful to my beloved family for their support and patience, which helped me achieve success in my life.

Finally, I thank the Saudi Ministry of Higher Education for providing me with the opportunity and financial support to pursue my master's degree in Canada.

Dedication

To my sweetheart,

My wife, Zainab

And my kids, Nawaf and Ariana

Table of Contents

List of Figures

List of Tables

Nomenclature

Acronyms

ASTM	American Society of Testing Materials
EMT	Eshelby–Mori–Tanaka
GN	Gauss-Newton
IFSS	Interfacial Shear Strength
IMM	Injection Molding Machines
LGFPP	Long Glass Fiber Reinforced Polypropylene
LM	Levenberg-Marquadt
NIST	National Institute of Standards and Technology
OOF	Object-Oriented Finite element
P	Permeation
PP-OMMT	Polypropylene Organically Modified Montmorillonite
PRESS	Prediction Error Sum of Squares
RVE	Representative Volume Element
SD	Steepest Descent
TM	Tensile Modulus
UTS	Ultimate Tensile Strength

Chapter 1
Introduction

1.1 Composite Material Products

In recent decades, the high demands of automotive industries and related applications have generated a new major field of polymer science that has rapidly grown and progressed to particulate composites for aerospace and other applications by modifying the commercial polymers to improve their mechanical properties and increase their shelf life. A composite material is basically synthesized of two components or more, known as a matrix system or filler system. Polymers such as thermoplastics and thermosets can be used as a matrix material to form a composite, as well as metals, ceramics and carbon. At the same time, the matrix system works as a binder for the filler system; fiberglass, graphite, aramid, silica and aluminum can be used for this purpose. Both matrix and filler retain their individual identities when they join to form a composite and directly affect the properties of the final composite (Peters, 1998).

Around 30% of total annual production of polymers is consumed in mixtures, and about 80% of these mixtures are processed to enhance toughness of the matrix polymer. Toughness of polymeric material is one of the crucial factors that affect the selection of appropriate materials to construct a composite for a wide variety of applications, including products for the automotive, construction, utilities, home and sporting industries. These products can be exposed to many different circumstances during their service time, such as impact loading, high strain rates, and low or high temperatures (which may lead to embrittlement of materials), even though they follow a ductile pattern at high temperatures or low stress rates. In engineering applications, brittle failure of materials is a great concern that must be considered (Karian, 1999).

In general, fibers are much stronger and stiffer several times more so than polymer and orthotropic (having different properties in two different directions). Reinforcing a polymer by adding fiber may improve some properties of a composite material. On the other hand, it might lead to the deterioration of other properties in the same composite. Therefore, the fiber concentration (weight fraction) or any other filler system used should be controlled depending on the application type used or the properties desired (Peters, 1998). Traditionally, the whole process of designing a composite material to meet the requirements of a specific design and function, which requires experimentation that typically involves trial and error, is time-consuming.

1.2 Research Objective

Finding the best combination between two or three components for a composite material is very challenging, especially if the desired values of two components occur in different weight fractions of each component. Trial and error is the traditional approach used to design composite material products, which is costly and time consuming. The objective of this study was to develop a computer-aided effective methodology for composite product design that uses the existing database of tensile strength, tensile modulus, flexural strength, flexural modulus, notched Charpy impact, and notched I-zod impact for long glass fiber reinforced polypropylene (LGFPP) composite. Additionally, these properties were modeled using either linear or nonlinear regression, which essentially depend on how the data points are distributed, and then the models were analyzed by checking the coefficients of determination. Finally, an inverted model technique was applied to generate the best combination of the composite based on specific needs. The results obtained from inverting the model were compared with the results obtained from minimizing the cost of the composite where the specific needs were the same, and that is the major objective of this work. This procedure was performed in two cases studies. From the point of view of the future, this study can contribute toward product development and can be augmented by further experiments and re-

analyzed by other models. Its findings can also be implemented in other categories of formulation development.

1.3 Research Approach

1.3.1 Modeling Mechanical properties of (LGFPP) Composite

Historical data describing the mechanical property behaviors of long glass fiber-reinforced polypropylene were available in the literature. The collected data were modeled using a polynomial regression method based on the least square approach. These models were analyzed using nonlinear regression analysis technique, and the best-fit model was chosen for each property. This composite represents the first case study.

1.3.2 Polymer-layered Silicate Nanocomposites (PP-OMMT)

Similar to the first case study, historical data were obtained from a literature review; however, the models that describe tensile modulus and permeation were available in the literature as well. Factorial and mixed design techniques were used for modeling the behavior of these properties. Analysis was conducted for various factors and components of the composites system using design modules to determine the most effective properties of PP-OMMT (Mittal, 2008).

1.3.3 Optimization

The method of Levenberg-Maquadt was used in performing the optimization to produce a new composite product with predefined properties. Two approaches were undertaken, in the approach the objective function was set to minimize the cost of the composite while using the mechanical properties expressed in the regression models as constraints. Also, some of the composite ingredients were limited to a certain weight fraction that can be presented as lower and upper bounds. In the second approach the problem was set to obtain the best combination

of composites for two or more properties by minimizing the variance between the predicted model and the desired value.

1.4 Thesis Outline

This thesis is divided into five main chapters that cover the following topics:

Chapter 1 General information on composite materials as well as the research objectives and approach.

Chapter 2 Literature review describing the behavior of mechanical properties of the composite, modeling these properties for both case studies, and optimization process.

Chapter 3 Description of the systematic technique that was followed in this work which involves regression modeling and optimization.

Chapter 4 Discusseion of the results obtained by performing an optimization for different objective functions.

Chapter 5 Summary of the important findings of this study and recommendations for future research.

Chapter 2
Literature Review

2.1 Design and Optimization of Composite Material Product

In general, designing a chemical product involves several steps. The first step is defining the product specifications based on the customer and market needs. The second step is to generate various prototypes and select the one that best meets the specific needs of the product for commercial development. The last step is to decide the outer appearance and features of the product, and then which technique will be used for manufacturing (Cussler and Moggridge, 2001).

In composite materials, designers seek the best possible design that consumes the least amount of resources, and the measure of quality depends on the application, typically referred to as ‘stiffness’ and ‘strength’, while the weight and cost are used for resource measurement. Consequently, either lowest weight or cost is desirable in design with respect to the limitations of the stiffness or strength properties. The requirements are defined for a given application and designed by engineers to obtain a product that meets these requirements. Then, a structural modification takes place to enhance the performance and minimize the weight or cost. Often, this process is tedious due to the large number of iterations required by the engineers, such modifications in the structural dimensions (cross-sectional areas, length, and thickness) in order to improve the performance. Furthermore, these modifications may lead to designs where strength or stiffness requirements are violated. Sometimes, it is difficult to meet the specific needs of a product and it may require more iterations to be conducted; in some cases, it is more difficult to satisfy the specific requirements from the beginning to become a final product. As a result, mathematical optimization has appeared to be a powerful tool for structural design, since it deals with the minimization or maximization of an objective function subject to different constraints. Using this tool for design has helped the engineers to avoid repeating iterations in many cases and

made the design process more well-organized and systematic. One more issue must be considered during the design process of laminated composite materials is their mechanics. This issue is studied at two different levels, namely, in relation to macromechanics and to micromechanics (Gurdal *et al.*, 1999). The examination of the interaction between the layers of the laminate with one another and their influence on the overall response quantities of laminate (e.g., temperature and moisture) can be defined in terms of macromechanics. On the basis of the rule of mixture at the micromechanical level, the elastic properties of an individual layer can be derived from the elastic properties of a composite constituent of fiber and matrix. Furthermore, the prediction of composite properties must be based on the micromechanics level (Gurdal *et al*., 1999).

2.2 Injection Molding Technique

The diversity of applications based on various factors, such as product performance, size, shape, and quantities, generated many different types of injection molding machines (IMM) to form final products; however, the process of manufacturing these different applications are the same. In processing, the material is fed into the plasticator barrel through the hopper, and the pressure in the barrel is between 2,000 and 30,000 psi (14 to 205 MPa). To meet pressure flow restrictions going from the plasticator into the mold cavity, the barrel pressure must be enough for a given cavity pressure. A rotating screw located inside the plasticator barrel helps the materials to move toward the nozzle, and during this motion, a heat system surrounding the plasticator barrel causes the materials to melt. The heating system is comprised of different sections (front, center, rear) each of which can be set to a different temperature depending on the type of material used, as shown in Figure 2.1. Also, another factor assists in the melting process – the friction between the rotating screw and the surface of the plasticator – and this is known as ‘shear heating’. When the melted materials reach the nozzle, they are injected into the mold that forms the product and its features. Commonly, steel or aluminum is used for molds due to their high heat resistance. In order to prevent back

flow of melted material during solidification, the injected materials should be under pressure for a certain amount of time (Rosato *et al.*, 2000).

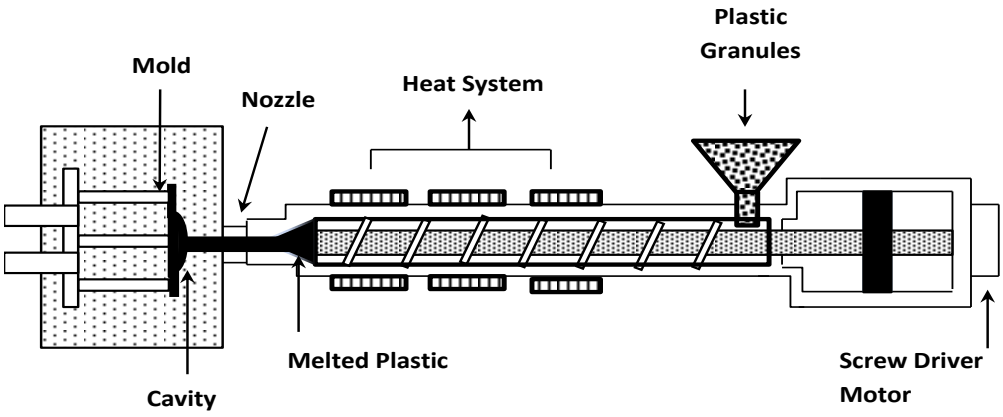

Figure 2.1: Injection Molding Machine. Adopted from (Rosato *et al*., 2000)

2.3 Introduction of Mechanical Properties

The use of plastic materials is common, due to the desirable mechanical properties at economically low cost and light weight. The polymer used in this project was Homo-polypropylene (see Figure 2.2), which is classified under thermoplastics polymers. Further, having good knowledge of the behavior of mechanical properties and how they can be adjusted by different factors will be very useful in the design of composite materials (Nielsen *et al*., 1994).

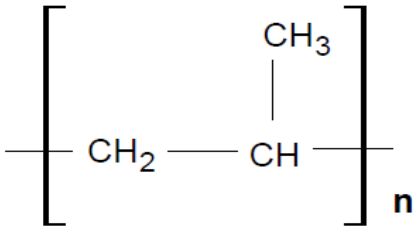

Figure 2.2: Polypropylene chemical structure.

2.3.1 Tensile Strength

A tensile strength test is used to measure how much stress can be applied to a material until failure. This test is conducted according to the standards of American Society of Testing Materials (ASTM), known as (D-638). The specimen is inserted in one side and it is stretched from the other until it fractures. The values of engineering stress and engineering strain can be obtained from the tensile test and are defined by the following equations:

$$Engineerin\ stress = S = \frac{F}{A_0} \tag{2-1}$$

$$Engineering\ strain = e = \frac{\Delta l}{l_0} \tag{2-2}$$

Where

- F is the force applied on the specimen;
- A_0 is the original cross-section area of the specimen before starting the test;
- Δl is the change in the length of the specimen; and
- l_0 is the original length of the specimen.

Recording the results of tensile test, the engineering stress-strain curve can be obtained as illustrated in Figure 2.3 (Askeland, 2011).

What properties can be obtained from the stress-strain curve? Yield point, also called 'yield strength', plays a significant role in distinguishing between the elastic deformation area and the plastic deformation area. In the elastic deformation area, a specimen is able to return to the original length once the applied stress is released; however, in the plastic deformation, area the specimen cannot return to the original length after the applied force is released. The highest point that can be reached on the stress-strain curve is called 'ultimate tensile strength' (UTS), where the values of UTS vary depending on the materials used. The slope of stress-strain curve in the elastic deformation area is defined as the modulus of elasticity, or Young's modulus (E). Hooke's law represents the relationship between stress and strain in elastic area.

$$E = \frac{S}{e} \tag{2-3}$$

In a composite material, the elastic modulus depends on the stiffness of components and their concentrations whereas the value of (E) lies between the values of the matrix and the filler elasticity.

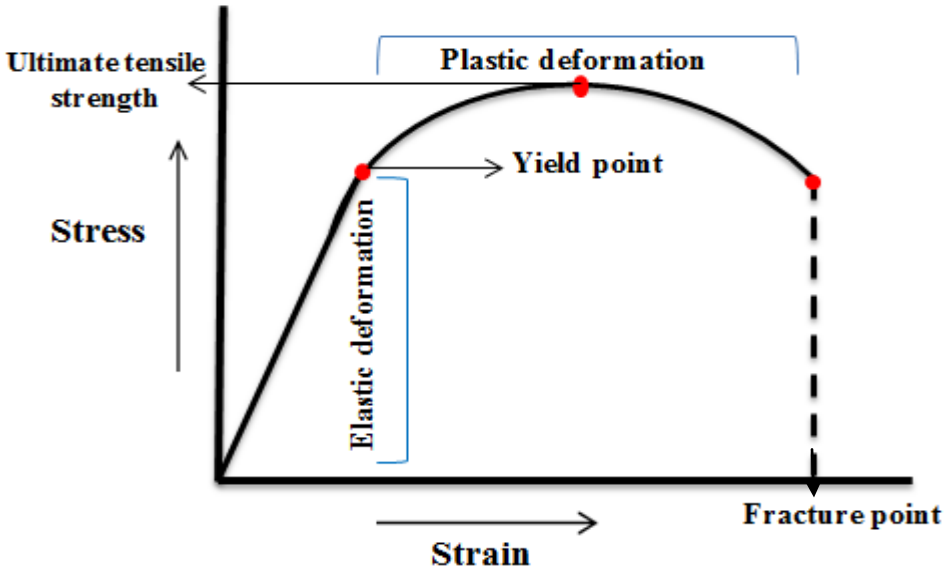

Figure 2.3: Typical stress-strain curve. Adopted from (Askeland, 2011)

Tensile toughness is the energy absorbed by a material before fracture and is measured by the area under the stress-strain curve. The ability of permanent deformation of a material without breaking when a stress is applied is known as 'ductility'. This phenomenon always occurs in the plastic deformation area, and there are two ways to measure ductility – either by using elongation or reduction in the area as defined by the following equation:

$$Elongation = \frac{l_f - l_0}{l_0} \times 100 \qquad (2\text{-}4)$$

Where l_f is the distance between the gage marks after the specimen breaks.

$$\text{Re}duction\ in\ area = \frac{A_0 - A_f}{A_0} \times 100 \qquad (2\text{-}5)$$

Where A_f is the final surface of cross-sectional area when the specimen breaks (Askeland, 2011).

2.3.2 Flexural Strength

Flexural strength is often used for brittle material to measure the ability of material to resist deformation under load. A three-point bend test is commonly used, known as (D-790) according to ASTM. The specimen is supported by two pins from beneath and force is applied at the middle from the other side. The flexural strength can be calculated by the following equation:

$$Flexutral\ strength\ for\ three\ pionts\ bend\ test\ \sigma_{bend} = \frac{3FL}{2wh^2} \qquad (2\text{-}6)$$

Where

- F is the force applied;
- L is the distance between the two pins;
- w is the specimen width; and
- h is the specimen height (thickness).

Although the stress-strain curve is obtained from the bend test, the stress is plotted versus deflection instead of strain. The flexural modulus (E_{bend}) is the ratio of stress to deflection or the material's tendency to bend which is determined from the slope of the stress-deflection curve and is calculated as follows:

$$E_{bend} = \frac{L^3F}{4wh^3\delta} \qquad (2\text{-}7)$$

Where δ is the deflection of the beam when force F is applied (Askeland, 2011; Driscoll & ASTM International., 1998).

2.3.3 Notched I-zod and Charpy Impact

The notched impact test measures the material's ability to absorb energy during fracture and can be defined as the impact toughness of a material. It has been mentioned that the toughness can be determined by the area under the stress-strain curve in the tensile test; however, in the impact test, to determine the energy absorbed is different due to the high rate of strain applied while in the tensile test the rate of strain is low. Furthermore, the material may behave in a brittle manner when extremely rapid strain is applied. Different measurements are used for the impact test. The I-zod impact test is commonly used for plastic material; the specimen is installed vertically, and the pendulum impacts the specimen on the same side of the notch. The specimen in a Charpy test is inserted horizontally, and the impact occurs on the other side of notch (Askeland, 2011; Driscoll & ASTM International, 1998).

2.4 Modeling Mechanical Properties of Composite Material

In the last two decades, there has been an acceleration of growth in the development of fiber-reinforced thermoplastic polymer composites and their applications. Simultaneously, there has been great attention to the behavior of the micro-mechanical parameters and their measurement in order to have a better understanding of the structure-property relationships in such composites. As a result of combining the fiber and matrix properties and the capability of transferring the stresses through the fiber-matrix interface, the final properties of thermoplastic composite are formed. The orientation factor, fiber content, fiber length, strength, aspect ratio, and interfacial strength are significant variables that influence the final balance of thermoplastic composite properties produced by injection molding (Thomason, 2002b). Generally, fibers longer that 1 mm are considered to be long fibers (Phelps and Tucker III, 2009).

The present tactic used to predict the elastic properties of a discontinuous fiber composite involves two significant stages. The first stage is to calculate the elastic stiffness of a 'reference' composite that has unidirectional fibers and the same structure, length distribution and volume fraction as the real composite. Second, the elasticity of the real as-formed composite is obtained from the elasticity of the reference composite that is averaged over all possible orientations by the orientation averaging method (Advani, 1987; Camacho, 1990).

The rule of mixtures, Cox's theory (Cox, 1952) is commonly used to model the stiffness of fiber-reinforced thermoplastic composites, and was further improved by Krenchel in 1964. Through interfacial shear stress, the applied load can be transferred from the matrix to the fiber where the maximum value of the shear is at the fiber end and decreases to zero at the center. In contrast, the tensile stress in the fiber is at its maximum value in the center and zero at the ends; however, the tensile stress in the matrix cannot exceed the maximum tensile stress along the length of the fiber. Despite increasing the efficiency of stress transfer with fiber length, it never reaches 100%. The efficiency factor η_1 of fiber length is introduced into the rule-of-mixtures equation of modulus composite E_c in order to contain the dependency of reinforcement efficiency on the fiber length (Thomason and Vlug, 1996).

$$E_c = \eta_1 V_f E_f + (1 - V_f) E_m \qquad (2\text{-}8)$$

Where

- V_f is fiber volume fraction; and
- E_f and E_m are fiber and matrix stiffness, respectively.

The shear lag model developed by Cox is given by

$$\eta_1 = \left[1 - \frac{\tanh(\beta L/2)}{\beta L/2}\right] \tag{2-9}$$

And

$$\beta = \frac{2}{D}\left[\frac{2G_m}{E_f \ln\left(\sqrt{r/R}\right)}\right]^{\frac{1}{2}} \tag{2-10}$$

Where

- L is the fiber length;
- D is the fiber diameter;
- G_m is the shear modulus of the matrix;
- r is the fiber radius; and
- R is related to the mean spacing of the fibers.

Taking into account the fiber orientation factor η_0 introduced by Krenchel and adding it into the rule of mixtures, we arrive at the following equation:

$$E_c = \eta_0 \eta_1 V_f E_f + (1 - V_f) E_m \tag{2-11}$$

The Halpin-Tsai model is another approach that can be used to predict the composite material's elasticity, which is based on the self-consistent micromechanics method. In addition, Halpin-Tsai equations were developed from the calculations of rigorous elasticity where the combinations of engineering elastic constants and differences in Poisson's ratios were expressed by the geometry factor η_0 (Halpin and Kardos, 1976).

$$E_c = \eta_0 E_1 + (1-\eta_0)E_2 \tag{2-12}$$

Where E_1 and E_2 can be calculated by following equations for the modulus of unidirectional reinforced laminate.

$$E_j = E_m\left[\frac{1+\xi_j \eta_j V_f}{1-\eta_j V_f}\right] \quad , \quad \eta_j = \frac{(E_f/E_m)-1}{(E_f/E_m)+\xi_j} \tag{2-13}$$

$$\xi_1 = \frac{2L}{D} \quad , \quad \xi_2 = 2$$

Where ξ is a measure of reinforcement geometry that depends on loading conditions (for more detail, see Halpin and Kardos, 1976). Thomason calculated the orientation factor η_0 of LGFPP prepared by injection molding technique, whereas the values of Young's modulus are obtained for both tensile and flexural using the two methods mentioned above in the Cox-Krenchel model in equations (2-11) and the Halpin-Tsai model in equations (2-12). The results of the orientation factor obtained from both models were very similar. They showed a good agreement with the experimental data; however, there was an exception with very high fiber glass weight fractions. Although the average orientation factor was computed from both models and compared with the orientation factor obtained from the optical method, the results were conflicting. Thomason claimed that possible reasons for these conflicting results could be either errors in the assumptions used in the equations to calculate the orientation factor or errors in the experimental measurements (Thomason, 2005).

The Eshelby-Mori-Tanaka (EMT) model term is a combination of Eshelby's equivalent inclusion technique (Eshelby, 1957) and the Mori-Tanaka model (Mori and Tanaka, 1973). The EMT model can be used effectively in terms of accuracy and efficiency to predict the

elastic stiffness for the aligned fiber composite (Benveniste, 1987). Further, reviewing and evaluating have been conducted by Tucker and Liang for standard micromechanical models of short-fiber composites in order to predict its elastic properties (Tucker III and Liang, 1999). The results of an accurate predictions have been shown by the authors where can be provided by EMT model and emphasized that can be one of the best choices for predicting the elastic stiffness properties of aligned short-fiber composites. Recently, the Monte-Carlo technique has been used by Hine with other authors to generate aligned fiber microstructures that are randomly non-overlapping, including distribution of fiber lengths (Hine *et al*., 2002). In addition, a numerical simulation of the generated microstructures has been performed, where the simulation results apparently agreed with the predictions of the Tandon-Weng model (Tandon and Weng, 1984). Furthermore, there is an analogy between the Tandon-Weng model and the EMT model. Later on, the same method was performed by Hine et al., (Hine, Lusti, & Gusev, 2004) to generate a randomly oriented fiber microstructure. Also, they showed that the results determined by numerical simulation for elastic and thermoelastic properties and the results obtained by the constant strain orientation averaging method (averaging the stiffness constants) are very close to each other (Advani and Tucker III, 1987; Camacho *et al.*, 1990). A recommendation was proposed by Hine et al. to combine the EMT model with the orientation averaging approach in order to compute the elastic and thermo-elastic properties of the short-fiber composite.

Based on the EMT model with experimental characterization of fiber orientation distribution and fiber length, Nguyen and his team developed a methodology by combining process modeling and micromechanical modeling (Ba *et al*., 2008). This technique is applied to determine the elastic stiffness properties of long-fiber thermoplastics (LF/PP) produced by injection molding method. The distribution of fiber orientation in LF/PP specimens cannot be predicted at a level of accuracy sufficient to yield accurate predictions for stiffness properties. Therefore, it is essential for both the fiber orientation distribution and the fiber length distribution to be accurate in order to reliably predict the composite properties.

Consequently, it has been recommended that there should be more focus on modeling the fiber orientation distribution for long-fiber thermoplastics.

Kelly and Tyson are developed a model based on the rule of mixture that is able to predict the ultimate tensile strength (σ_{uc}) of a polymer composite reinforced with discontinuous fiber (Kelly & Tyson, 1965). It is widely known as the Kelly-Tyson model, which can be written in simplified form as follows:

$$\sigma_{uc} = \eta_0 (X + Y) + Z \tag{2-14}$$

Where

- X is the contribution of fiber with length less than a critical fiber length L_c (sub-critical length);
- Y is the contribution of fiber with length greater than a critical fiber length L_c (super-critical length); and
- Z is the contribution of matrix.

The critical fiber length can be determined as follows:

$$L_c = \frac{\sigma_{uf} D}{2\tau} \tag{2-15}$$

Where

- σ_{uf} is the fiber strength;
- D is the average fiber diameter; and
- τ is the interfacial shear strength (IFSS).

Keeping in mind the assumption of the Kelly-Tyson model that all fibers are aligned toward the direction of loading, the original concept of Kelly-Tyson was further extended by Bowyer and Bader, who have developed the model of the stress-strain curve of the composite before failure. Their argument was based on the existence of a critical fiber length $L_\varepsilon = \left(E_f \cdot \varepsilon_c \cdot D/2\tau\right)$ at any strain value $\left(\varepsilon_c\right)$. The average stress $= L \cdot \tau / D$ if the fibers are shorter than L_ε, while fibers longer than L_ε carry an average stress $= E_f \varepsilon_c \left(1 - \left(E_f \varepsilon_c D/4L\tau\right)\right)$ (Bader and Bowyer, 1972; Bader and Bowyer, 1973). Hence, at any strain level, the composite stress can be obtained by the following:

$$\sigma_c = \eta_0 \left(\sum_i \left[\frac{\tau L_i V_i}{D} \right] + \sum_j \left[E_f \, \varepsilon_c V_j \left(1 - \frac{E_f \, \varepsilon_c D}{4\tau L_j} \right) \right] \right) + \left(1 - V_f\right) E_m \, \varepsilon_c \qquad (2\text{-}16)$$

Generally, the values of orientation $\left(\eta_0\right)$ and interfacial shear strength $\left(\tau\right)$ factors are unknown. The common approach to account for the average fiber orientation is by fitting the experimental data using a simple numerical orientation factor, while the value of interfacial shear strength can be obtained by the macro-method analysis that was originally suggested by Bowyer and Bader. Further, an improved version has been thoroughly reviewed by Thomason in three different research papers (Thomason and Groenewoud, 1996; Thomason, 2002a; Thomason, 2002b; Thomason, 2002c). The procedures of this methodology were used by Thomason in 2005 to predict the composite tensile strength values of injection-molded, long glass fiber-reinforced polypropylene for different fiberglass weight contents. The experimental data of the tensile strength test, which was used in this project, shows a nonlinear pattern where the composite strength increases with the fiber content and reaches the maximum strength at around (40-50%wt) then decreases to almost the same level as the starting point. The fiber content ranged from 0 to73% by weight. In these composites, both the average of fiber length and the average of fiber orientation linearly decrease with increasing fiber content, but their results may involve high levels of experimental error.

There was a good correlation between the prediction by the Kelly-Tyson theory and the experimental data of composite strength; however, one should be aware of the all assumptions that lie behind any model. According to Thomason, the assumptions are as follows:

- Stress transfer through the interface is linearly increased from the tips of the fiber inwards to some maximum value;
- No fiber-matrix debonding occurs;
- The composite matrix properties and the resin properties are the same;
- The factor η_0 is independent of strain and identical for all fiber lengths;
- The fiber modulus is identified;
- IFSS τ is independent of loading angle.
- Fiber diameter is monodisperse;
- The stress–strain curves for both fiber and matrix are linear; and
- An orientation correction factor η_0 may be applied to account for fibers not oriented in the loading direction (Thomason, 2002b).

The testing of notched impact strength of discontinuous fiber-reinforced composites may operate various energy dissipation mechanisms that have been suggested by different authors (Cooper, 1970; Cottrell, 1964; Piggott, 1974). In the front area of the crack tip, fracture and deformation of the matrix occur. Meanwhile, debonding may occur when the strength of the fiber-matrix interface exceeds by the applied stress and is transferred by shears to the fibers. If the fiber stress level exceeds the local fiber strength, fibers may fracture. Energy dissipation may be involved if the fibers pull out of the matrix from the crack interface. Due to the frictional forces along the interface, there is a possibility of transfer of stress to a debonded fiber. The common approach used to predict the impact energy of discontinuous fiber-reinforced composites is the Cottrell model, which takes into account all mechanisms that mentioned above. Moreover, the model was developed for unidirectional reinforcement.

The Cottrell model has two parts based on whether the length of fiber in a composite is subcritical or supercritical. In order to predict the impact energy U_c for a composite with fiber length $L < L_c$ (critical fiber length), the following equation is used.

$$U_c = (1 - V_f)U_m + \left[\frac{V_f L U_d}{D}\right] + \left[\frac{V_f L^2 \tau_f}{6D}\right] \qquad (2\text{-}17)$$

Where the three terms in the equation represent the matrix fracture, the fiber-matrix debonding, and the fiber bull-out, respectively. In case of $L > L_c$

$$U_c = (1 - V_f)U_m + \left[\frac{V_f (L - L_c)U_f}{L}\right] + \left[\frac{V_f L_c^2 U_d}{DL}\right] + \left[\frac{V_f L_c^3 \tau_f}{6DL}\right] \qquad (2\text{-}18)$$

Where the four terms cover matrix fracture, fiber fracture, debonding, and pull-out limited to the critical fiber length.

- $U_{m,d,f}$ are the fracture energy of the matrix, interface, and fiber, respectively;
- D is the fiber diameter; and
- τ_f is the interfacial friction during fiber pull-out.

Notice that the value of τ_f is not necessarily equal to the value of τ that was used to calculate the value of L_c. Because of the existence of the fibers that prevent large deformation, the dissipated energy by the matrix is small, (Friedrich, 1985). It becomes important to accurately evaluate the value of τ_f when the energy absorption mechanism is controlled by the fiber pull-out. Raghava, 1998 considers the radial stresses (σ_R) because of

thermal shrinkage $\tau_f = \rho\sigma_R$. The interfacial friction can be calculated from the following equation:

$$\sigma_R = \frac{(\alpha_m - \alpha_f)(T_s - T_t)E_f E_m}{(1+\upsilon_f + 2V_f)E_f + (1+\upsilon_m)E_m} \qquad (2\text{-}19)$$

Where

- ρ is the coefficient of friction;
- $\alpha_{m,f}$ are the thermal expansion coefficients for the matrix and fiber, respectively;
- T_s is the matrix solidification temperature;
- T_t is the testing temperature; and
- υ is Poisson's ratio. (Raghava, 1988)

In case of fiberglass polypropylene, Schoolenberg proposed that the primary factors which governed the τ and τ_f in this system are dynamic friction (ρ_d) and static friction (ρ_s) (Karger-Kocsis, 1995).

The Cottrell model has been applied by Thomson to predict the impact strength of glass fiber polypropylene. As experimentally observed, the Charpy impact increases with increasing fiber content. Also, the temperature in the range from -50 to +40 significantly influenced the Charpy strength in the system. As a result of a Thomason study, the predictions of a pull-out dominated model for composite impact energy did not correlate well with the experimental data; however, there was a good correlation between the composite impact strength and tensile strength, the fiber length is required to be > 8 mm (Thomason and Vlug, 1997). Another study by Thomason experimentally showed the behavior of both the notched Charpy and Izod impact for injection molding of long glass fiber-reinforced polypropylene over a range of 0-73%wt of fiber. Both Charpy and Izod impact follow the same pattern where the

energy impact increases as the content of fiber increases and reaches a maximum around 40-50%wt, then decreases toward the starting point (Thomason, 2005).

2.5 Modeling Mechanical Properties of Nanocomposite Material

There has been remarkable growth since 1980 in research studies dealing with the prefix 'nano', characterization and modeling having received a great portion of these studies. The length of the nanocomposite is estimated about (1-100) nanometers that the matrix material can be reinforced with more than one nanomaterial (the filler) for enhancement of its properties' performance with respect to the filler to be smaller than 100 nm in length. A distinguishing aspect of nanocomposites is that, at low filler volume fractions, its properties can be significantly improved without damaging the homogeneity or the density of the material (Hu *et al*., 2010).

Polymer-layered silicate has been chosen to be part of this work as a second case study. A multi-scale modeling approach presented by Liu and Chen is extended to the concept of representative volume element RVE in order to investigate the compressive behavior of carbon nanotube/polymer composites (Tsu-Wei Chou and Li, 2006). The nanotube was modeled at the atomic scale and the deformation of matrix was analyzed via the continuum finite element technique proposed by Shi *et al*. (2005). There were simulations conducted for the interactions of van der Waals between carbon atoms and the finite element nodes of the matrix, which revealed the stress distribution at the interface of carbon-nanotube/polymer under both iso-strain and iso-stress loading conditions (Tsu-Wei Chou and Li, 2006). Also, Tserpes and other authors used the method of multi-scale RVE modeling to study the tensile behavior of carbon- nanotube/polymer composites. The RVE is a rectangular solid whose the whole volume is occupied by the matrix, while a nanotube is modeled as a three-dimensional (3D) elastic beam. The 3D solid elements and beam elements are used to individually model the matrix and nanotube. Predictions of the stiffness were obtained and verified by the rule of mixtures. The result showed an agreement at low strain; however, there was a deviation at

high values of strains due to the nonlinear behavior of carbon nanotubes (Tserpes *et al*., 2008).

The finite element method is also commonly used to determine the mechanical properties of nanocomposites with unit cell technique. The Young's modulus of nanoclay/polymer nanocomposites was examined by Hbaieb's group, who used the finite element method, creating 2D and 3D aligned and oriented nanoclay particles models of four-unit cells. Two types of boundary conditions were applied – periodic and symmetrical boundary conditions. The numerical results obtained indicate that the elastic modulus predictions of clay/polymer nanocomposites for the 2-D models were not accurate (Hbaieb *et al*., 2007); however, the EMT model accurately predicted the stiffness of nanocomposites with volume fractions below 5% for aligned particles, while underestimating the stiffness at higher volume fractions (Mori and Tanaka, 1973).

Dealing with complex and highly heterogeneous nanocomposites can be seriously limited by using either multiscale RVE modeling or unit cell modeling. For instance, the complex morphology, size, and spatial distribution of the reinforcement cannot be captured by using an approximation of simple geometrical particles for filler with highly variable and irregular angular structures. Consequently, a new approach has been presented – namely, object-oriented finite element modeling (OOF), which has a potential to precisely predict the overall properties by capturing the actual microstructure morphology of the nanocomposites (Hu et al., 2010). At National Institute of Standards and Technology (NIST), where OOF modeling was developed (Langer *et al*., 2001), Dong and other researchers studied the mechanical properties of polypropylene/organoclay nanocomposites as well as various clay contents ranging from 1 to 10 wt%. The investigation was begun with the specimen fabrication in consequence of experimental characterization where numerical modeling of OOF was used for predictions. The results that were obtained for predicting the tensile modulus showed agreement with the experimental data (Dong *et al*., 2008).

Despite the good predictions that can be obtained by the Halpin-Tsai model for tensile properties with a variety of reinforcement geometries, there were number of assumptions that have prevented the theory from correctly predicting the properties of the layered silicate nanocomposites, which was confirmed by various authors. Assumptions such as close bonding of filler and matrix, accurate alignment of the platelets in the matrix, and the filler particles in the matrix taking uniform shape and size make it very hard to achieve correct predictin about the properties of nanocomposites. There is another concern, namely, the existence of the distribution of tactoid thicknesses due to the unfinished exfoliation of the nanocomposites. In reality, these assumptions mentioned above are rarely true, especially in nonpolar polymer matrix composites, due to interactions not occurring between the organic and inorganic components. For the sake of containing the effect of unfinished exfoliation and misorientation of the filler, the models have been adjusted; however, the mixture needs to be more amalgamated to reduce the influence of impaired adhesion at the surface (Al-Malaika *et al*., 2001; Brune and Bicerano, 2002; Fornes and Paul, 2003).

The use of design modules experiments by Mittal in 2008 generated various factorial and mixtures design models to predict the properties of polymer-layered silicate nanocomposites. He suggested that the factorial and mixture design models might be a much better way, particularly where the assumptions of Halpin-Tsai theory do not work in nonpolar polymer systems due to the use of oversimplified assumptions. The analyses indicated that the tensile modulus and oxygen permeation were the most significant factors influencing the system. In addition, further analysis was conducted to determine the interaction quantities of the components in the system, such as the amount of polymer, inorganic filler, and surface modifications. The variation in the general properties of the composites is due to variation in the components' contents, such as the morphology of the composite, which is significantly influenced by the interactions at the interface and the number of octadecyl chains in the modification. Thus, it was necessary to constrain the mixture amounts of the components where they cannot be applied within the range of 0-100% of total weight. Hence, the polymer comprised 84 to 100%, inorganic filler 0 to 11%, and organic modification 0 to 5% of the

total weight of the composite. The models successfully showed accuracy in predicting the tensile modulus and gas permeation behaviors of the polypropylene-organically modified montmorillonite (PP-OMMT) nanocomposites where the models follow a nonlinear pattern (Mittal, 2008).

Chapter 3
Mathematical Models and Optimization Mechanism

3.1 Introduction

In this chapter we are trying to develop an effective methodology for composite product design in order to obtain the best combination of the composite. At the same time, we are seeking for the optimum cost of the composite. This methodology was applied on two case studies. The first case study was the LGFPP composite that can be formed of glass fiber and polypropylene. The weights of the two components were optimized for specific needs in terms of mechanical properties using regression models as can be seen in detail in section 3.3. The PP-OMMT nanocomposite was the second case study in this work where involves three components to form the composite. The weights of the three components also were optimized in terms of desired properties of tensile modulus and permeation as illustrated in section 3.4. The results of performing the simulations for different objective functions for both cases are shown and discussed in Chapter 4.

3.2 Methodology for Composite Product Design

The systematic technique that is followed in this study is illustrated in Figure 3.1. Analysis takes place when the regression models were performed to assess the accuracy of the model. After verifying the accuracy of the model, it will be involved in the optimization process, which can be done by defining the optimization problem and the objective function as well as designing the constraints. Next, we run the simulation and check the findings. If the results do not meet the requirements, it needs to be refined. If the requirements are met, then that means the product has been optimized.

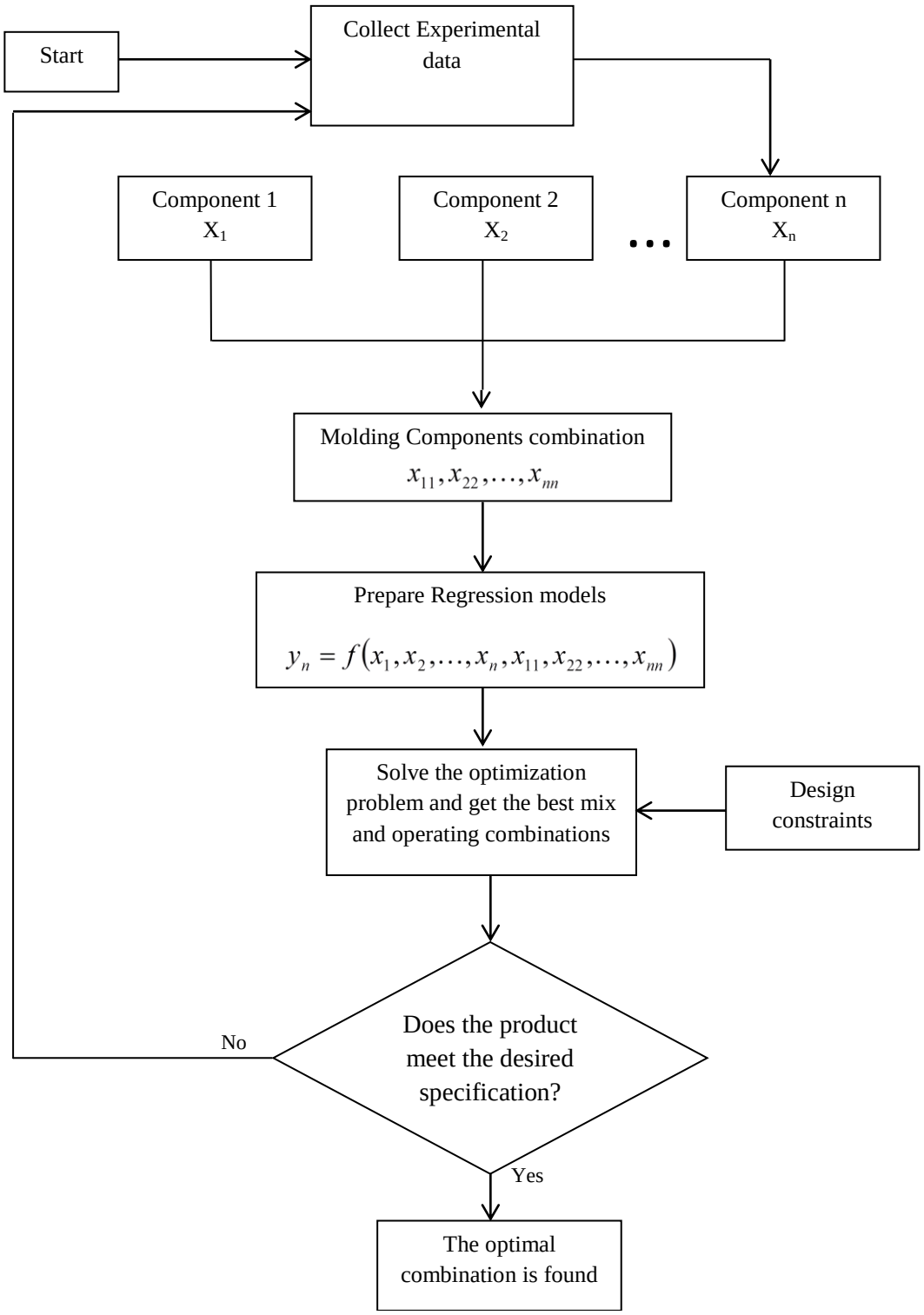

Figure 3.1: Systematic modeling and optimizing product design.

3.2.1 Regression Models

Performing regression analysis is useful in determining the physical characteristic of a system by extracting the parameters from measured data. In this work, polynomial regression is used that statistically is a form of linear regression where can be modeled the relationship between X the independent variable and y the dependent variable and k which represents the order of the polynomial. The following equation represents the general form of the k^{th} order of polynomial.

$$y_i = a_0 + a_1 X_i + a_2 X_i{}^2 + ... + a_i X_i{}^k + \varepsilon_i \qquad (3\text{-}1)$$

Where

- $a_{0,1,2}$ are the intercept, linear effective parameter, and quadratic effect parameter, respectively.

Also, it can be expressed in matrix form, where X is a design vector, y_i is a response vector, a is a parameter vector, and ε is a random error vector.

$$X = \begin{bmatrix} 1 & x_1 & x_1^2 & \dots & x_1^k \\ 1 & x_2 & x_2^2 & \dots & x_2^k \\ \vdots & \vdots & \vdots & & \vdots \\ 1 & x_i & x_i^2 & \dots & x_i^k \end{bmatrix}$$

$$y_i = \begin{bmatrix} y_1 \\ y_2 \\ \vdots \\ y_i \end{bmatrix} \quad , \quad a = \begin{bmatrix} a_0 \\ a_1 \\ \vdots \\ a_k \end{bmatrix} \quad and \quad \varepsilon = \begin{bmatrix} \varepsilon_1 \\ \varepsilon_2 \\ \vdots \\ \varepsilon_i \end{bmatrix}$$

The least square approach is used to estimate the coefficients of the polynomial regression a_i. If the model is linear, then the following equation is applied.

$$\hat{\vec{a}} = \left(X^T X\right)^{-1} X^T \vec{y} \tag{3-2}$$

Where X^T is transpose matrix; however, if the model is nonlinear, which is the case of modeling the mechanical properties of fiberglass-reinforced polypropylene in this study, the following equation is applied. In order to estimate the value of parameters a, numerical algorithms are used which minimize the objective .

$$a_i^{k+1} = a_i^k + \Delta a_i \tag{3-3}$$

Where

- k is an iteration number and the vector of increments; and
- Δa_i is known as a 'shift vector'.

$$Min \sum_{i=1}^{n} \left(y_i - \hat{y}_i\right)^2 \tag{3-4}$$

Where

- y_i is the absorbed value; and
- $\hat{y}_i$ is the predicted value.

3.2.2 Optimization

The optimization process can be defined in terms of seeking either maximizing or minimizing a single-valued objective function $f(x)$, where x is a vector of n real variables $x_1, x_2, ..., x_n$. The objective function can be subjected to a limited number of constraints that are presented as inequalities or equalities (equations). Generally, it can be defined as follows:

$$Min \quad f(x) \tag{3-5}$$

Subject to:

$$g_i(x) \geq 0 \qquad i = 1,..., m_1 \tag{3-6}$$

$$h_j(x) = 0 \qquad j = 1,..., m_2 \tag{3-7}$$

Where

- $g_i(x)$ is a vector of inequalities of dimension m_1;
- $h_j(x)$is a vector of equations of dimension m_2; and
- The total number of constraints is $m = (m_1 + m_2)$. (Avriel, 2003).

Optimization algorithms are iterative. A solution can be obtained by generating a sequence of improved estimates where the iterations start with an initial assumption of the optimal values of the variables. Further, the way in which the iteration moves from each to the next distinguishes one algorithm from another. Several strategies can benefit from the values of objective function f, the constraints c, and usually the first and second derivatives of these functions. The accumulated information of some algorithms are gathered from previous

iterations, whereas others are gathering local information from the current point. In spite of these details, the robustness, efficiency, and accuracy should be considered to be good algorithms. In order to perform perfectly with a variety of problems, the robustness is needed as well as efficiency in term of speed and minimal computer time and storage. A conflict may occur in seeking to achieve these targets. For instance, nonlinear optimization of a large problem may need plenty to computer storage when a rapidly convergent method is used. Additionally, a robust technique may also be very slow (Nocedal and Wright, 1999).

Among the concepts of nonlinear optimization, the Levenberg-Marquadt (LM) method was used in this work. The Gauss-Newton (GN) method is an improvement of LM by amalgamating the Steepest Descent (SD) into the iterative update scheme. The initial estimate gets close to the optimum area and behaves like Steepest Descent method if it is far from the optimum point, after that converges like the Newton methods.

In optimization, the Steepest Descent is the most direct method due to the computation of the gradient direction followed by a one-dimensional (1D) search. The minimum point of the objective function in parameter space of Steepest Descent is iteratively approached. SD can be mathematically defined as follows:

$$x^{k+1} = x^k - \lambda^k \nabla F\left(x^k\right) \tag{3-8}$$

The suffering of SD from convergence slowness is due to the use of the information of the first-order derivative alone. On the other hand, when the initial guess is far from the actual value, it is relatively robust.

Newton's technique goes a step further than SD, since the second-order derivative term is involved in computing the update in the Taylor’s expansion of the objective function at the current point.

$$x^{k+1} = x^k - \left[H_f\left(x^k\right)\right]^{-1} \nabla F\left(x^k\right) \tag{3-9}$$

Where the term $\left[H_f\left(x^k\right)\right]$ represents the Hessian matrix of function $F(x)$ at x^k, that denotes the second-order derivative.

The convergence in Newton's method is faster than SD. As a result, the robustness is reduced, i.e., the sensitivity toward the initial guess is much greater than SD. Another difficulty is the need of calculating the Hessian matrix H, which could be a serious issue in many various applications where the analytical form of $F(x)$ is unavailable. For a particular set of optimization problems – least-square optimization, i.e.

$$\min F(x) = \left\| f(x) \right\|_2^2 = f^T(x) f(x) \tag{3-10}$$

Gauss-Newton (GN) is improved by replacing the Hessian matrix $\left[H_f\left(x^k\right)\right]$ by the multiplication of two first-order derivatives (Jacobian matrix) of the function f in Newton's method; hence, the "pseudo-Hessian" matrix has the form of $\left[J_f\left(x^k\right)^T\left(J_f\left(x^k\right)\right)\right]$. Consequently, GN is more commonly used where the equation can be rewritten in two forms as follows:

$$x^{j+1} = x^k - \left| J_f\left(x^k\right)^T J_f\left(x^k\right) \right|^{-1} J_f\left(x^k\right)^T f(x) \tag{3-11}$$

Or

$$\left[J_f\left(x^k\right)^T\left(J_f\left(x^k\right)\right)\right](\Delta x)^k = -J_f\left(x^k\right)^T f(x) \qquad (3\text{-}12)$$

In GN, the savings in computation are due to only need of calculating the $J\left(x^k\right)$. Nonetheless, the price to pay is the convergence rate (GN method has first-order convergence, while in Newton's method, the second-order convergence is in its place). There are oscillatory features during iterations in both Newton's method and the Gauss-Newton method, which is not the case in the SD method. A hybrid of GN and SD was offered by Levenberg-Marquardt. This system proposed a steering factor λ, which is able to shift between the GN method and SD method. The new equation form in LM can be defined as follows:

$$\left[J_f\left(x^k\right)^T J_f\left(x^k\right) + \lambda I\right](\Delta x)^k = -J_f(x)^T f(x) \qquad (3\text{-}13)$$

If $\lambda \to \infty$, LM comes close to the SD method. If $\lambda \to 0$, LM method is reduced toward GN. The way of selecting the values of λ through the iterative process are as follows: setting λ to a large value at the beginning of the iteration, thus, the LM method displays the robustness of SD and the initial guess can be chosen with less attention. For the sake of accelerating the convergence in every iteration, if $F\left(x^k + \Delta x^k\right) < F\left(x^{k-1} + \Delta x^{k-1}\right)$, decreases the λ value by certain amount such as (divided by 2); otherwise, the λ value can be increased to expand the searching area (trust-region) (Levenberg, 1944; Marquardt, 1963).

3.2.3 Processing Optimization

MATLAB software version 7.10.0.499 (R2010a) was used to predict the minimum cost of the tested composite under different conditions. MATLAB is a high-level programming

language and provides an interactive environment that can complete intensive algorithmic jobs faster than traditional programming.

3.3 First Case study

The experimental data that were used in this case were collected from a literature review reported by Thomason in 2005. GetData Graph Digitizer software version 2.24 was used to determine the data points. These experimental data describe the behavior of mechanical properties of LGFPP as follows:

- Tensile strength
- Tensile modulus
- Flexural strength
- Flexural modulus
- Notched Charpy impact
- Notched I-zod impact

We performed a curve fitting on the experimental data, where the notched Charpy impact is taken as an example.

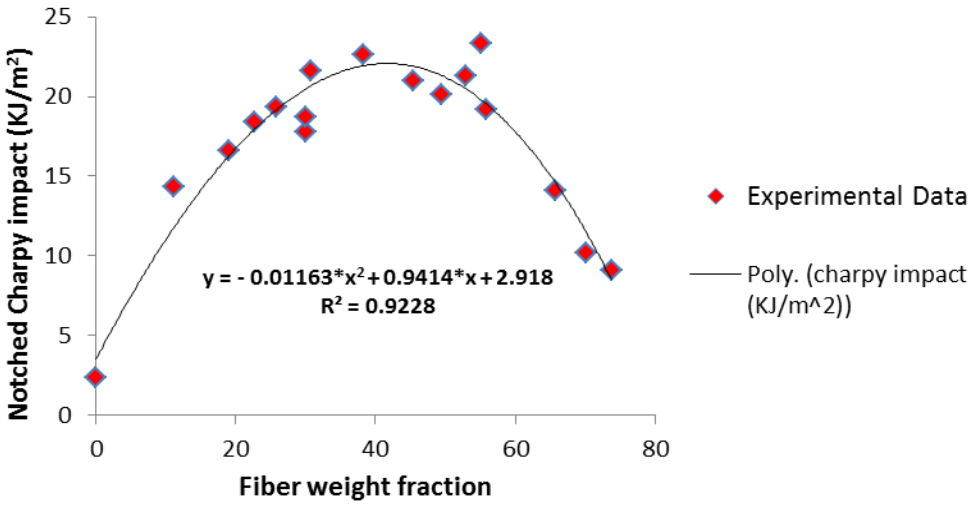

Figure 3.2: Curve fitting on experimental data of notched Charpy impact.

Figure 3.2 shows that the fitting is nonlinear (second-order polynomial), which depends on how the experimental data is distributed. The best way of determining whether the curve fitting is good or not for the available data is by examining the coefficient of determination, which is frequently used to judge the performance of a regression model. First of all, R^2, which is a statistical measurement of how well the regression line evaluates the actual data point, can be mathematically expressed as follows:

$$R^2 = \left[1 - \frac{SS_E}{SS_T}\right] \tag{3-14}$$

Where

- SS_E is residual sum of squares; and
- SS_T is the total sum of squares (proportional to the sample variance).

If the value of R^2 approaches 1, then that indicates that the regression model is perfectly fit to the actual data point; however, if R^2 approaches zero, then that means the regression line is too poor to evaluate the real data. The value of R^2 is increased each time by adding a new term to the model (increasing the order of polynomial), even if the new term is not significant; however, this increase cannot be taken as a sign that the new model is better than the previous one. Therefore, a better statistic to use is the $R^2_{Adjusted}$, which can be defined as follows:

$$R^2_{Adjusted} = 1 - \left[\frac{N-1}{N-p} \cdot \left(\frac{SS_E}{SS_T} \right) \right] \tag{3-15}$$

Where

- N is the sample size; and
- p is the order number of polynomial.

The value of $R^2_{Adjusted}$ cannot be increased unless significant terms are added to the model. In addition, the value of $R^2_{adjusted}$ cannot exceed the value of R^2.

Another coefficient that should be considered is $R^2_{\Pr edicted}$, which can be written as:

$$R^2_{\Pr edicted} = \left[1 - \frac{PRESS}{SS_T} \right] \tag{3-16}$$

$PRESS$ is an acronym for 'prediction error sum of squares', and can be defined as the differences between each observation y_i of the sum of squares and the corresponding predicted value when a point is excluded from the sample data, $\hat{y}_{(i)}$.

$$PRESS = \sum_{i=1}^{n} \left(y_i - \hat{y}_{(i)} \right)^2 \qquad (3\text{-}17)$$

Both $PRESS$ and $R^2_{\Pr edicted}$ are indicators of how well the regression model is likely to perform when predicting new observation data (Montgomery, 2011).

For instance, high values of $R^2_{\Pr edicted}$ or low values of $PERSS$ imply that the predictions of the model are excellent and vice versa. In case of modeling the notched Charpy impact, the R^2, $R^2_{Adjusted}$ and $R^2_{\Pr edicted}$ are calculated for both second and third order polynomials as shown in Table 3.1.

Table 3.1: Coefficients of determination results of notched Charpy impact.

Model Degree	R^2	$R^2_{Adjusted}$	$R^2_{\Pr edicted}$
Quadratic polynomial	0.9228	0.9113	0.8918
Cubic polynomial	0.9258	0.9086	0.7221

It can be seen in the above table that the value of R^2 is increased when a new term is added to the model. The fit in second-order is about 92.23% and increases slightly when the third-order is applied to around 92.58%. Also, there is a slight difference between the values of $R^2_{Adjusted}$ for second and third order, which is about 0.27%. To simply judging the models by which one is the best fit based on the values of R^2 and $R^2_{Adjusted}$ is not adequate. Therefore, it is necessary to compare the values of $R^2_{\Pr edicted}$ for second order that estimated (estimated at about 89.18%) and third order (about 72.21%) because they measure the accuracy of the model with new observation data. Also, it can be done by calculating the difference between

$R^2_{Adjusted}$ and $R^2_{Predicted}$. This difference in cubic polynomial is about 0.1865%, which is much greater than the quadratic polynomial, which equals 0.0195%. Hence, it has been decided that the quadratic polynomial model is the best fit.

Further analysis of regression models takes place to investigate the performance of the model through plotting the residual and normal probability. The residuals are $e_i = y_i - \hat{y}_i$.

Plotting the residual is useful in checking the assumption that the errors are approximately normally distributed. If the points are randomly dispersed, then that indicates that the model is appropriate for the data; however, if the distribution of the points follow a specific pattern, such as a U-shape or inverted U, that means the regression model is inappropriate to predict new points. As seen in Figure 3.3, the residual of notched Charpy impact is randomly distributed.

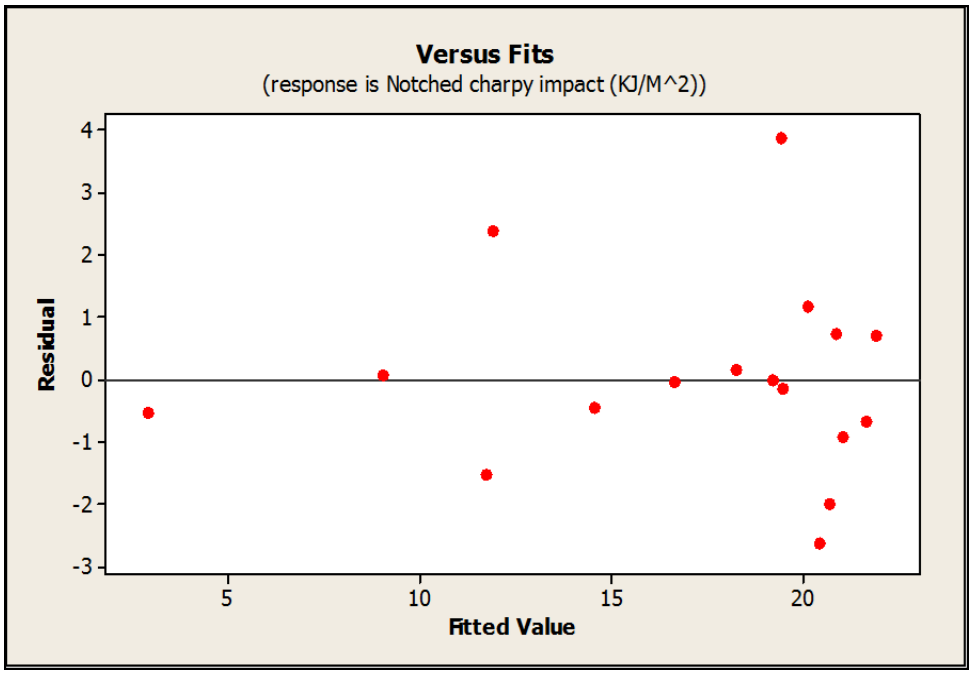

Figure 3.3: Plotting the residual of notched Charpy impact.

Another way of checking the normality is by plotting the normal probability of the residual. The general idea is that the plot of the theoretical p^{th} percentile of the normal distribution against the experimental data sample percentiles should be nearly linear if the data tracks a normal distribution through mean μ and variance σ^2. The model is appropriate if the points are approximately located in a straight line; this is the case with the notched Charpy impact as illustrated in Figure 3.4.

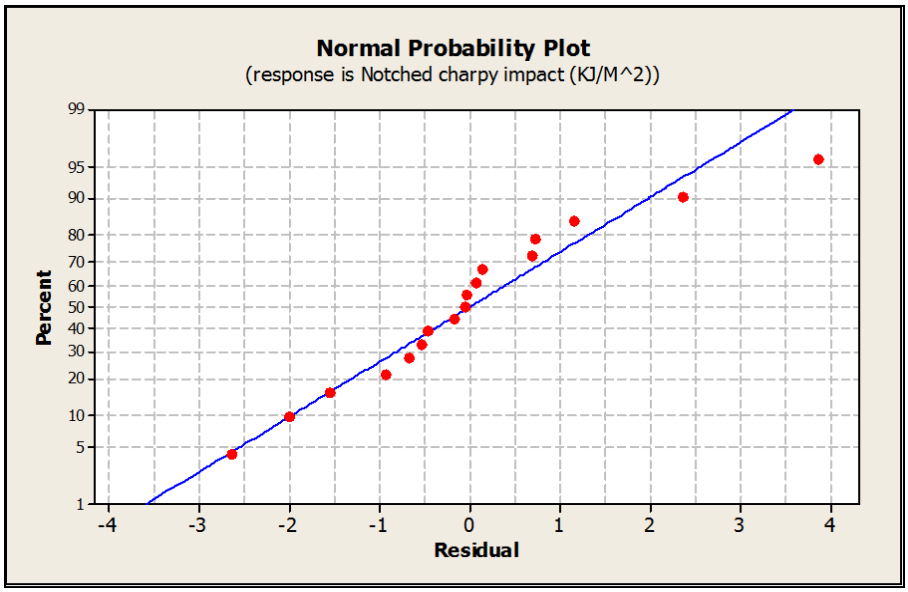

Figure 3.4: Normal probability plot of residual for notched Charpy impact

The regression is used in modeling the mechanical properties of long glass fiber-reinforced polypropylene due to two main reasons:

- The models described earlier in the literature review involve many parameters that are not preferred in performing optimization, and some of these parameters involve uncertainty when its estimate such as the orientation factor and interfacial shear stress especially with long glass fiber as a filler.

- Regression models are amenable to MATLAB software when an optimization is performed.

The other mechanical properties follow the same procedures that we have mentioned above, which involve modeling and analysis. The mathematical model of each property is presented in Table 3.2.

Table 3.2: Regression models of mechanical properties

Mechanical Property	Regression Model
Tensile Strength (MPa)	$-0.0616 * X^2 + 4.55 * X + 31.849$
Tensile Modulus (GPa)	$-0.00004 * X^3 + 0.004 * X^2 + 0.06 * X + 2.37$
Flexural Strength (MPa)	$-0.086 * X^2 + 6.52 * X + 47.98$
Flexural Modulus (GPa)	$0.0013 * X^2 + 0.121 * X + 1.895$
Notched I-zod Impact (J/m)	$-0.139 * X^2 + 11.013 * X + 25.014$
Notched Charpy Impact (KJ/m^2)	$-0.011 * X^2 + 0.941 * X + 2.918$

Where

- X represents the filler weight (long glass fiber) in composite system.

Often, the order of model is preferred to be as low as possible. Most of the properties in Table 3.3 have a second-order polynomial, except one that has a third-order polynomial. Also, the table illustrates the values of coefficient of determinations which are reasonably

large, indicating that the models have good predictive capability. Therefore, these models are the best fit for the data available.

Table 3.3: Coefficient of determination of each property model.

Property	**Model Order**	R^2	$R^2_{Adjusted}$	$R^2_{\text{Predicted}}$
Tensile Strength	Quadratic	0.965	0.961	0.955
Tensile Modulus	Cubic	0.991	0.989	0.966
Flexural Strength	Quadratic	0.962	0.956	0.949
Flexural Modulus	Quadratic	0.992	0.991	0.987
Notched I-zod Impact	Quadratic	0.909	0.896	0.876
Notched Charpy Impact	Quadratic	0.922	0.905	0.891

3.3.1 Minimizing the Cost of Composite

The function that performed the simulations in MATLAB was fmincon, which is an abbreviation of 'find minimum of constrained nonlinear multivariable function'. This function was fixed to obtain the local optimum cost of the LGFPP composite.

In this composite, three properties were selected to minimize the cost: tensile modulus, flexural modulus, and notched I-zod impact. The reason for choosing only three of the composite's properties is that the tensile strength and tensile modulus are dependent on each as illustrated in literature; the same holds true for the flexural strength and flexural modulus.

The notched I-zod impact and notched Charpy impact measure the same concept but with different scale measurements.

The objective function of cost minimization $f(x)$ is defined as follows:

$$Min\left(\sum_{i=1}^{n} C_i \cdot X_i\right) \Big/ 100 \qquad , \; i = 1, \; 2 \qquad \text{(3-18)}$$

Where

- C_1 is the cost of glass fiber;
- X_1 is the weight of glass fiber in percentage;
- C_2 is the cost of polypropylene; and
- X_2 is the weight of PP in percentage.

The total was divided by 100 because of the use of weight percentage. The function $f(x)$ is subjected to nonlinear inequality constraints, which can be presented by the regression models obtained for each property. These constraints were used to define the desired properties that we would like to obtain from the composite, while nonlinear equalities constraints did not exist in either case study. The following equation stands for the linear equality that is used to control the weight of the composite.

$$X_1 + X_2 = 100 \qquad \text{(3-19)}$$

Lower and upper bounds were defined based on the weight of the matrix and filler systems. The procedure that was followed to run the simulations involved making one property constant and changing the values of the others each runs. Next, the other properties take

turns being the constant. This procedure is useful in assessing how effective these properties arevin minimizing the cost of the composite.

3.3.2 Minimizing the Variance

In this objective function, we were seeking to obtain the best combination of the components where quality of the composite cannot be compromised (while the cost of the composite is secondary). The objective function was fixed to minimize the variance between the values predicted from the regression model and the desired properties values.

The function $f(x)$ can be written as follows:

$$Min \quad \sum_{i=1}^{n}\left(\frac{(M_i - d_i)}{H_i}\right) \quad , \quad i = 1,\ 2,\ 3 \qquad (3\text{-}20)$$

Where

- $M_{1,2,3}$ are the regression models of tensile modulus, flexural modulus, and notched I-zod impact, respectively;
- $d_{1,2,3}$ are the desired property values that we would like to obtain for tensile modulus, flexural modulus, and notched I-zod impact, respectively; and
- $H_{1,2,3}$ are the maximum values of regression models that can be used for tensile modulus, flexural modulus, and notched I-zod impact, respectively.

The regression models were divided by H_i in order to be normalized; this makes it possible to avoid the bias in the objective function toward any property. The bias occurs because there are different magnitude scales; for instance, the notched I-zod impact has a high magnitude scale that starts from 40 J/m and the maximum is 240 J/m, while the tensile modulus ranges from 2.2 to 14.2 GPa. Therefore, the objective function always targets to satisfy the model

that has a big value on account of the small one. The nonlinear inequality constraints need to exist because the model of I-zod impact takes an inverted U-shaped when it is plotted as shown in Figure 3.5. This type of shape provides two solutions one of which is smaller than the other in the magnitude of the variance. In this case, the objective function will prefer to choose the solution with the smallest variance value; however, this solution might violate the requirements, while the other solution would not even though the value of the variance is bigger. Consequently, the best way to get rid of this problem is by constraining the models with the values of the desired properties. Also, the linear equality in equations (3-19) should exist. The values of the desired properties that were used in the first objective function to minimize the cost were also used in the second objective function for the sake of comparison. Surface plots of tensile modulus, flexural modulus and notched I-zod impact are shown in Figure 3.5, which is a good way of checking whether there is a feasible solution or not. Looking at this figure, we can see that there is a feasible solution for both objective functions.

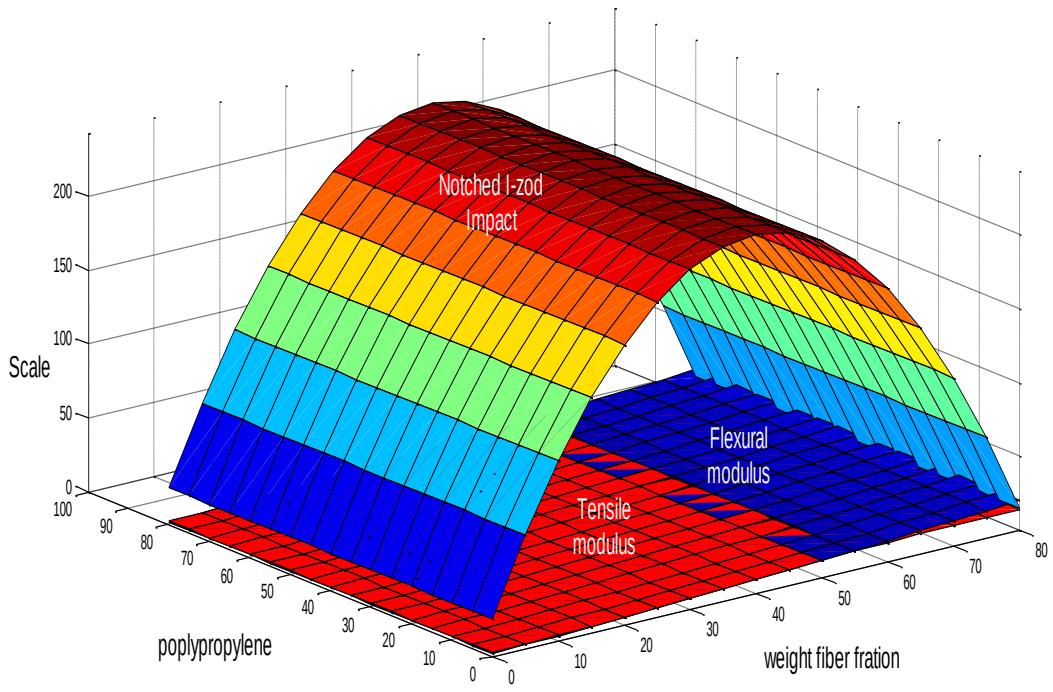

Figure 3.5: Surface plot of notched I-zod impact, tensile modulus and flexural modulus models for LGFPP

3.4 Second Case Study

In the case of PP-OMMT nanocomposites, the mathematical models of tensile modulus and oxygen permeation were proposed in literature review by Mittal, (2008).

Mittal, found that tensile modulus and oxygen permeation have a significant influence on the composites' properties as a result of performing a factorial and mixture design technique. A nonlinear model was produced after the regression for the tensile modulus that can be written in the form of a numerical equation.

$$E = 15.3 * X_1 - 109.53 * X_2 + 58.96 * X_3 + 1.91 * X_1 \cdot X_2 \qquad (3\text{-}21)$$

Where

- E is the tensile modulus of the composites in MPa;
- X_1 is the weight of the polymer in percentage;
- X_2 is the weight of the organic modification in percentage; and
- X_3 is the weight of the inorganic filler in percentage.

The value of ($R^2 = 98.59\%$) is given through regression analysis which indicates an excellent fit of the data. Furthermore, the magnitude of the residual error as compared to the main effects was low. Likewise, a model was produced for oxygen permeation which is also nonlinear as written in the following equation.

$$P = 0.89 * X_1 + 12.21 * X_2 - 3.32 * X_3 - 0.14 * X_1 \cdot X_2 \qquad (3\text{-}22)$$

Where

- P is oxygen permeation.

The accuracy of the model is confirmed through regression analysis, which achieves about a 98.74% fit of the data.

3.4.1 Minimizing the Cost of Nanocomposite

The PP-OMMT nanocomposite, contains three types of components, and its objective function $f(x)$ can be expressed as follows:

$$Min \left(\sum_{i=1}^{n} C_i \cdot X_i \right) \Big/ 100 \quad , \quad i = 1, 2, 3 \tag{3-23}$$

Where

- $C_{1,2,3}$ are the costs of polypropylene, inorganic filler, and organic modification, respectively; and
- $X_{1,2,3}$ are the weights in percentage of polypropylene, inorganic filler, and organic modification, respectively.

The nonlinear inequality constraints can be expressed by the equations of tensile modulus (3-21) and oxygen permeation (3-22). Lower and upper bounds for the inorganic filler and organic modification are limited, which means that they cannot be worked in a full range of weight from 1 to 100%; however, they do not exceed 17% of weight when combined together. The reason behind this is explained in the literature review, Chapter 2. The linear equality can be written as the following equation.

$$X_1 + X_2 + X_3 = 100 \tag{3-24}$$

3.4.2 Minimizing the Variance

Similarly, what has been done in case 1 for the second objective function is done with the case 2, where the objective function $f(x)$ is as follows:

$$Min \sum_{i=1}^{n} \left(\frac{(M_i - d_i)}{H_i} \right)^2 \quad , \quad i = 1, 2 \qquad (3\text{-}25)$$

Where

- $M_{1,2}$ are the regression models of tensile modulus and oxygen permeation, respectively; and
- $d_{1,2}$ are the desired properties value that we would like to obtain for tensile modulus and oxygen permeation, respectively.

The only exception here is that there is no need for the nonlinear inequalities constraints otherwise, it would be redundant. We do not have the same issue as in case 1, which means we have only one solution based on the requirements that can be provided by running the simulation in the case of PP-OMMT nanocomposite. The surface plots of tensile modulus and oxygen permeation models can be clearly seen in Figure 3.6, and it can be concluded that a feasible solution can be found. All results obtained from performing the simulations will be discussed in Chapter 4.

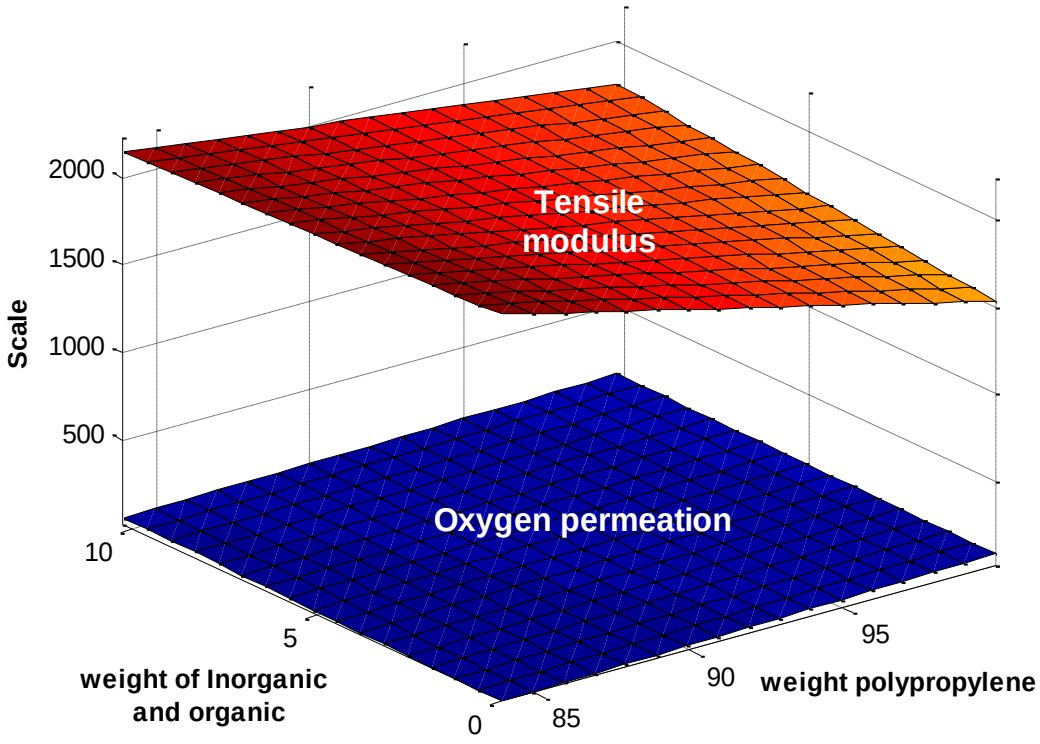

Figure 3.6: Surface plots of tensile modulus and oxygen permeation models of PP-OMMT nanocomposite.

Chapter 4
Results and Discussion

4.1 Model Accuracy

A function in MATLAB software was formulated to predict the desired properties. Further, the accuracy of this function (which in turn is the model for LGFPP composite) was validated with the available experimental data. Table 4.1 shows that, for the composite with 30% of glass fiber and 70% of polypropylene, the predicted values and the actual values of almost all properties are reasonably close.

Table 4.1: comparison of predicted and experimental mechanical properties of 30% of glass fiber and 70% of polypropylene composite.

Mechanical Property (Y)	Acceptable Criteria	Predicted Value	Actual Value[1]
Tensile Strength	$33 \leq Y \leq 121$	113.05	114
Tensile Modulus	$0 \leq Y \leq 14.5$	7.16	6.97
Flexural Strength	$46.8 \leq Y \leq 178$	166.36	165.42
Flexural Modulus	$0 \leq Y \leq 18.2$	6.74	6.87
Charpy Impact	$2.3 \leq Y \leq 22.6$	20.69	18.7
I-zod Impact	$33.6 \leq Y \leq 257$	230	214

[1] Adapted from Thomason (2005)

4.2 Minimizing the Cost of Composite

4.2.1 Case (1) LGFPP

MATLAB software was used to simulate the output of different combinations of tensile modulus, flexural modulus, and I-zod impact. Each time, one of the variables was held constant, and the other two were varied. The tensile modulus was between 4 and 14 GPa, while the flexural modulus was from 4 to 18 GPa and the notched Izod impact was in the range of 100-240 J/m. The results of minimum cost as a function of tensile modulus at different flexural modulus are shown in Figure 4.1. Figure 4.1a, b, c, d, e, and f present the minimum cost versus tensile modulus, at different I-zod impact values. In Figure 4.1a when the I-zod impact is 100 J/m, it was observed that the cost of the composite remains same at different levels of flexural modulus; however, the cost would increase with increasing tensile modulus. The starting point of the increase in the cost occurs at a higher value of tensile modulus as the flexural modulus is increased.

For example, at a flexural modulus of 10 GPa, as the tensile modulus increases, the cost stays at a constant level; however, it starts to increase when the value of the tensile modulus reaches 10 GPa. The reason for this is that the properties are constrained. Basically, if one of the variables' properties value (tensile or flexural) is constrained to be higher than the other, then the function stops when the higher property value is satisfied. Therefore, whenever the value used is less than the fixed property's value, the result will be the same, and that is what keeps the cost constant. Once the fixed property's value becomes equal to or is exceeded by the other property, then the cost starts to increase. There is an exception here, i.e., a linear increase when the value of flexural modulus is fixed at 4 GPa, because the tensile modulus value starts at 4 GPa, which means that they are equal. In fact the values of tensile modulus and flexural modulus that can be obtained at any weight fraction are close to each other. It has also been observed that high values of the flexural modulus, such as 18 GPa, are not presented in Figure 4.1 because they cannot be achieved (no feasible solution).

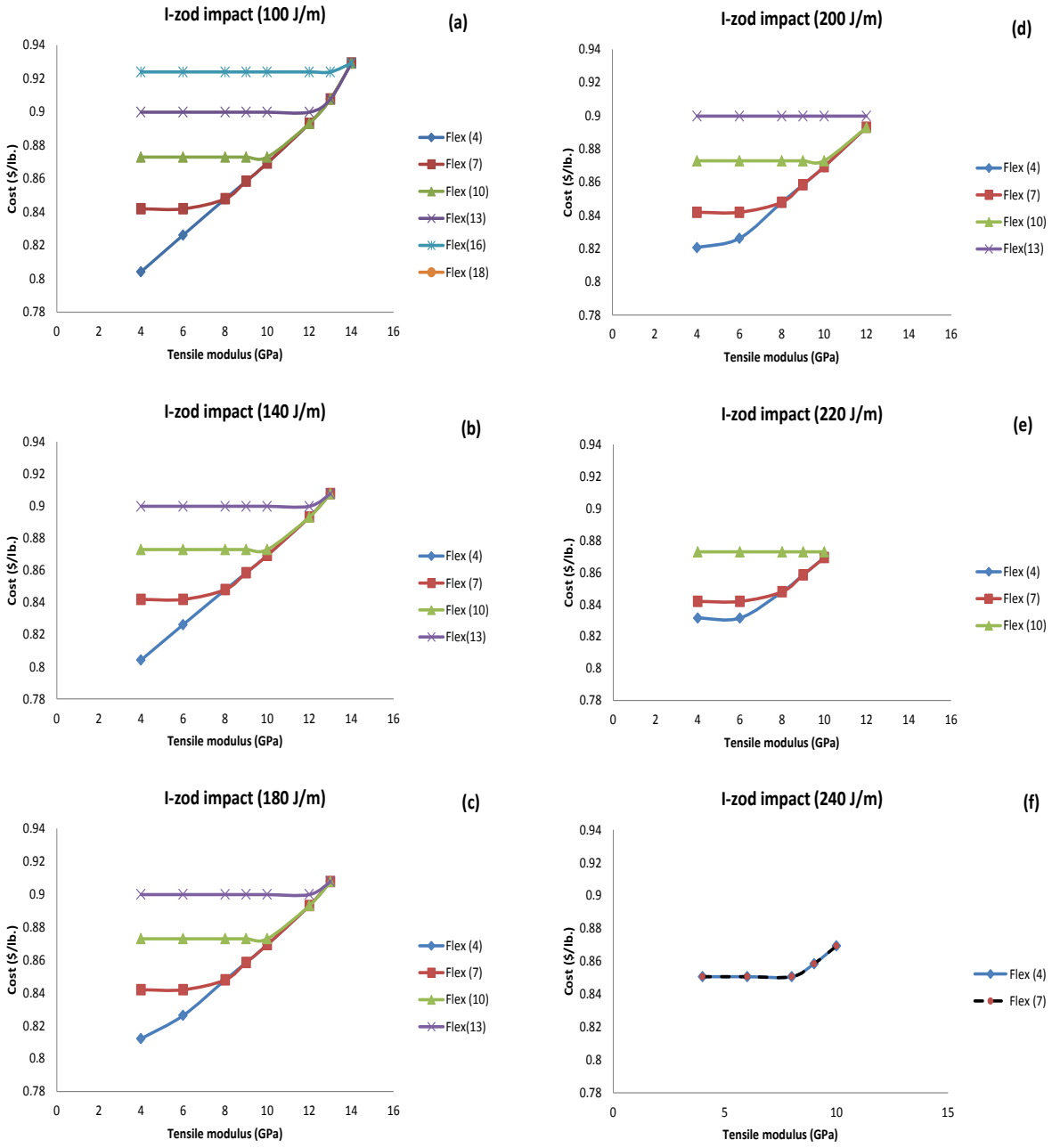

Figure 4.1: Result of minimizing the cost of LGFPP where the notched I-zod impact is constant and the tensile modulus and flexural modulus (which is symbolized as Flex.) are variables. (a) I-zod impact 100 J/m, (b) I-zod impact 140 J/m, (c) I-zod impact 180 J/m, (d) I-zod impact 200 J/m, (e) I-zod impact 220 J/m, and (f) I-zod impact 240 J/m.

Figure 4.1 (b) through 4.1 (f) follow almost the same pattern as Figure 4.1 (a). Gradually, as the value of I-zod impact increases, the high values of flexural modulus and tensile modulus become unachievable. Also, an increase in I-zod impact led to a slow increase in the cost of the composite for flexural modulus equals to 4 GPa, e.g., comparing the cost of flexural modulus at 4 and 7GPa at low value of tensile modulus when the I-zod impact fixed at 100 J/m, the cost was different as been observed; however, increasing I-zod impact value causes raising in the cost of flexural modulus at 4GPa and approaching the cost of flexural modulus at 7GPa until it became identical with the cost of flexural modulus at 7 GPa. This is evident from Figure 4.1.

Secondly, the results of holding flexural modulus constant and the minimum cost as a function of tensile modulus at different values of I-zod impact is illustrated in Figure 4.2. The minimum cost versus tensile modulus at different flexural modulus values are presented through the charts (a) to (f) in Figure 4.2. It can be noticed that the cost is slightly increased with increasing the levels of I-zod impact in Figure 4.2a, but the disparity in cost soon fades away as the flexural increases, and the lines that represent each different value of I-zod impact become identical (see Figure 4.2b, c, d). Further, for different values of I-zod impact, the cost of the composite increases as the value of the constant (flexural modulus) increases. For example, in Figure 4.2c, where the flexural modulus was fixed at 10 GPa, the composite's cost at different levels of I-zod impact starts at 0.875 $/lb.; however, increasing the flexural modulus to 13 GPa increases the cost, which starts at 0.9 $/lb. as shown in Figure 4.2d.

An additional observation is that a combination of high values of the three properties cannot be achieved simultaneously. For instance, at 16 GPa of flexural modulus, the only combinations that can be achieved are, when the I-zod impact equals 100 J/m with any value of tensile modulus, as shown in Figure 4.2e. In case of the flexural modulus being 18 GPa, as shown in Figure 4.2f, there is no combination that can satisfy the objective; thus, no product can be achieved with these levels of properties.

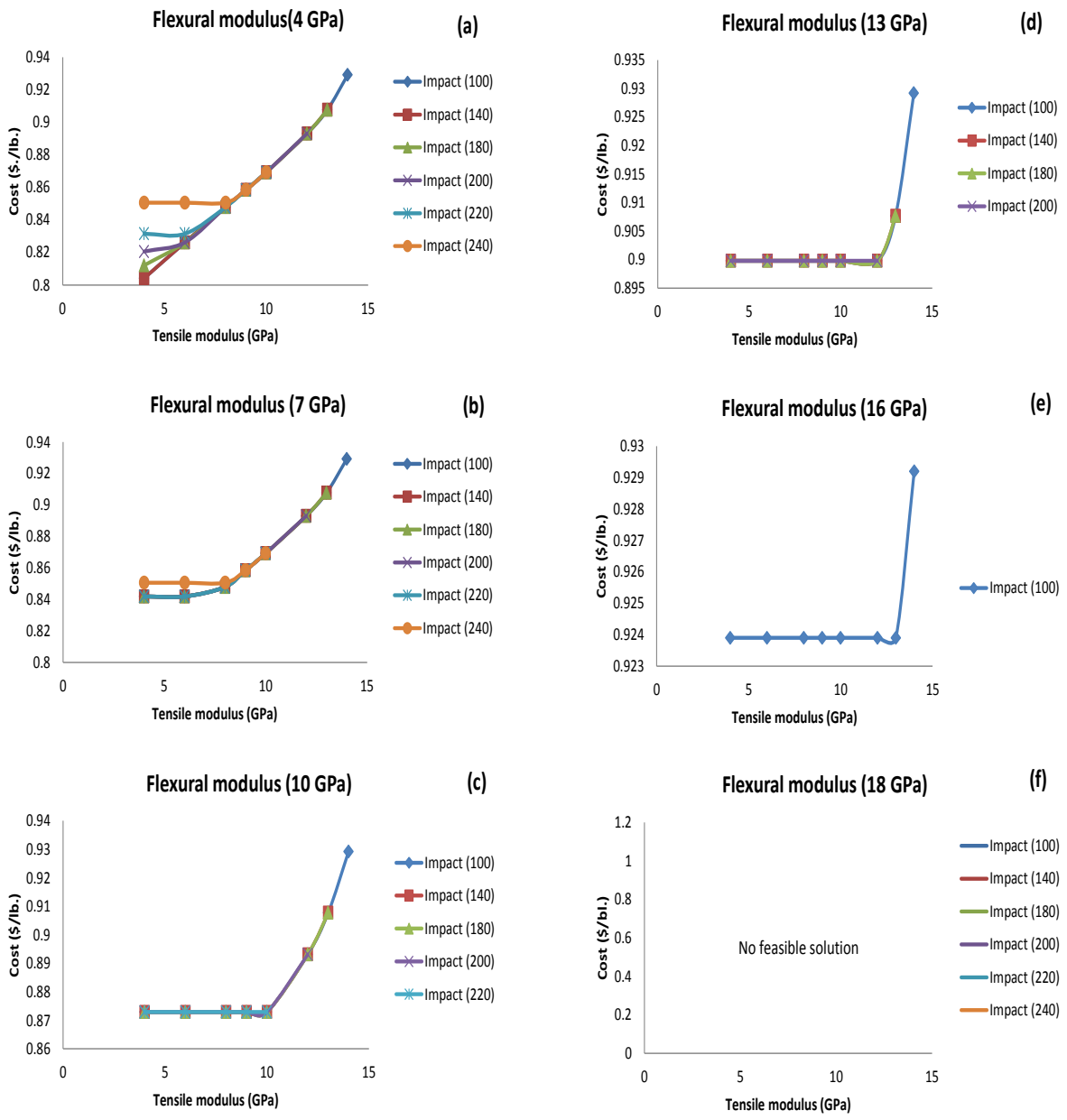

Figure 4.2: Results of minimizing the cost of LGFPP where the flexural modulus is constant and the tensile modulus and notched I-zod impact (which is symbolized as impact) are variables. (a) flexural modulus 4 GPa, (b) flexural modulus 7 GPa, (c) flexural modulus 10 GPa, (d) flexural modulus 13 GPa, (e) flexural modulus 16 GPa, and (f) flexural modulus 18 GPa.

Finally, Figure 4.3 shows the results obtained for minimum cost as a function of flexural modulus for different values of I-zod impact, where the tensile modulus was held constant. The charts from (a) to (h) in Figure 4.3 represent the constant (tensile modulus) at different levels, where the cost is plotted against the flexural modulus with changing the values of I-zod impact.

In Figure 4.3a, it can be observed that the composite's cost is progressively increases for different values of I-zod impact with an increase in the flexural modulus, where this increase follows the same tone for all different values of the I-zod impact; however, there is a slight difference in the cost with low values for both flexural modulus and I-zod impact. The small disparity in cost begins to fade away gradually with the raising of the level of tensile modulus, as illustrated through charts (a) to (d) in Figure 4.3. Also, raising the tensile modulus value makes it possible for the cost of the composite to gradually approach one and stay steady at different values of flexural modulus; however, there is a little increase with high values of flexural modulus and I-zod impact, as can be seen in charts (e) to (g) in Figure 4.3. Moreover, this increase is accompanied by a limitation of forming a composite that combines high values of the three properties.

For example, examining charts (f) to (h) in Figure 4.3 and comparing them with each other, it is observed that the number of combinations begin to reduce as the tensile modulus value increases until only one combination can be formed at 14 GPa, which is the maximum value of tensile modulus as shown in Figure 4.3(h). The cause of the reduction in number of combinations is that the surface plot of I-zod impact model takes an inverted U-shaped based on the increase of the fiber weight fraction, while the tensile and flexural modulus increase linearly with increasing the fiber weight fraction. The maximum value of I-zod impact is 240 J/m, which is located around 45% of fiber glass weight; after this weight, the value of I-zod impact begins to decrease. At the same time, the values of tensile and flexural modulus continue to increase with the increase of the weight of fiber.

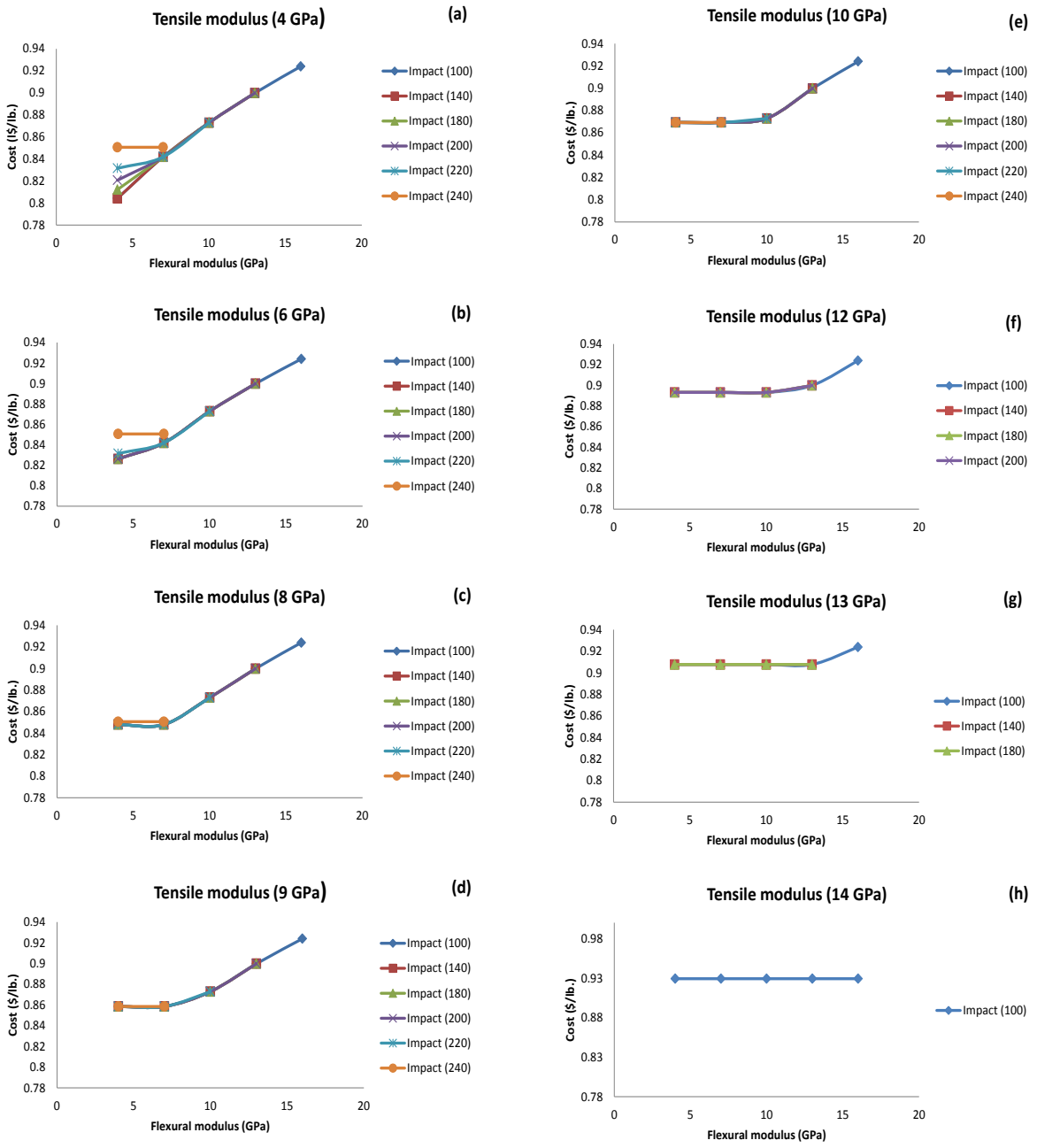

Figure 4.3: Result of minimizing the cost of LGFPP with constant tensile modulus and the flexural modulus and notched I-zod impact (which symbolized as impact) are variables. (a) tensile modulus 4 GPa, (b) tensile modulus 6 GPa, (c) tensile modulus 8 GPa, (d) tensile modulus 9 GPa, (e) tensile modulus 10 GPa, (f) tensile modulus 12 GPa, (g) tensile modulus 13 GPa, and (h) tensile modulus 14 GPa.

As a result, a combination at high values for all three properties cannot be achieved because if a high level in the I-zod impact is obtained, for instance, then the other properties cannot be obtained at higher levels, which means that the constraints (the requirements) are violated and vice versa. In other words, there is no feasible solution. This reason is also valid for the two previous cases that were discussed in Figure 4.1 and Figure 4.2.

Figure 4.4 shows how the weight fraction of composite components were distributed as a function of tensile modulus for various amounts of I-zod impact, while the flexural modulus was held constant at 4GPa. It can be clearly seen in Figure 4.4a, the fiber component weight was distributed in exactly the same way as the cost was distributed at the same conditions. Also, the weight fraction for polypropylene system was plotted at the same conditions; however, the properties increase by decreasing the weight of polypropylene, as illustrated in Figure 4.4b. Similarly, the same trend and results were observed for different conditions and are illustrated in Appendix A.

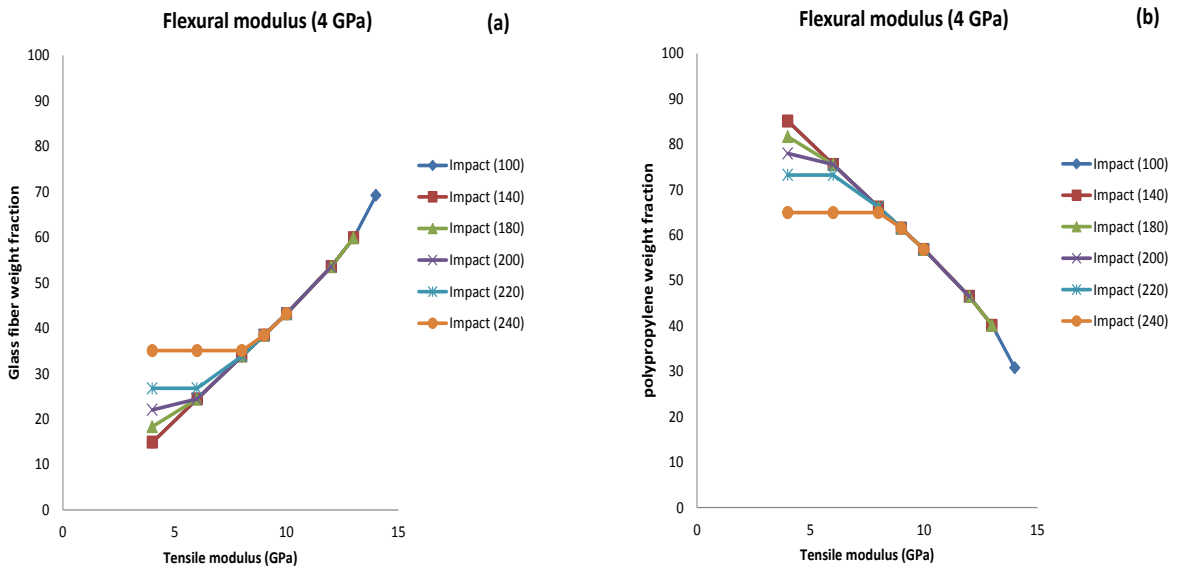

Figure 4.4: (a) Weight fraction of fiber glass versus tensile modulus for different values of I-zod impact, (b) weight fraction of polypropylene versus modulus for different values of I-zod impact.

Hence, we can conclude that the cost increases with the increase in the properties of the composite; furthermore, increasing the weight of the fiberglass also increases the same properties' values, which indicates that the main factor affecting the cost is the weight of fiberglass.

4.2.2 Case (2) PP-OMMT

Charts (a) to (e) in Figure 4.5 represent the results of cost as a function of tensile modulus at different values of oxygen permeation. The range used for tensile modulus was from 1550 to 2150 MPa, while the oxygen permeation was between 57 and 89 $cm^3 \cdot \mu m/m^2 \cdot d \cdot mmHg$.

In general, the cost is slowly increased with increasing the tensile modulus, but this increase cannot be seen in graphs (a) to (d) in Figure 4.5 due to the use of a high cost scale; however, it can be seen clearly in Figure 4.5e, where the result in graph (e) is almost to those shown in the graphs a, b, c, and d, where the oxygen permeation is equal to 57, 60, 65, and 70, respectively. The values of permeation that are equal to 80, 85, and 89 are not presented because they cannot be achieved within the tensile modulus range. Furthermore, the oxygen permeation does not influence the cost at all when the cost is minimized. Also, it can be noticed that the increase in the cost increases sharply after the point of 2000 MPa of tensile modulus, as shown in Figure 4.5a, b, c, and d. The cause for the sudden increase in the due to the high cost of one of the components of PP-OMMT called as 'modified organic' (modified montmorillonite).

In order to clarify the reason, the weight fraction of each component was varied and plotted as a function of tensile modulus for various level of permeation. The weight fraction of the organic modification remains to be zero through the tensile modulus and the permeation increase, as illustrated in Figure 4.6.

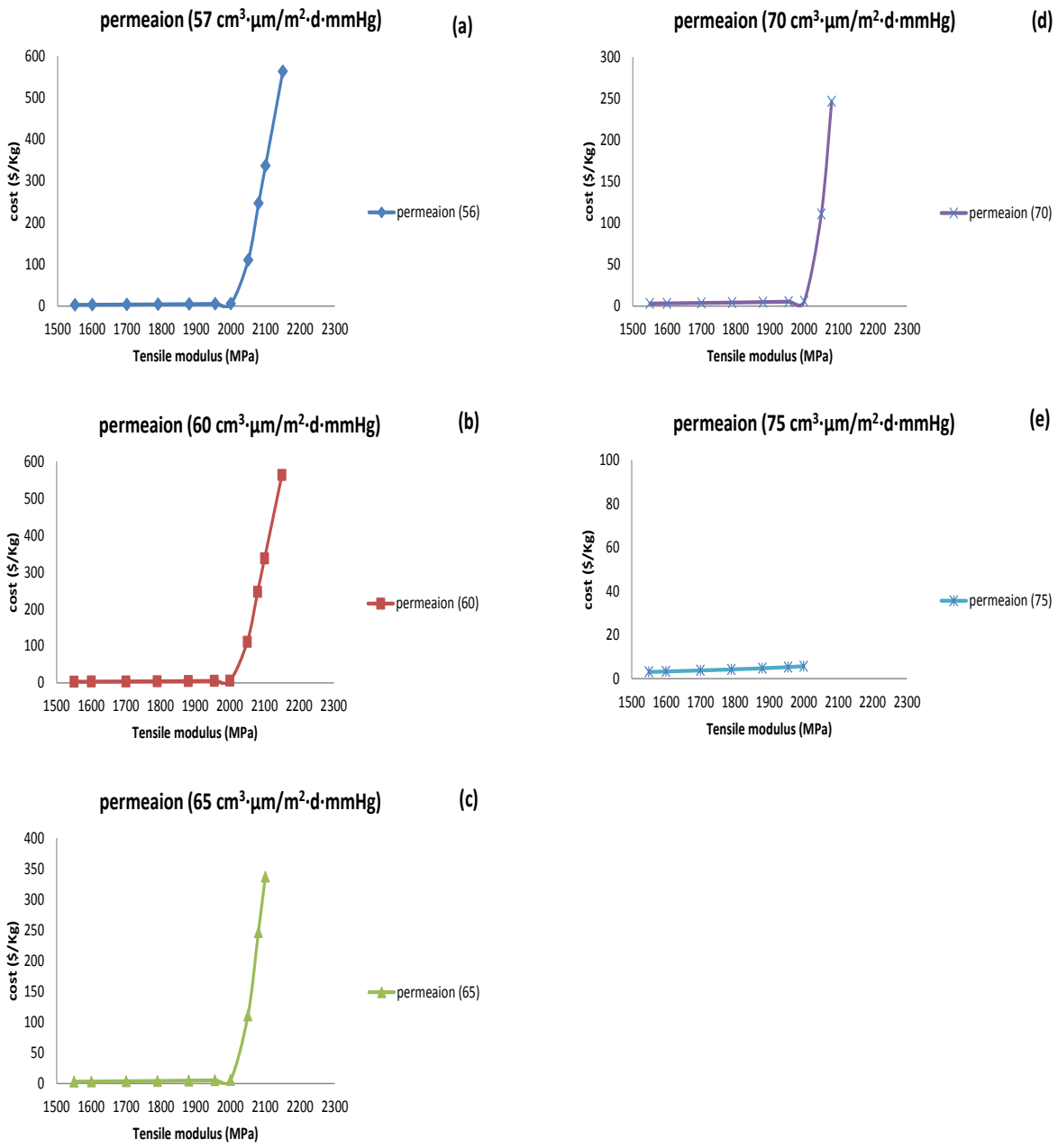

Figure 4.5: Plotting the result of the cost versus tensile modulus at different levels of permeation. (a) Permeation 57, (b) permeation 60, (c) permeation 65, (d) permeation 70, (e) permeation 75.

Once the tensile modulus exceeds 2000 MPa, the organic modification component is being used in the mixture and the modified organic weight begins to increase dramatically as the tensile modulus increases, (and this is the reason for the sharp increase in cost). In Figure 4.7, the gradual drop in the weight of polypropylene leads to an increase in the value of the tensile modulus. On the other hand, it can be clearly seen that an increase in the weight of inorganic, increases the tensile modulus till it becomes constant at about 2050 MPa, which means the use of this component reaches the maximum, which was estimated to be about 11% of the total mixture (as illustrated in Figure 4.8). While the influence of decreasing or increasing the weight fraction of any components of the mixture on different levels of permeation were constant in this function, as shown through the Figure 4.6, Figure 4.7, and Figure 4.8. This conclusion also applied on the results of cost function.

Accordingly, the most significant component that strongly influences the cost of the composite is the organic modification, whereas the weight of polypropylene and inorganic have a minor effect on the cost compared to the weight of the organic modification.

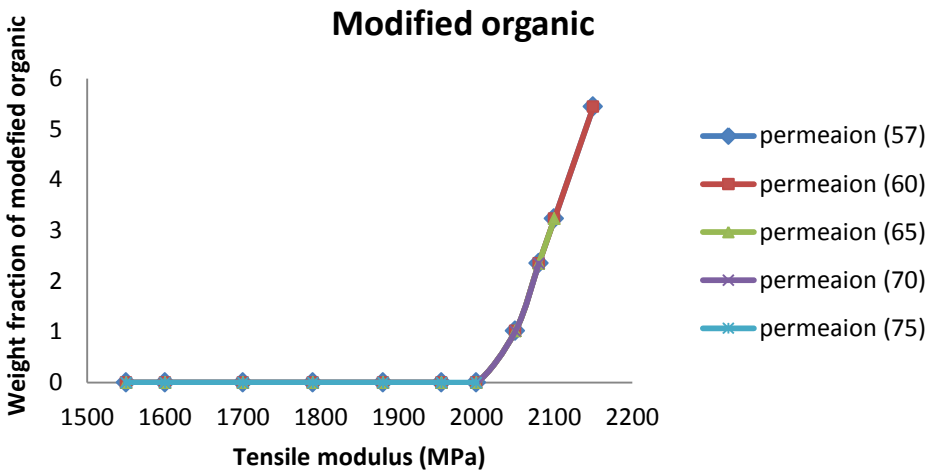

Figure 4.6: Plot of the weight fraction of modified organic versus the tensile modulus for different permeation levels.

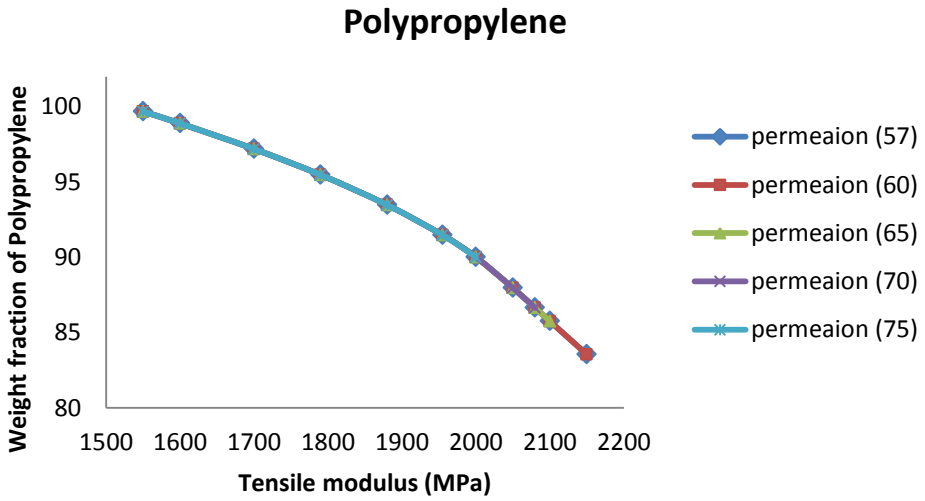

Figure 4.7: Plot of the weight fraction of polypropylene versus the tensile modulus for different permeation levels.

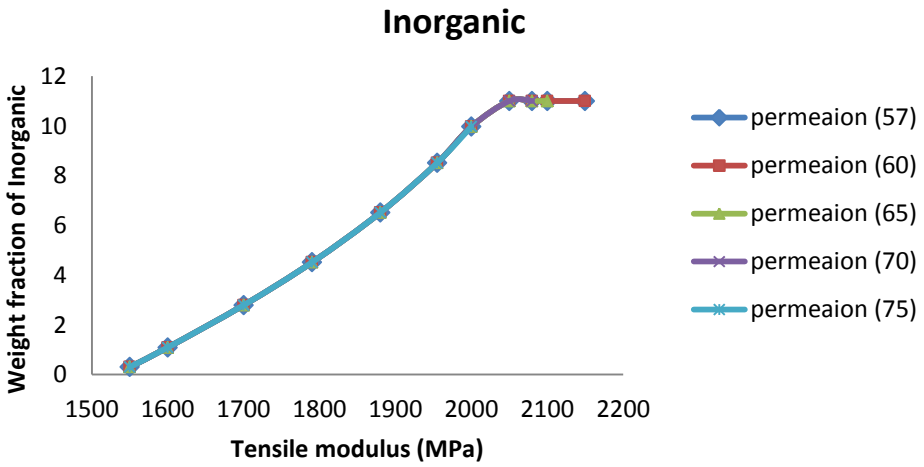

Figure 4.8: Plot of the weight fraction of inorganic versus the tensile modulus for different permeation levels.

4.3 Minimizing the Variance between Desired Properties

4.3.1 Case (1) LGFPP

The objective function was called in MATLAB software to minimize the variance between the desired properties to obtain the best proportion of weight fractions, that would satisfy the constraints (the minimization of cost was secondary). The same conditions that were used in minimizing the cost were applied in minimizing the variance in order to compare between the two functions' results.

In general, the results of the composite cost of the variance function show a similarity with the results of the cost function in some cases; however, there was a difference in other cases. These similarities and differences can be demonstrated by comparing between the results of each combination of the two functions individually. Simulations were performed to minimize the variance of the desired properties as a function of tensile modulus at different levels of flexural modulus, and the I-zod impact is kept constant.

For example, in Figure 4.9 the cost is plotted against the tensile modules for the two functions; the blue line represents the variance minimization function and is represented by ($*$), while the dashed line shows the cost minimization function. Graphs (a) to (f) represent flexural modulus at 4, 7, 10, 13, 16, and 18 GPa respectively, while the I-zod impact is equal to 100 J/m (constant). It can be seen that there is a slight difference in the composite cost between the two functions in Figure 4.9a when the tensile modulus is 12 GPa with the flexural is at a low level, which is about 4 GPa. This difference in the cost becomes significant with an increase of in the flexural modulus, where the cost from minimizing the variance function is greater than the cost from minimizing the cost function, as illustrated in the graphs (b) to (e) in Figure 4.9. At a high value of flexural modulus, such as 18 GPa, there is no feasible solution for both functions, as shown in Figure 4.9f.

Further analysis was conducted to show the effect of various levels of the I-zod impact (constant) on the cost as shown in Figure 4.10. Figure 4.10 shows the corresponding effect where flexural modulus, is 10 GPa. It can be clearly observed that increasing I-zod impact leads to a reduction in the cost and the profiles are identical with those of minimizing the cost function as clearly illustrated through graphs (a) to (e), while graph (f) has I-zod impact of 240 J/m, which is unachievable.

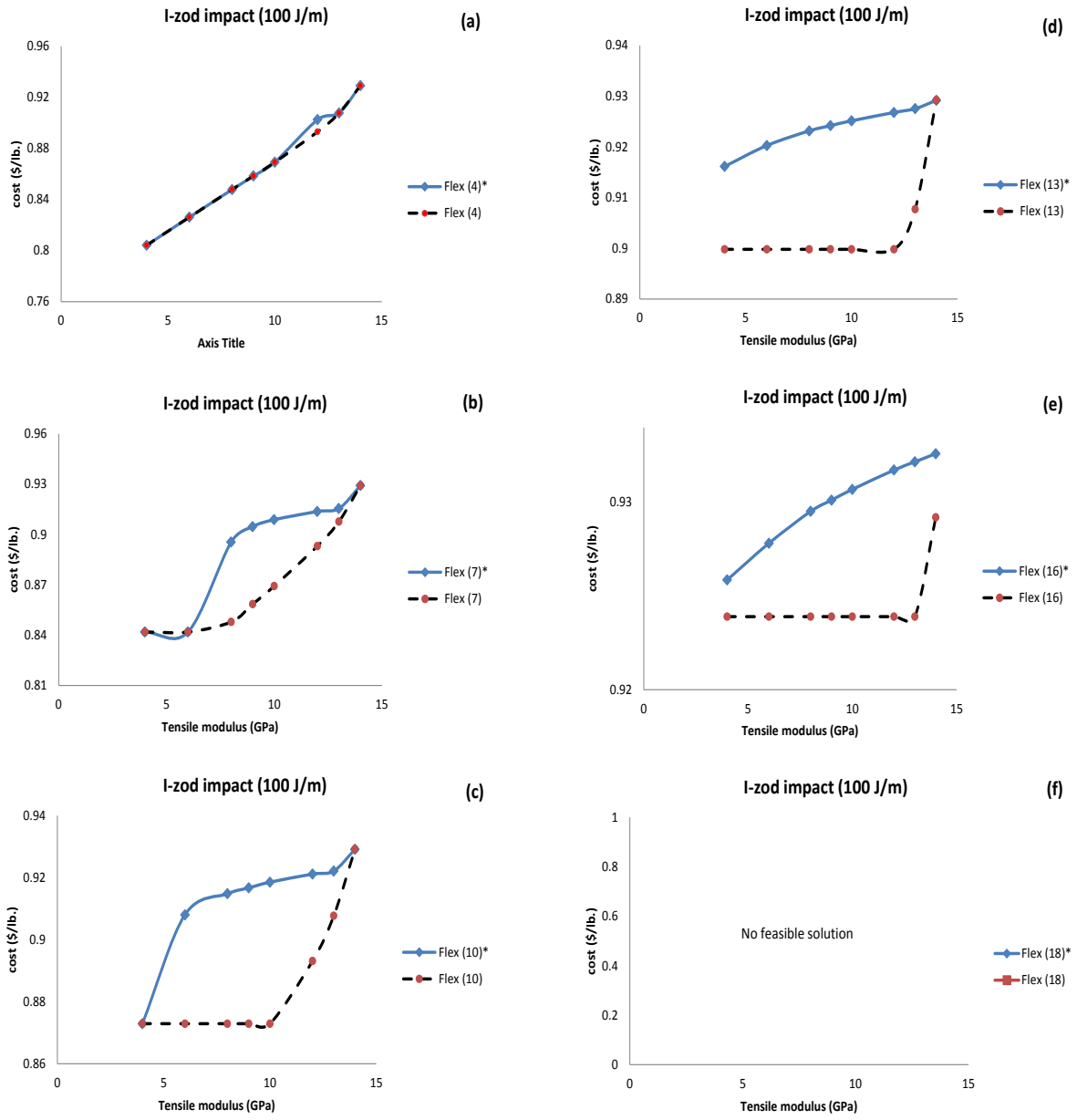

Figure 4.9: The result of comparing the cost of variance and cost function versus the tensile modulus at constant value of I-zod impact. (a) flexural modulus 4 GPa, (b) flexural modulus 7 GPa, (c) flexural modulus 10 GPa, (d) flexural modulus 13 GPa, (e) flexural modulus 16 GPa, and (f) flexural modulus 18 GPa.

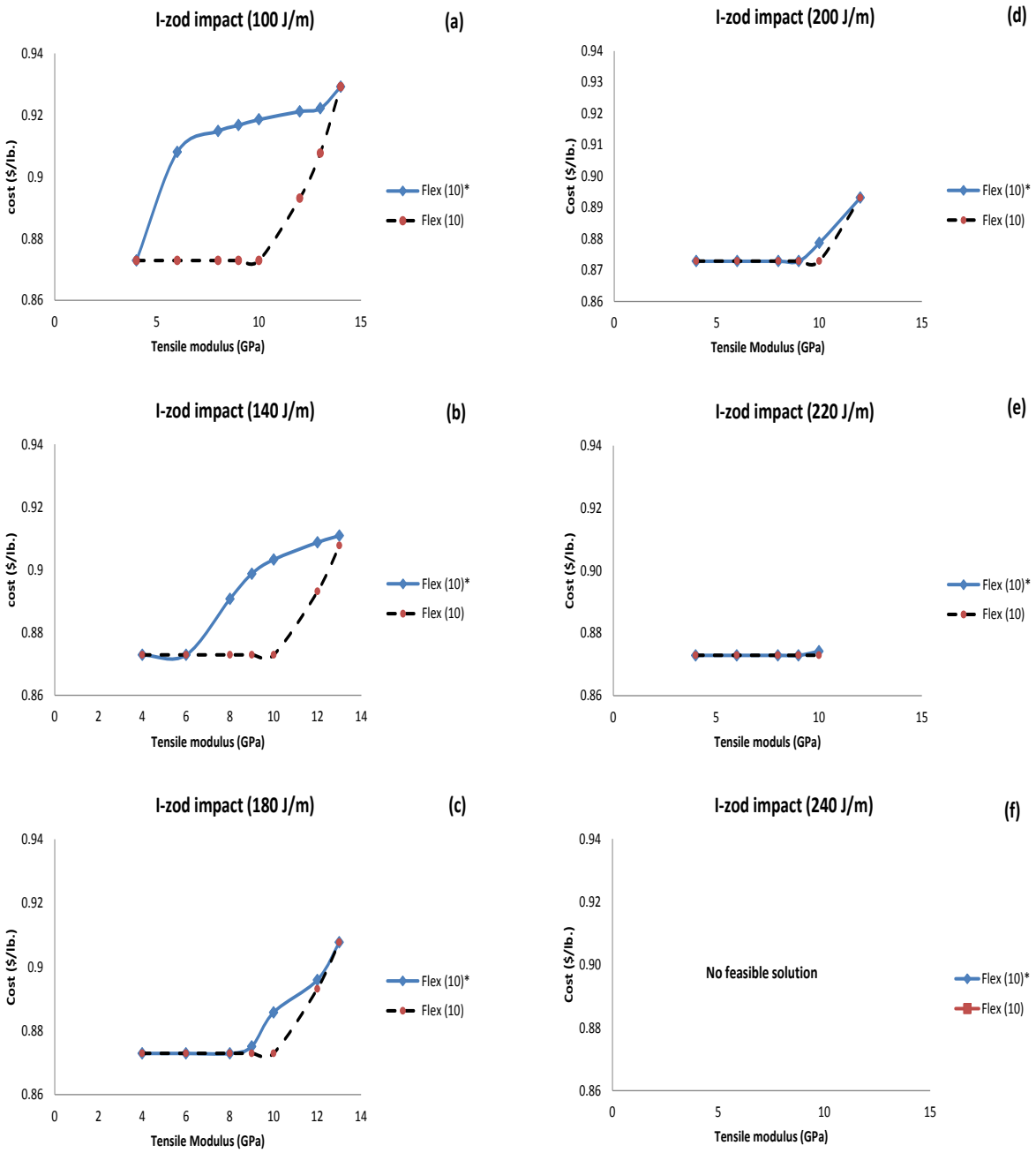

Figure 4.10: The result of comparing the cost of variance and cost function versus tensile modulus at variance amount of I-zod impact, while the flexural modulus (which symbolized as flex.) equals 10 GPa in all cases. (a) I-zod impact 100 J/m, (b) I-zod impact 140 J/m, (c) I-zod impact 180 J/m, (d) I-zod impact 200 J/m, (e) I-zod impact 220 J/m, and (f) I-zod impact 240 J/m.

In other conditions, the tensile modulus is kept constant while the I-zod impact and flexural modulus are varied. It has been observed that the cost obtained from the variance function remains identical with that obtained from cost function at low values of tensile modulus as a constant, such as 4 GPa. The exception is when the I-zod impact is equal to 100 J/m and the flexural modulus is about 13 GPa; then, the cost of the variance function is slightly higher than the cost of the cost function, as shown in Figure 4.11a.

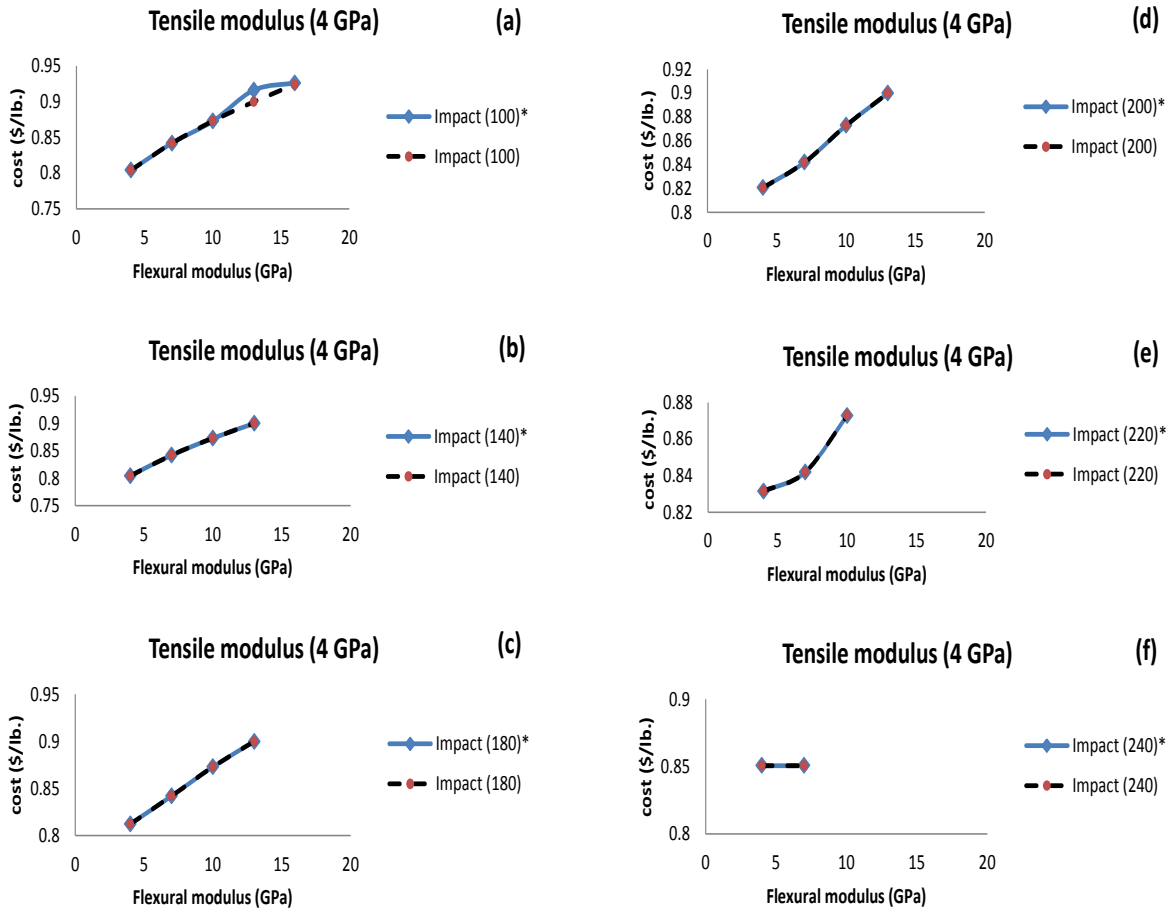

Figure 4.11: The result of comparing the cost of variance and cost function versus the flexural modulus at constant value of tensile modulus 4 GPa. (a) I-zod impact 100 J/m, (b) I-zod impact 140 J/m, (c) I-zod impact 180 J/m, (d) I-zod impact 200 J/m, (e) I-zod impact 220 J/m, and (f) I-zod impact 240 J/m.

Increasing the tensile modulus leads to an increase in the cost for the variance function, causing it to be higher than the cost of minimizing the cost function, where the difference between those becomes significant with lower values of I-zod impact, thereby increasing the value of flexural modulus as seen in Figure 4.12a, b, c, d, and e, while in f the cost remains identical for both functions. The difference in the cost between the two functions at very high values of tensile modulus, such as 13 and 14 GPa reduced especially with high level of I-zod impact as well as the number of combinations. Also, the difference appears at high values of flexural modulus, while at lower values these appear identical with the cost function, as clearly shown in Figure 4.13 and Figure 4.14.

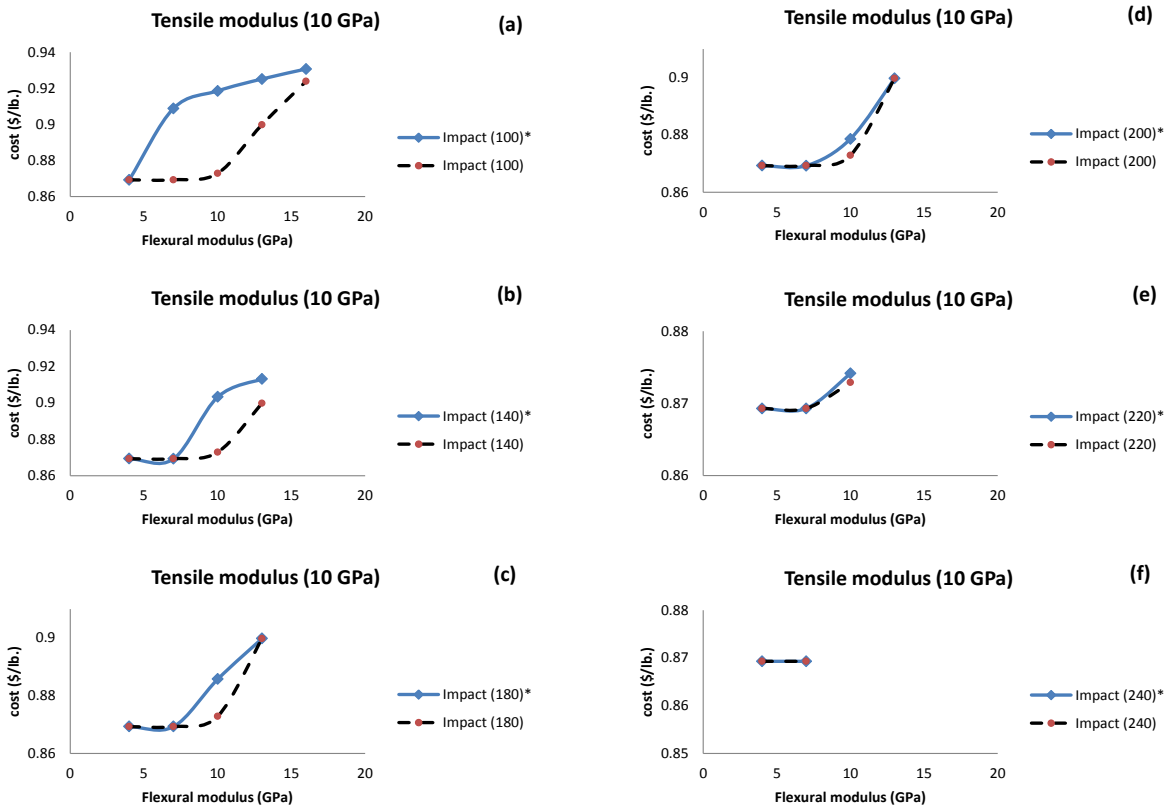

Figure 4.12: The result of comparing the variance and cost function versus the flexural modulus at constant value of tensile modulus 10 GPa. (a) I-zod impact 100 J/m, (b) I-zod impact 140 J/m, (c) I-zod impact 180 J/m, (d) I-zod impact 200 J/m, (e) I-zod impact 220 J/m, and (f) I-zod impact 240 J/m.

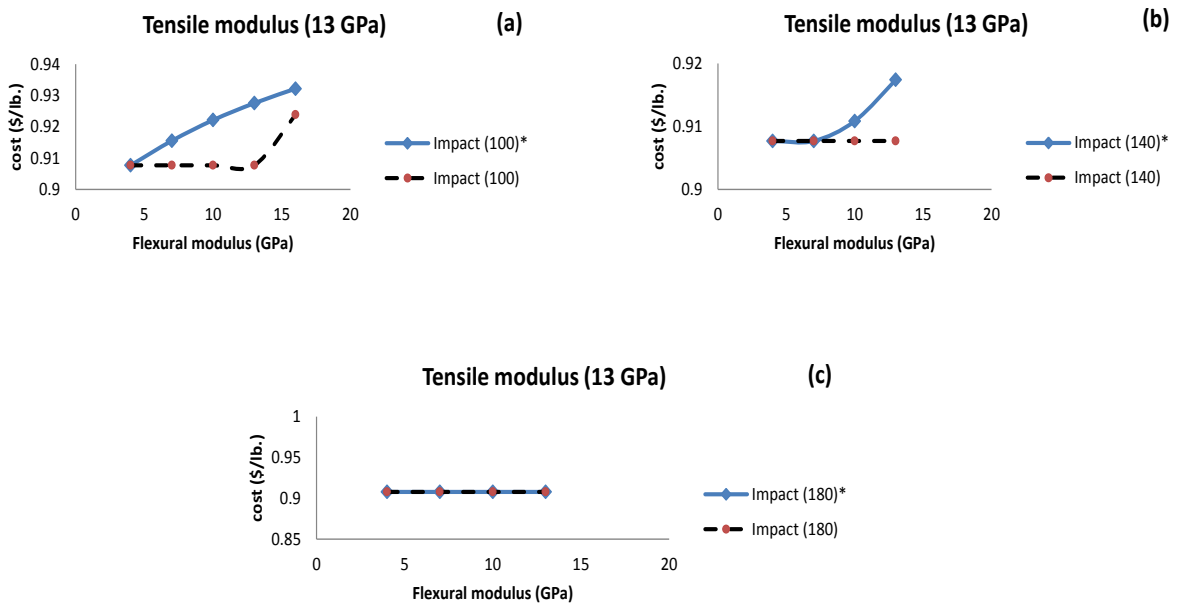

Figure 4.13: The result of comparing the variance and cost function versus the flexural modulus at constant value of tensile modulus 13 GPa. (a) I-zod impact 100 J/m, (b) I-zod impact 140 J/m, and (c) I-zod impact 180 J/m.

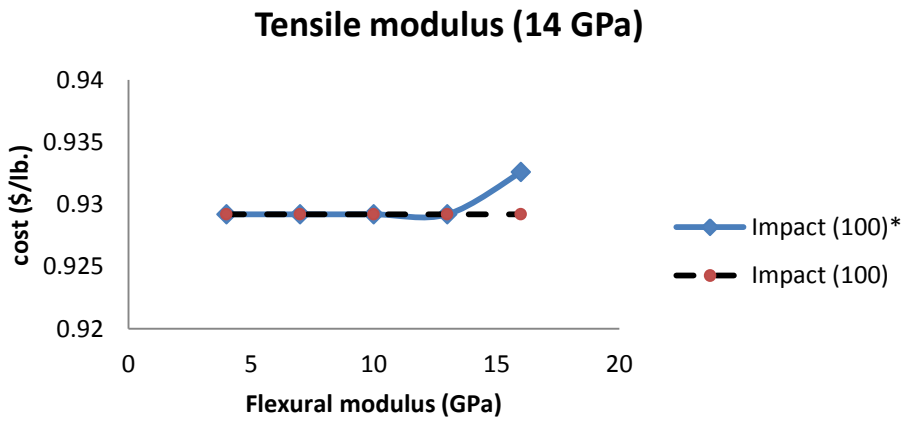

Figure 4.14: The result of comparing the variance and cost function versus the flexural modulus at constant value of tensile modulus 14 GPa.

From the results obtained by minimizing the variance function, it can be concluded that increasing both tensile modulus and flexural modulus causes an increase in the cost. At the same time, the difference in the cost increases for the variance function and the cost function; however, the I-zod impact reduces the disparity in cost between the two functions when it is increased and the cost of the composite becomes constant in both the cost and the variance functions. Moreover, combining high values of the three properties is unachievable. Additionally, the rest of the results with all other conditions can be seen in Appendix B.

4.3.2 Case (2) PP-OMMT

A similar function was used to minimize the variance between the desired properties where the conditions that were applied in case (1) for this composite were the same. The conditions were in terms of desired properties (requirements) and within a particular range of tensile modulus and permeation.

Table 4.2 and Table 4.3 represent the variances of tensile modulus values and permeation, respectively obtained from the simulation results. The results can be interpreted as follows: if the results of the variance are equal to or greater than zero (positive value), it means these combinations of desired properties are achievable; however, it cannot be achievable with negative values. The reason is that a negative value means that the requirement has violated the desired property value. Moreover, the requirements for both tensile modulus and permeation must be satisfied for any combination. For example, if we try combining 80 $cm^3 \cdot \mu m/m^2 \cdot d \cdot mmHg$ of permeation and 2,000 MPa of tensile modulus to form a composite of these properties, a variance value of tensile modulus at permeation of 80 $cm^3 \cdot \mu m/m^2 \cdot d \cdot mmHg$ was obtained in Table 4.2 and was equal to (+26.8). In Table 4.3, however, the variance of permeation at 2,000 MPa of tensile modulus was also obtained and was equal to (-3.5). As a result, these properties cannot be combined because one of them has a negative value, which basically mean that one of the requirements was violated.

Table 4.2: The results of the variance between the predicted and desired values of tensile modulus.

Desired value of tensile modulus	ΔTM at Permeation (cm^3·µm/m^2·d·mmHg)							
	57	**60**	**65**	**70**	**75**	**80**	**85**	**89**
1550	263.3	237.1	193.3	149.5	105.7	61.9	18.1	-9.7
1600	221.1	194.8	151.1	107.3	63.5	19.7	0	-33.5
1700	135.6	110.4	66.6	22.8	0	0	-28.8	-78.4
1790	46.8	34.4	0	0	0	-2.9	-63.1	-114.4
1880	13	0	0	0	0	-26.5	-88.9	-143.4
1955	0	0	0	0	0	-27.5	-94.7	-156.8
2000	0	0	0	0	12	26.8	26.8	26.8
2050	0	0	0	0	-9.7	-23.2	-23.2	-23.2
2080	0	0	0	0	-36.4	-53.2	-53.2	-53.2
2100	0	0	0	-16.4	-54.2	-73.2	-73.2	-73.2
2150	0	0	-23.2	-60.9	-98.7	-123.2	-123.2	-123.2

Table 4.3: The results of the variance between the predicted and desired values of permeation.

Desired value of Permeation	ΔP at Tensile modulus (MPa)										
	1550	**1600**	**1700**	**1790**	**1880**	**1955**	**2000**	**2050**	**2080**	**2100**	**2150**
57	4.7	3.9	2.5	2.5	0.8	0	0	0	0	0	0
60	4.2	3.5	2	0.6	0	0	0	0	0	0	0
65	3.4	2.7	1.2	0	0	0	0	0	0	0	-0.3
70	2.7	1.9	0.4	0	0	0	0	0	0	-0.2	-0.9
75	1.9	1.1	0	0	0	0	0	-0.1	-0.5	-0.8	-1.4
80	1.1	0.04	0	-0.2	-1.9	-3.4	-3.5	-3.5	-3.5	-3.5	-3.5
85	0.3	0	-1.4	-3.3	-5.3	-7.1	-8.5	-8.5	-8.5	-8.5	-8.5
89	-0.4	-1.5	-3.6	-5.5	-7.6	-9.5	-12.5	-12.5	-12.5	-12.5	-12.5

The results of the cost were plotted as a function of tensile modulus at various amounts of permeation, as shown in Figure 4.15. These results show that increasing the permeation decreases the cost, whereas raising the tensile modulus value leads to gradually increasing the cost; however, this increase in the cost starts to shift toward a drop when the tensile modulus is high and the permeation is low, such as a permeation of about 57cm^3·µm/m^2·d·mmHg. Moreover, it is observed that each time the permeation is increased, the shifting point in the cost occurs earlier than in the previous one.

For example, when the permeation is 57cm^3·µm/m^2·d·mmHg, the dropped point in the cost starts from 1,880 MPa of tensile modulus. While it starts to drop from 1600 MPa of tensile modulus when the permeation is 80 cm^3·µm/m^2·d·mmHg, as shown in Figure 4.15. Another observation is that combining desired properties at high levels or values for both tensile modulus and permeation cannot be accomplished.

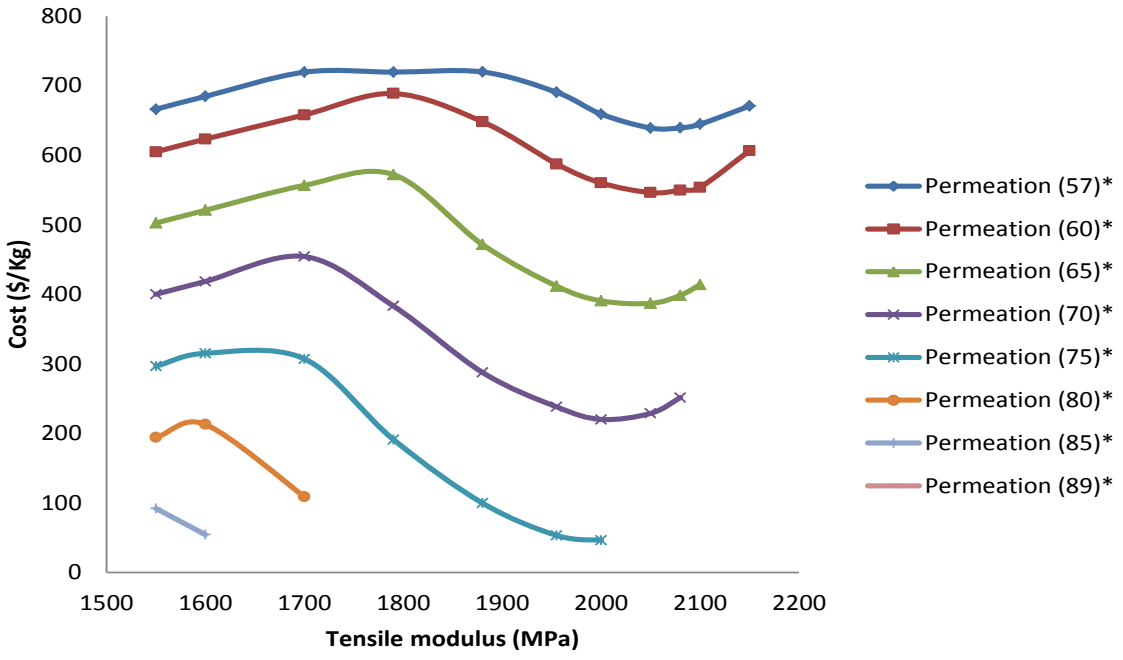

Figure 4.15: The result of the cost versus tensile modulus at different values of permeation.

The results in Figure 4.16 shows the comparison in the composite cost between the variance function and the cost function as a function of tensile modulus for different levels of permeation. A significant difference in the cost between the two functions is observed in Figure 4.16a where the cost obtained from the variance function is very high, especially for low values of tensile modulus. Nonetheless, the dramatic increase in the composite cost from the cost function that starts from 2,000 MPa of tensile modulus reduces the variance in the cost between them. Therefore, the cost from the two objective functions becomes similar. Further, increasing the level of permeation in the variance function gradually reduces the cost of the composite. For instance, for permeation levels of 60, 65, 70, and 75$cm^3 \cdot \mu m/m^2 \cdot d \cdot mmHg$, the composite cost starts at 600, 500, 400, and 300 $ respectively. This behavior is clearly shown in Figure 4.16b, c, d, and e. In the cost function, however, the permeation level has no effect at all on the cost of the composite, as illustrated earlier.

An increase in the permeation has another effect in addition to its effect on the composite cost, which was the reduction of forming a combination of desired properties at high value of tensile modulus, where that is valid for both functions, as shown in graphs (b) to (e) in Figure 4.16. If the permeation is equal to 80 or 85 $cm^3 \cdot \mu m/m^2 \cdot d \cdot mmHg$ in the variance function, a couple of combinations can be achieved at lower values of tensile modulus such as 1550, 1600, and 1700 MPa. Whereas the cost function cannot accomplish any combination at the same permeation levels, as shown in graphs (f) and (g) in Figure 4.16. On the other hand, optimum combination for any value of tensile modulus when the permeation is equal to 89 $cm^3 \cdot \mu m/m^2 \cdot d \cdot mmHg$ was not feasible (see Figure 4.16h).

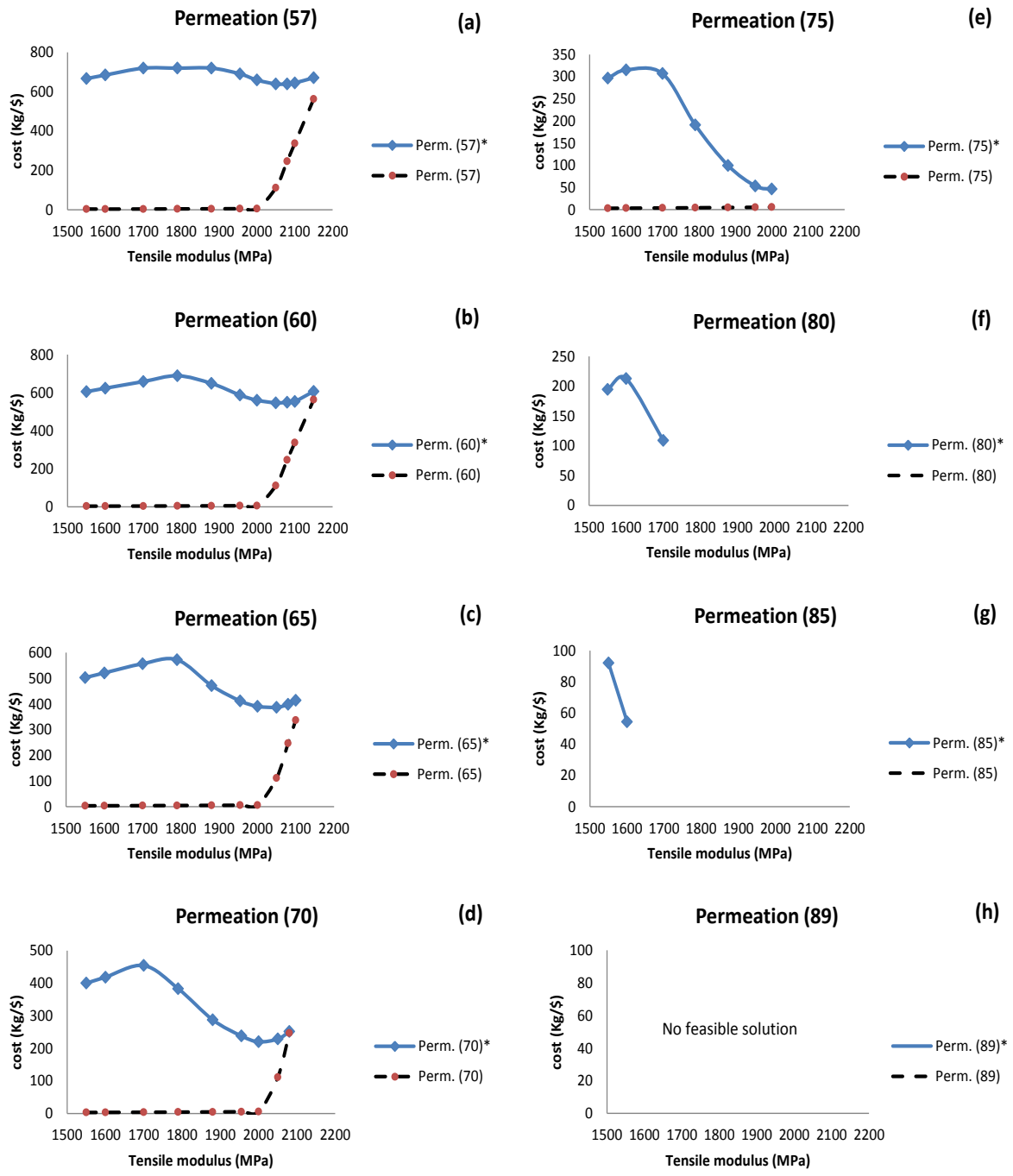

Figure 4.16: comparison of the variance and cost function versus tensile modulus at different levels of permeation. (a) permeation 57, (b) permeation 60, (c) permeation 65, (d) permeation 70, (e) permeation 75, (f) permeation 80, (g) permeation 85, and (h) permeation 89.

The decrease and increase in the composite cost can be justified by examining the components' weight of the composite, which directly influences the cost behavior. Firstly, the effect of tensile modulus and permeation on the behavior of each component will be discussed. It is followed by the explanation on the relationship between the components and cost behavior. As mentioned above, the weight fraction range of the matrix (polypropylene) was between 80 and 100% of the total mixture weight. Figure 4.17 shows the polypropylene weight fraction as a function of tensile modulus at various levels of permeation. The use of polypropylene component increases as the level of permeation increases, while it was gradually reduced with increasing tensile modulus.

For instance, at low values of permeation say, 57 $cm^3 \cdot \mu m/m^2 \cdot d \cdot mmHg$, the weight of polypropylene is about 93.5%, whereas it is equal to 99% when the permeation is around 85 $cm^3 \cdot \mu m/m^2 \cdot d \cdot mmHg$. These results occur when the desired tensile modulus is equal to 1,550 MPa; however, the weight of polypropylene gradually drops as the tensile modulus increases. Moreover, the variance in the polypropylene weight caused by different levels of permeation decreases as the desired tensile modulus increases.

In Figure 4.18, the inorganic weight fraction of different permeation values was plotted as a function of tensile modulus. The inorganic weight fraction ranged from 0 to 11%. It can be observed that the inorganic weight fraction increases linearly with increasing the resired tensile modulus; however, as the permeation increases, higher inorganic weight was achieved at lower tensile modulus. Also, the use of inorganic weight with low tensile modulus values is zero, especially at low levels of permeation.

In the cases where the levels of organic modification component are varied, the results obtained for weight fractions were plotted as a function of tensile modulus for different amounts of permeation as shown in Figure 4.19. The modified organic weight fraction ranged from 0 to 7%. It clearly shows that increasing the permeation leads to decreasing the weight fraction of modified organic.

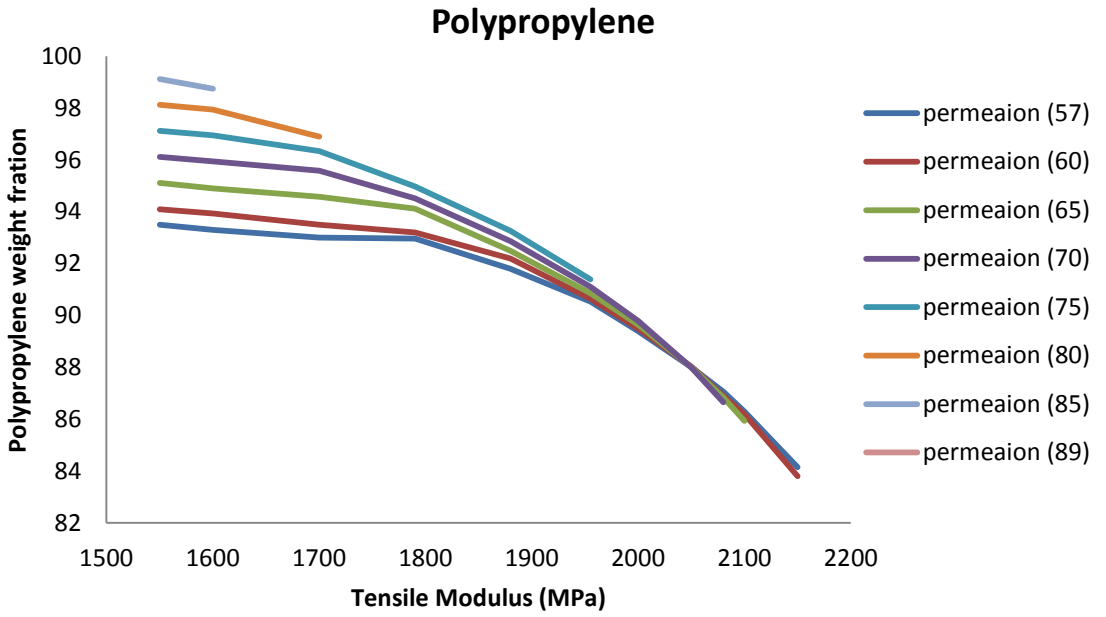

Figure 4.17: The result of plotting the weight fraction of polypropylene versus the tensile modulus for different values of permeation.

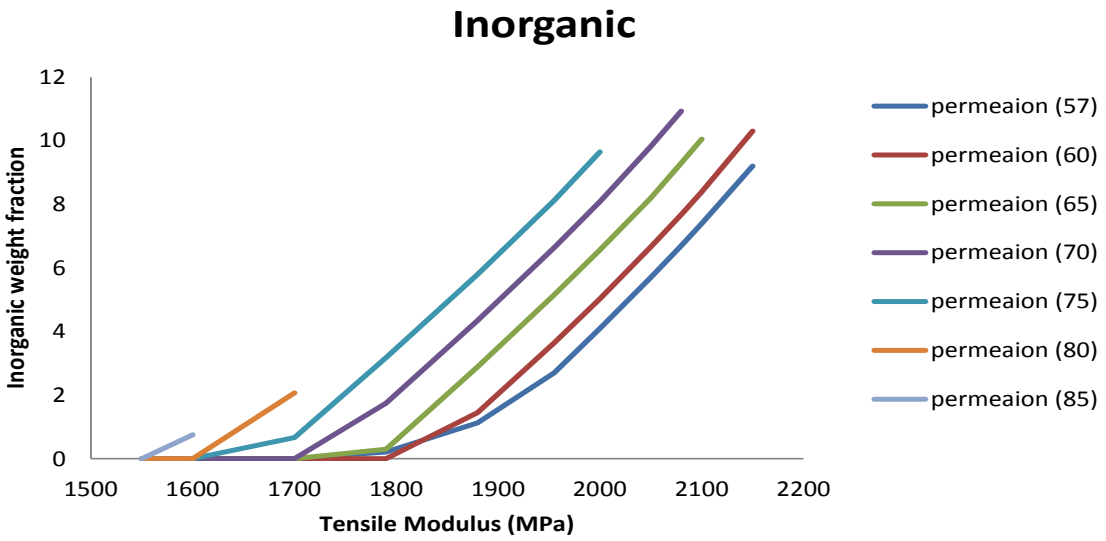

Figure 4.18: The result of plotting the weight fraction of inorganic versus the tensile modulus for different values of permeation.

Also, the weight fraction of modified organic is slightly increased by increasing the tensile modulus at lower and higher levels. In the middle range of the values, however, the weight fraction begins to gradually decrease. This pattern can be seen when the permeation equals to 57, 60, 65, and 70 but not with 75, 80, and 85 due to the limitation of forming combinations at high values of both tensile modulus and permeation.

Further it is important to know the effect of weight fraction of the component on the cost. As shown, in Figure 4.15, the composite cost follows almost the same pattern for different levels of permeation when the tensile modulus is increased, which is exactly the case with the variation in the weight fraction of modified organic as a function of tensile modulus for various levels of permeation.

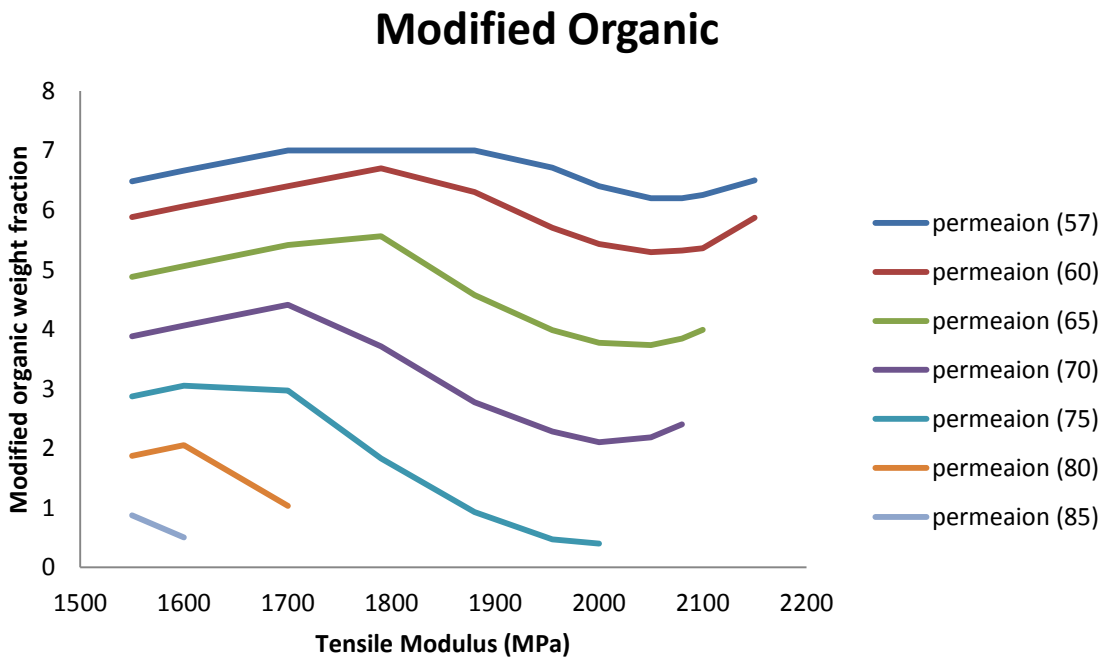

Figure 4.19: The result of plotting the weight fraction of organic modification versus the tensile modulus for different values of permeation.

The use of modified organic component causes a slight increase in the cost at lower values of tensile modulus whereas the use of an inorganic component does not. When an inorganic is used, however, the cost begins to decrease slightly as well as the weight of the modified organic component. Also, it is observed that there is a slight increase in the cost at higher tensile modulus values, due to an increase in the use of modified organic weight. The reason for the higher cost of the composite is due to the fact that the modified organic being expensive than the other components. Similarly, the effect of weight fraction of polypropylene is very minor (as it is cheaper compared to other components), both on the cost and on the properties.

Table 4.4: Comparison of the cost and the weight fraction between the cost function and variance at the same desired properties.

Function applied	Tensile modulus (MPa)	Permeation ($cm^3 \cdot \mu m/m^2 \cdot d \cdot mmHg$)	Weight fraction			Cost ($/Kg)
			PP	Inorganic	Organic	
Cost	1600	60	98.9	1.09	0	3.29
Variance	1600	60	93.9	0	6.06	623.24

Furthermore, the effect of modified organic component shown in Figure 4.16, where the results of the cost for the two functions were compared. The cost that resulted from the cost function was very low at low tensile modulus compared with the cost that resulted from the variance function at the same conditions. The most important element of the cost function was to minimize the cost of composite as much as possible. Consequently, the function tried to avoid using the cost of modified organic component in order to obtain the minimum cost. In case of the variance function, the cost was not that significant; however, minimizing the variances between the desired properties was the optimal goal. Therefore, the modified organic component was used irrespective of the cost. For example, the cost and the weight of

each component at the same combination were compared, as shown in Table 4.4. The two functions were set to form a combination of desired properties of the tensile modulus and the permeation to be 1600MPa and 60$cm^3 \cdot \mu m/m^2 \cdot d \cdot mmHg$, respectively. The cost of the composite was significantly different where the cost of variance function was higher than the cost of minimizing the cost function by about 619.96$. Further, it observed that the weight fraction of the components to form the same desired properties were different. As mentioned before, the most significant component that affects the composite cost is the weight fraction of modified organic. Therefore, the weight fraction of modified organic in the cost function was 0% of the total mixture and that what made the cost very low. While in case of variance function was 6.06% of the total mixture which caused the high cost of the composite.

The results thus obtained from the simulations of the second objective function, i.e., the variance function, can serve as a very useful tool for engineers in designing a product that requires high performance and long endurance. Furthermore, the diversity in applications needs demands composites of different specifications, depending on the type of application used. Hence, this technique would save time for designers as an alternative compared to the traditional method that depends on experiments.

Chapter 5
Conclusions

Designing products with desired properties by using inverse modeling is very advantageous in terms of saving time in comparison to the conducting of experiments, which is very time-consuming. Furthermore, it can be used directly to build a controller where the input variables are included in the model. These input variables can be treated as desired properties, and the output variables is the action of it. Therefore, when a new requirement is requested, the controller can ask the model to predict the action needed. The important thing in this process is how reliable the model is when predicting new data.

In this work, nonlinear regression models were conducted and analyzed to assess the accuracy of the predictions. These models were constructed in terms of mechanical properties of the LGFPP composite, which represented the first case study. The properties that have investigated were the tensile modulus, flexural modulus, and notched I-zod impact. The properties of PP-OMMT nanocomposite, which represented the second case study, were the tensile modulus and permeation. Moreover, the regression models that express the tensile modulus and the permeation were obtained from the literature review.

A simulation was performed on both cases for different objective functions, and MATLAB software was used to run the simulations. According to the result of minimizing the cost of LGFPP, there was a positive relationship between the composite cost and the weight of glass fiber. In addition, the trade-off principle was applied in terms of characterizing the mechanical properties. In case of finding the minimum cost of PP-OMMT nanocomposite, the weight of modified organic was the most significant component influencing the composite cost.

The variance between the desired properties was minimized to form the best combination of the composite, while the cost was secondary. There was a difference in the cost when the two functions of the LGFPP composite were compared, that, the variance function has given a higher cost because the tensile modulus and flexural modulus were the major reasons of increasing the cost, while the effect of increasing the level of notched I-zod impact was in the opposite direction, which resulted in lowering the cost.

In the case of PP-OMMT, the cost that resulted from the variance function was significantly higher than that resulting from the cost function. The reason for that was the use of modified organic component from the beginning at low values of the tensile modulus. In the cost function, though, the use of a modified organic component was avoided at low values where began used at high values of tensile modulus. Therefore, the cost of the two functions became much closer to each other at high levels of tensile modulus. Besides, the cost was not affected by any level of permeation in the cost function, while increasing the permeation in the variance function caused a reduction in the cost.

The simulation of the variance function can be useful in designing a product where the quality is the most significant (irrespective of the composite cost).

Appendix A

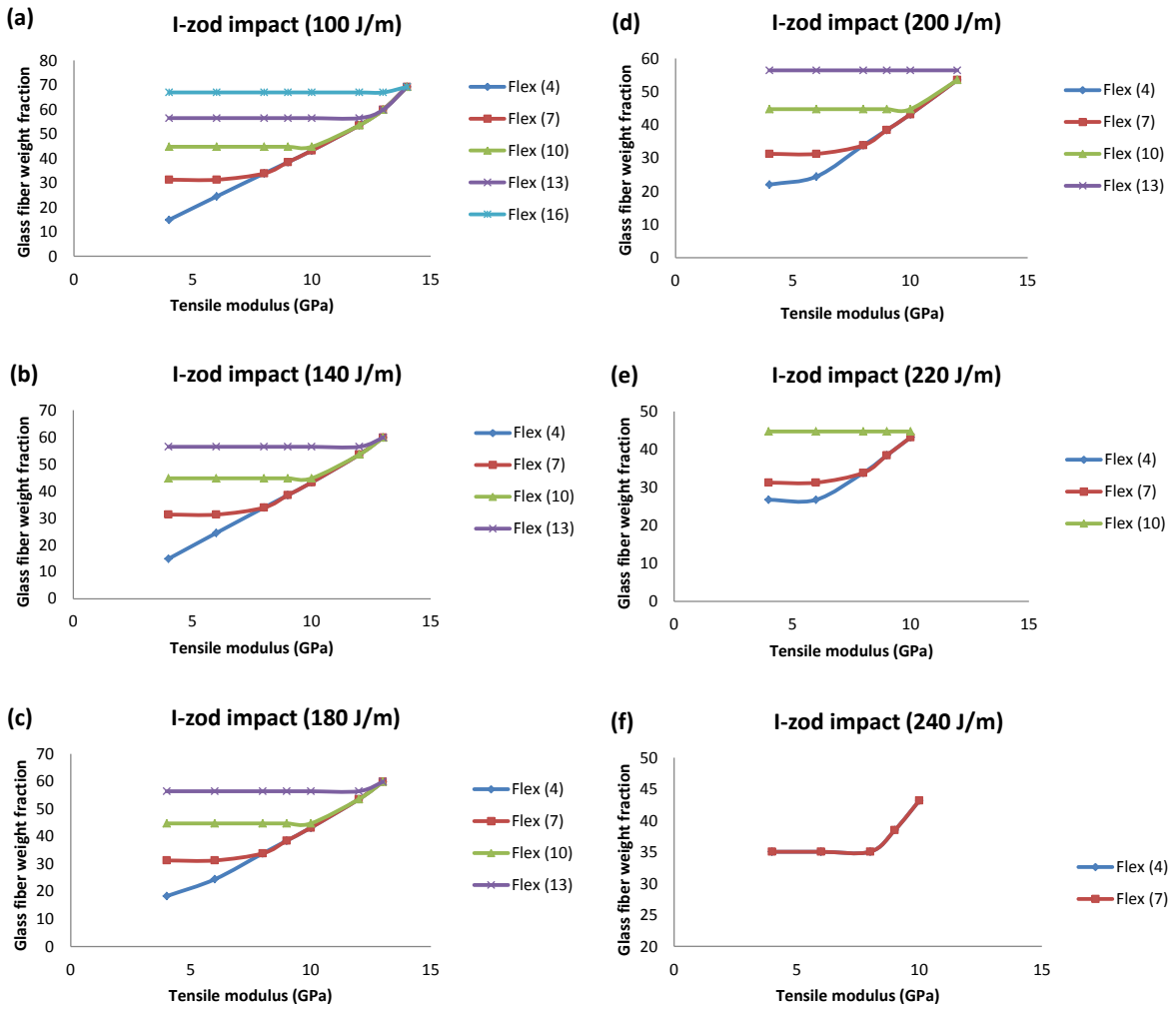

Figure A.1: Result of weight fraction of glass fiber versus the tensile modulus at different values of flexural modulus, while the notched I-zod impact was held constant. (a) I-zod impact 100 J/m, (b) I-zod impact 140 J/m, (c) I-zod impact 180 J/m, (d) I-zod impact 200 J/m, (e) I-zod impact 220 J/m, and (f) I-zod impact 240 J/m.

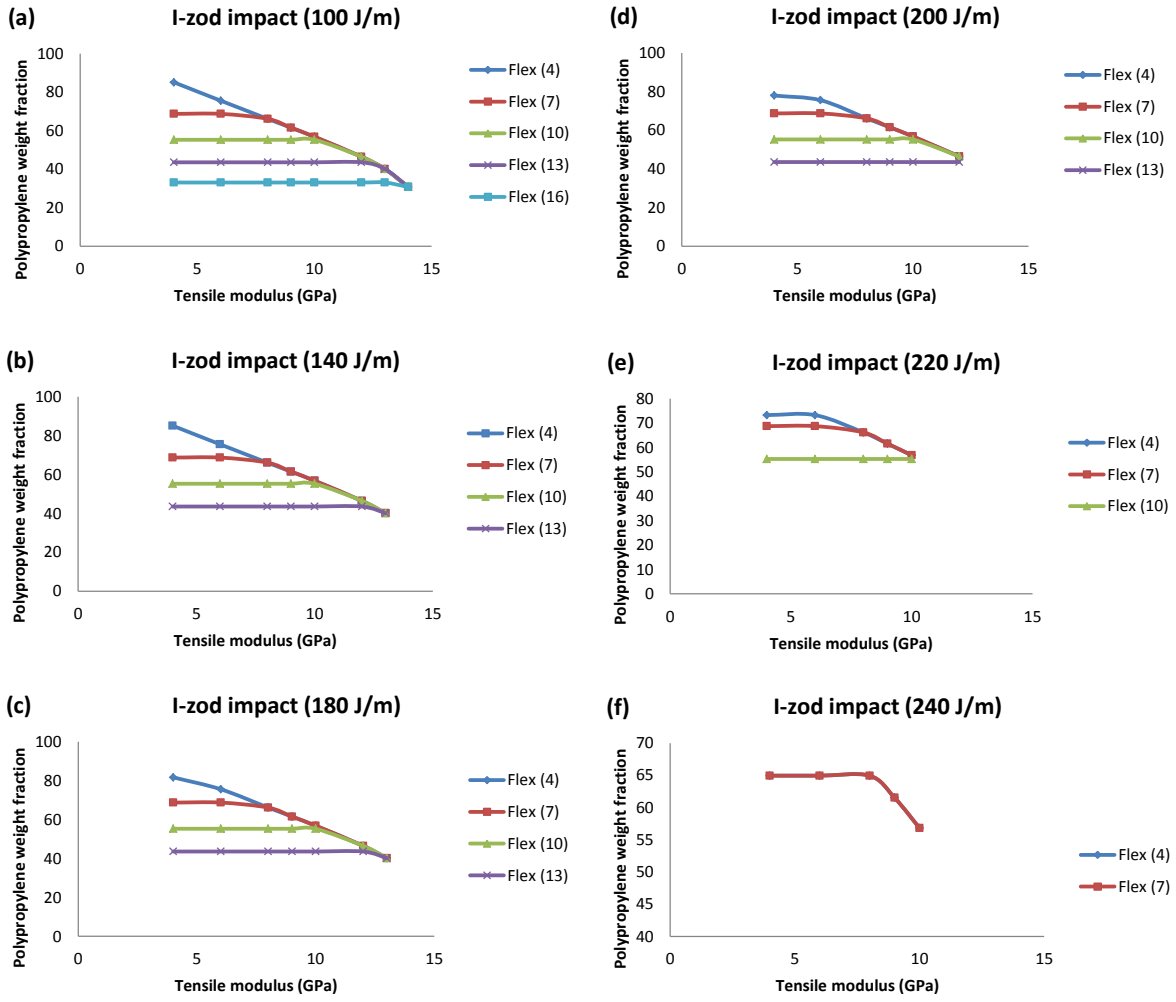

Figure A.2: Result of weight fraction of polypropylene versus the tensile modulus at different values of flexural modulus, while the notched I-zod impact was held constant. (a) I-zod impact 100 J/m, (b) I-zod impact 140 J/m, (c) I-zod impact 180 J/m, (d) I-zod impact 200 J/m, (e) I-zod impact 220 J/m, and (f) I-zod impact 240 J/m.

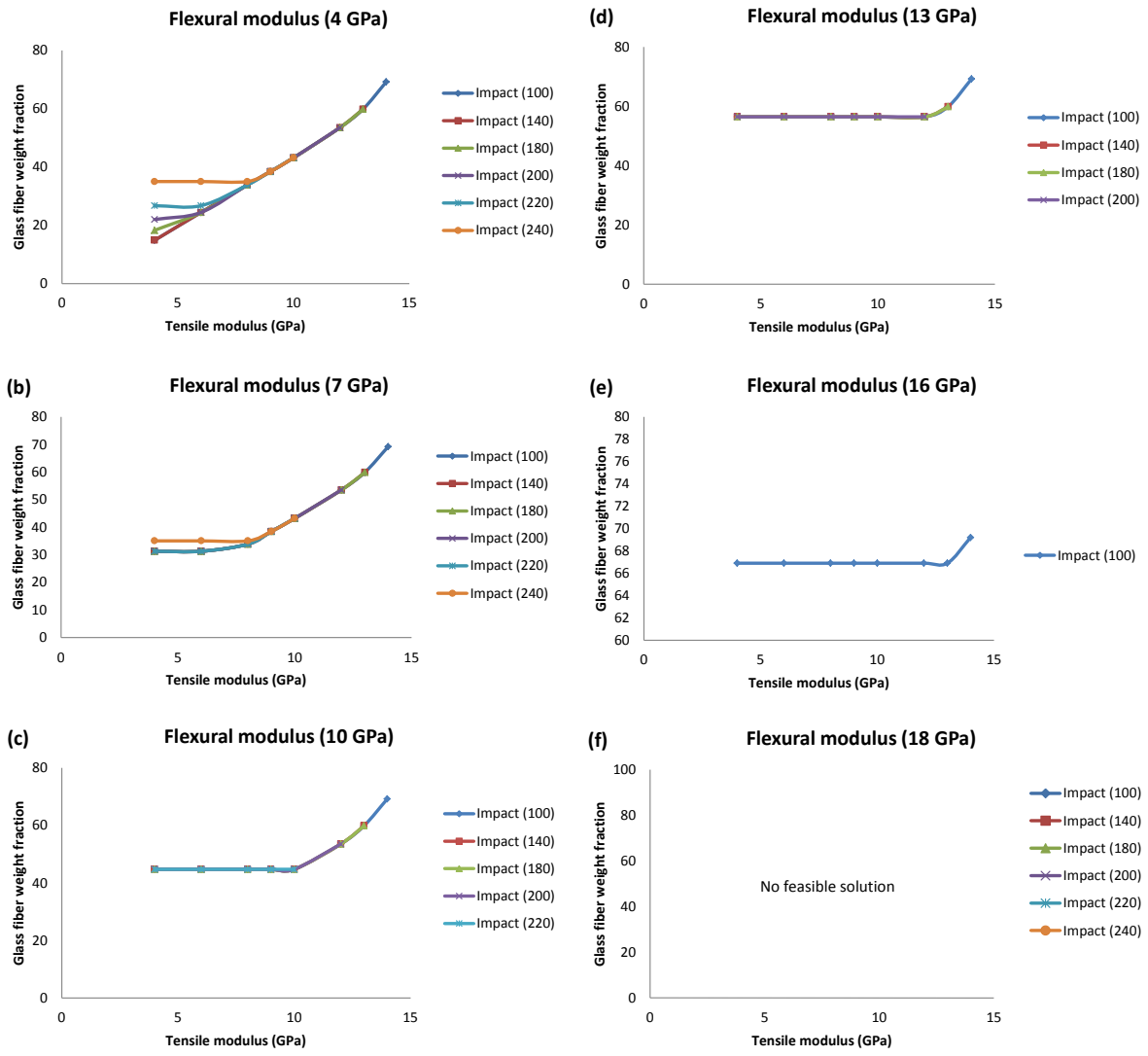

Figure A.3: Result of weight fraction of glass fiber versus the tensile modulus at different values of notched I-zod impact, while the flexural modulus was held constant. (a) flexural modulus 4 GPa, (b) flexural modulus 7 GPa, (c) flexural modulus 10 GPa, (d) flexural modulus 13 GPa, (e) flexural modulus 16 GPa, and (f) flexural modulus 18 GPa.

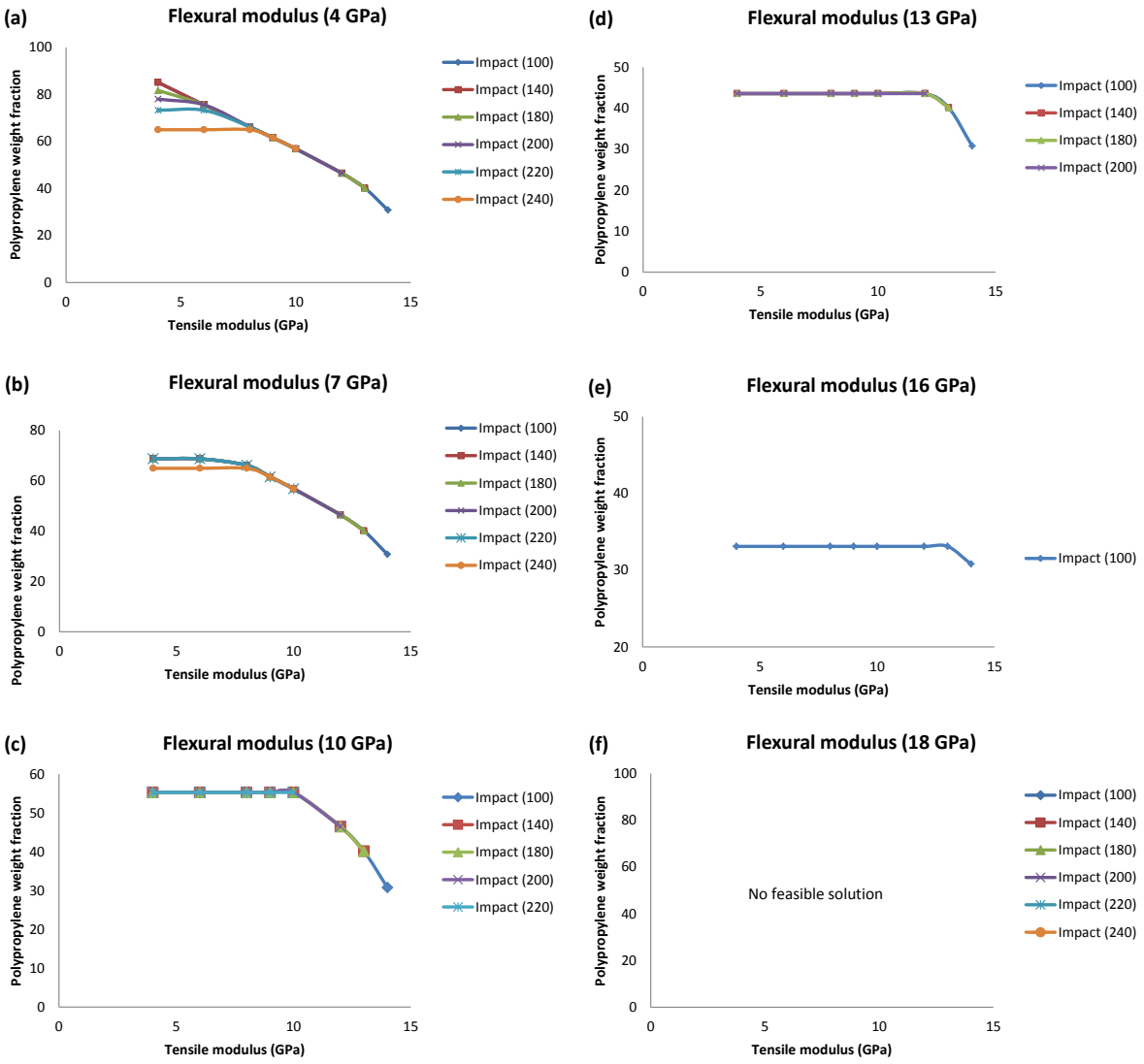

Figure A.4: Result of weight fraction of polypropylene versus the tensile modulus at different values of notched I-zod impact, while the flexural modulus was held constant. (a) flexural modulus 4 GPa, (b) flexural modulus 7 GPa, (c) flexural modulus 10 GPa, (d) flexural modulus 13 GPa, (e) flexural modulus 16 GPa, and (f) flexural modulus 18 GPa.

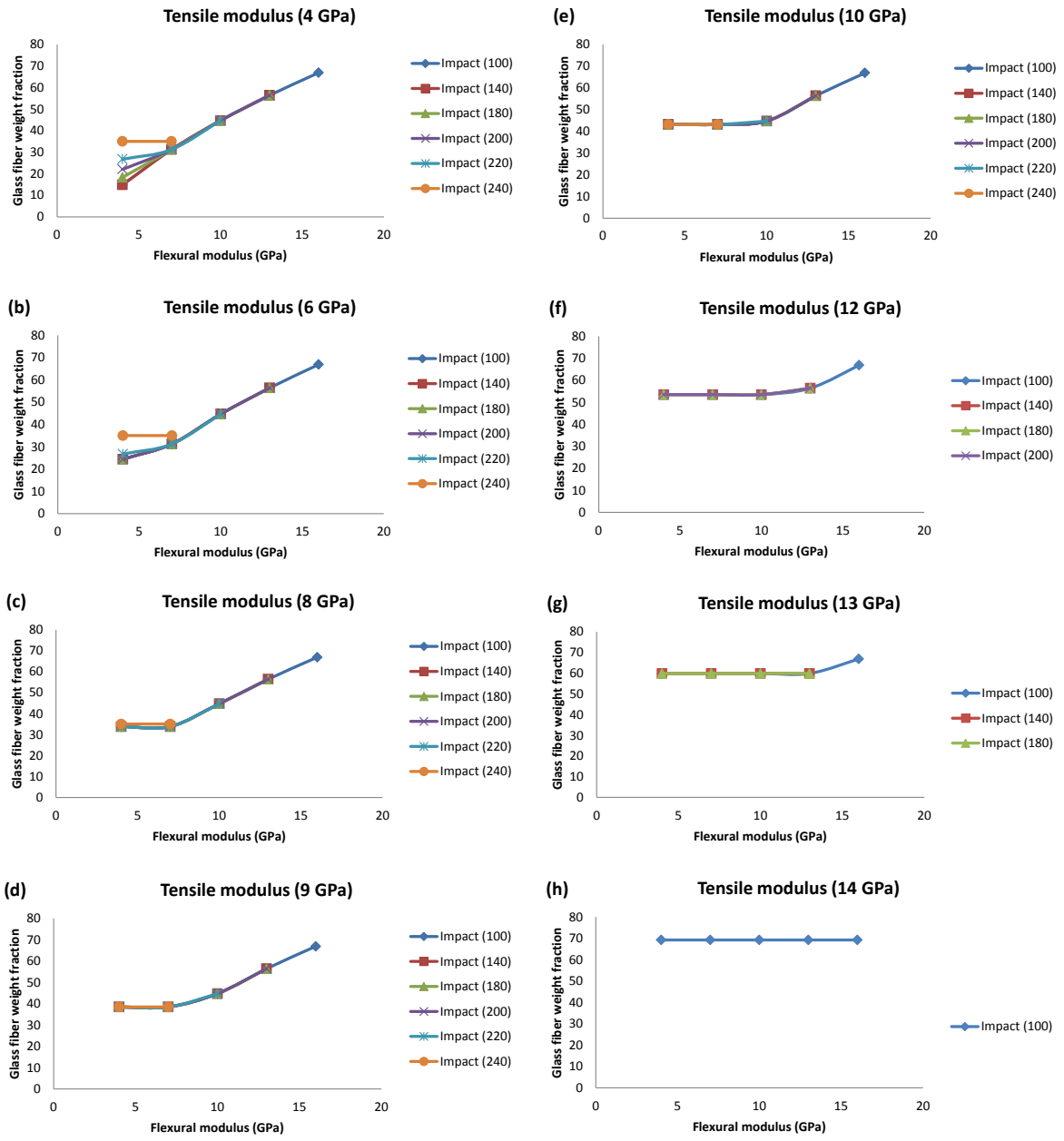

Figure A.5: Result of weight fraction of glass fiber versus the flexural at different values of notched I-zod impact, while the modulus tensile modulus was held constant. (a) tensile modulus 4 GPa, (b) tensile modulus 6 GPa, (c) tensile modulus 8 GPa, (d) tensile modulus 9 GPa, (e) tensile modulus 10 GPa, (f) tensile modulus 12 GPa, (g) tensile modulus 13 GPa, and (h) tensile modulus 14 GPa.

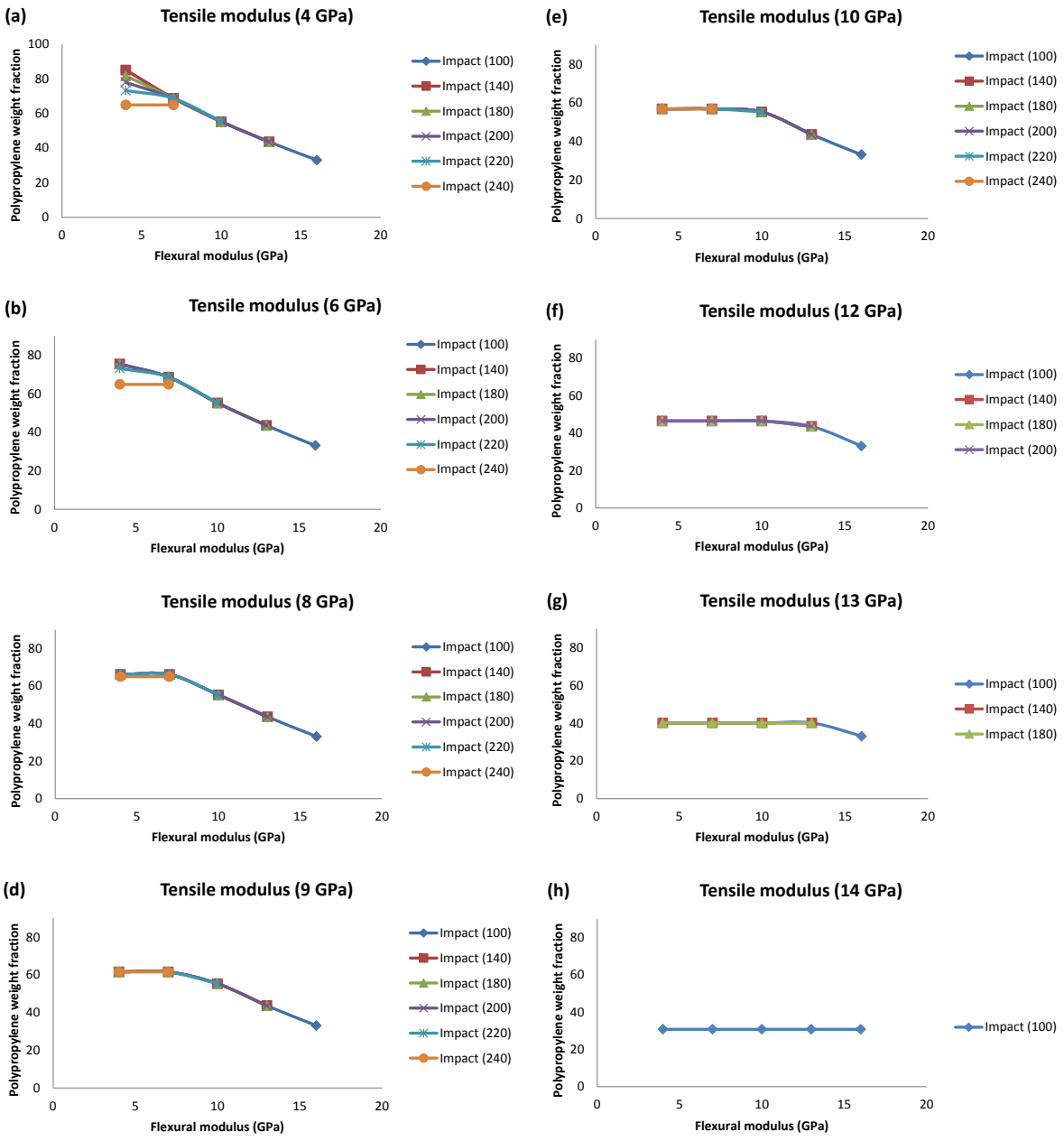

Figure A.6: Result of weight fraction of polypropylene versus the flexural at different values of notched I-zod impact, while the modulus tensile modulus was held constant. (a) tensile modulus 4 GPa, (b) tensile modulus 6 GPa, (c) tensile modulus 8 GPa, (d) tensile modulus 9 GPa, (e) tensile modulus 10 GPa, (f) tensile modulus 12 GPa, (g) tensile modulus 13 GPa, and (h) tensile modulus 14 GPa.

Appendix B

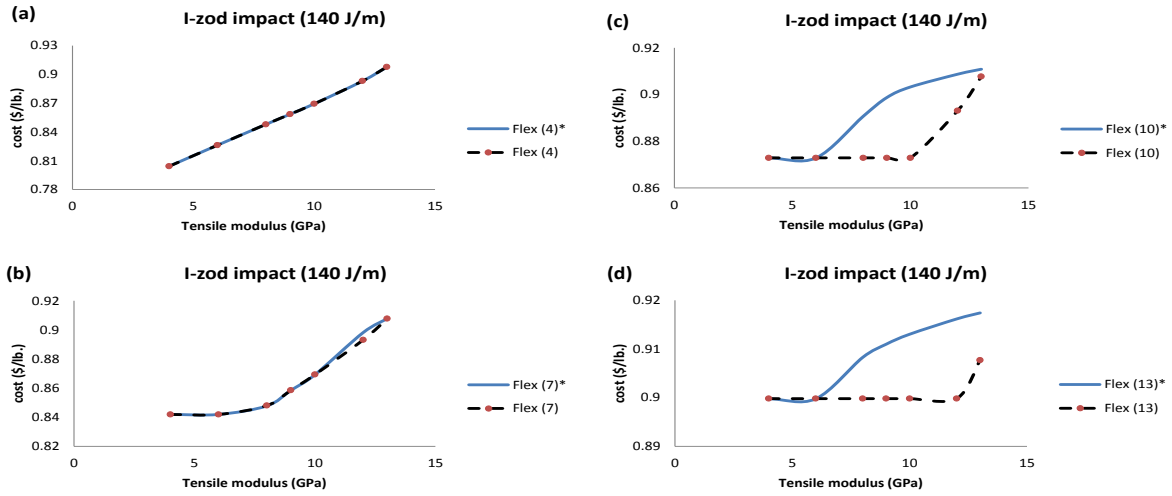

Figure B.1: The result of comparing the variance and cost function versus the tensile modulus at 140 J/m of I-zod impact. (a) flexural modulus 4 GPa, (b) flexural modulus 7 GPa, (c) flexural modulus 10 GPa, (d) flexural modulus 13 GPa.

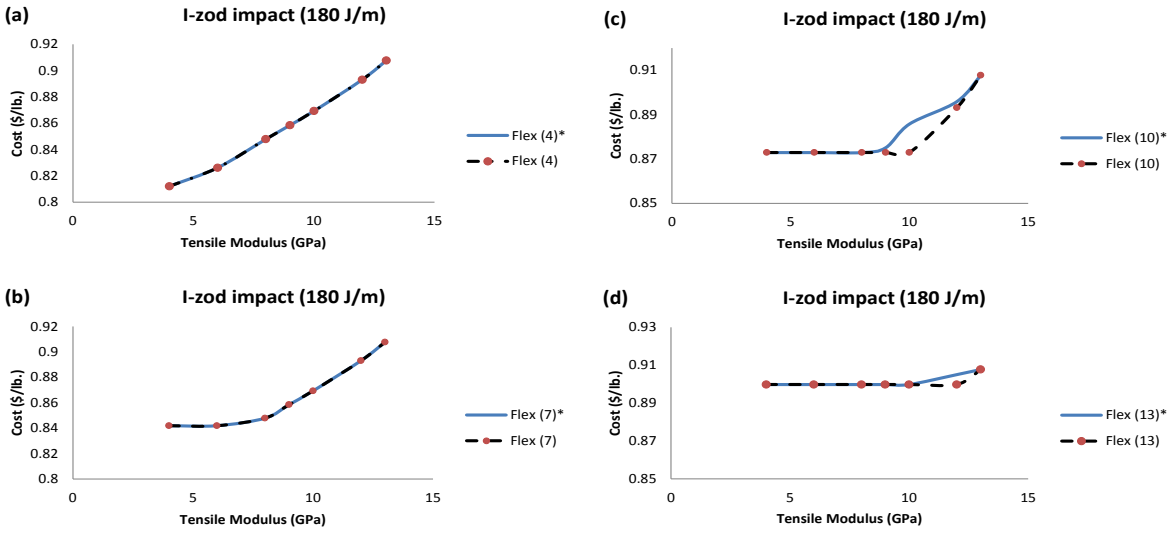

Figure B.2: The result of comparing the variance and cost function versus the tensile modulus at 180 J/m of I-zod impact. (a) flexural modulus 4 GPa, (b) flexural modulus 7 GPa, (c) flexural modulus 10 GPa, (d) flexural modulus 13 GPa.

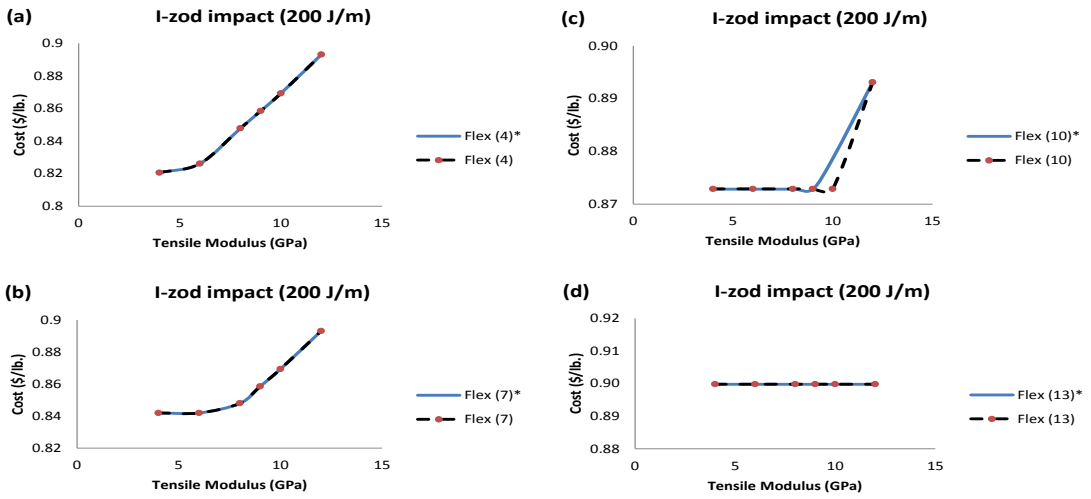

Figure B.3: The result of comparing the variance and cost function versus the tensile modulus at 200 J/m of I-zod impact. (a) flexural modulus 4 GPa, (b) flexural modulus 7 GPa, (c) flexural modulus 10 GPa, (d) flexural modulus 13 GPa.

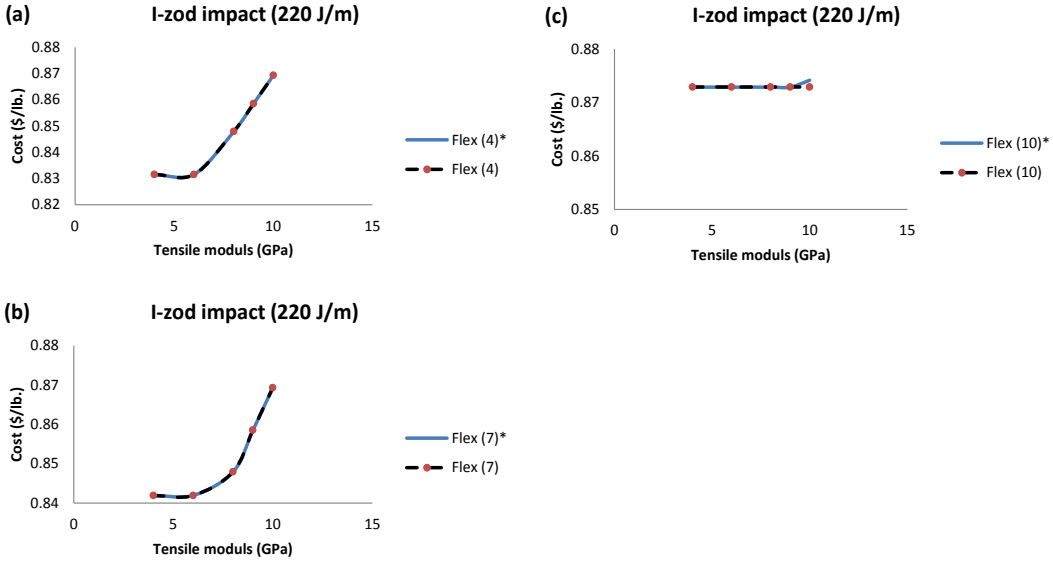

Figure B.4: The result of comparing the variance and cost function versus the tensile modulus at 220 J/m of I-zod impact. (a) flexural modulus 4 GPa, (b) flexural modulus 7 GPa, (c) flexural modulus 10 GPa.

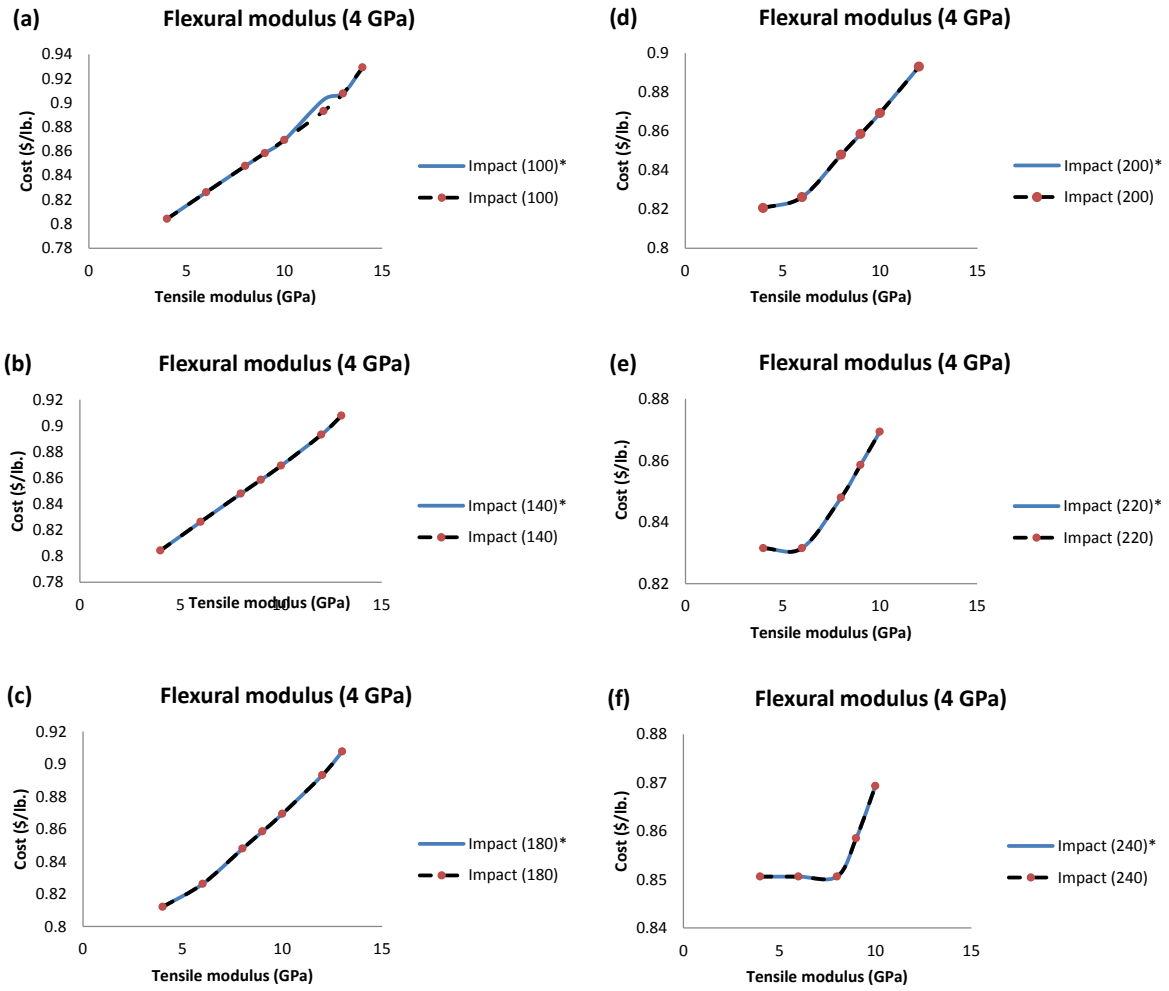

Figure B.5: The result of comparing the variance and cost function versus the tensile modulus at 4 GPa of flexural modulus. (a) I-zod impact 100, (b) I-zod impact 140, (c) I-zod impact 180, (d) I-zod impact 200, (e) I-zod impact 220, (f) I-zod impact 240.

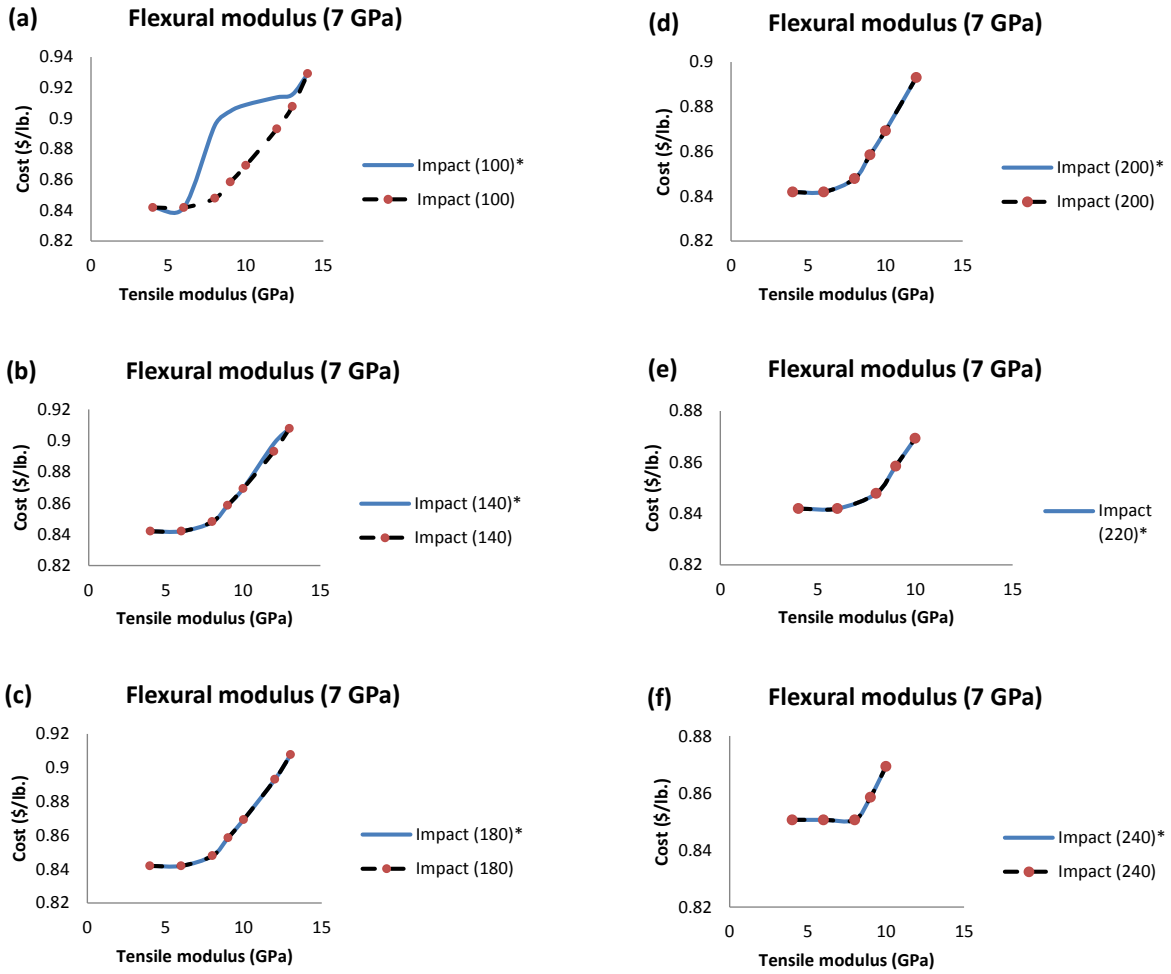

Figure B.6: The result of comparing the variance and cost function versus the tensile modulus at 7 GPa of flexural modulus. (a) I-zod impact 100, (b) I-zod impact 140, (c) I-zod impact 180, (d) I-zod impact 200, (e) I-zod impact 220, (f) I-zod impact 240.

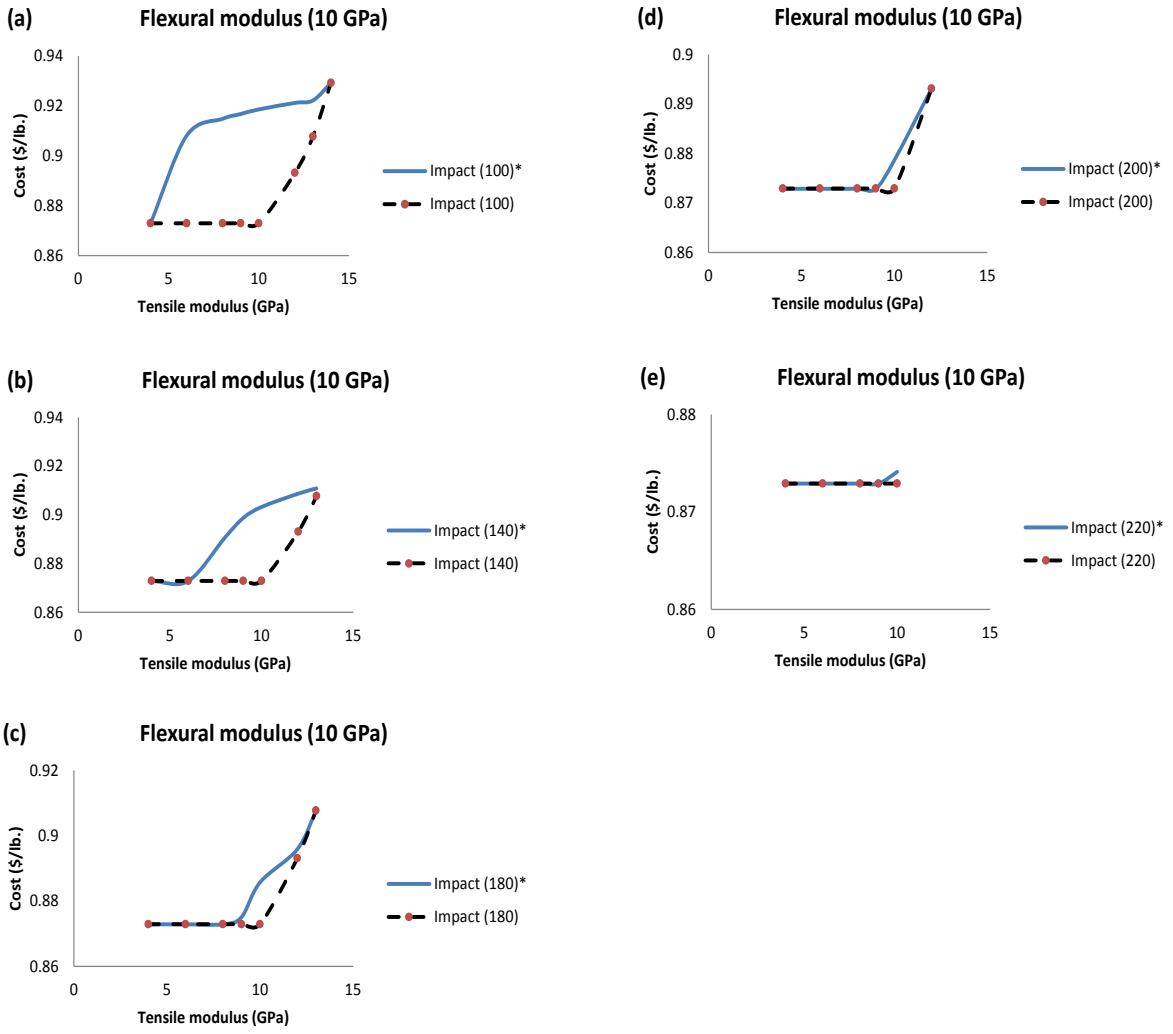

Figure B.7: The result of comparing the variance and cost function versus the tensile modulus at 10 GPa of flexural modulus. (a) I-zod impact 100, (b) I-zod impact 140, (c) I-zod impact 180, (d) I-zod impact 200, (e) I-zod impact 220.

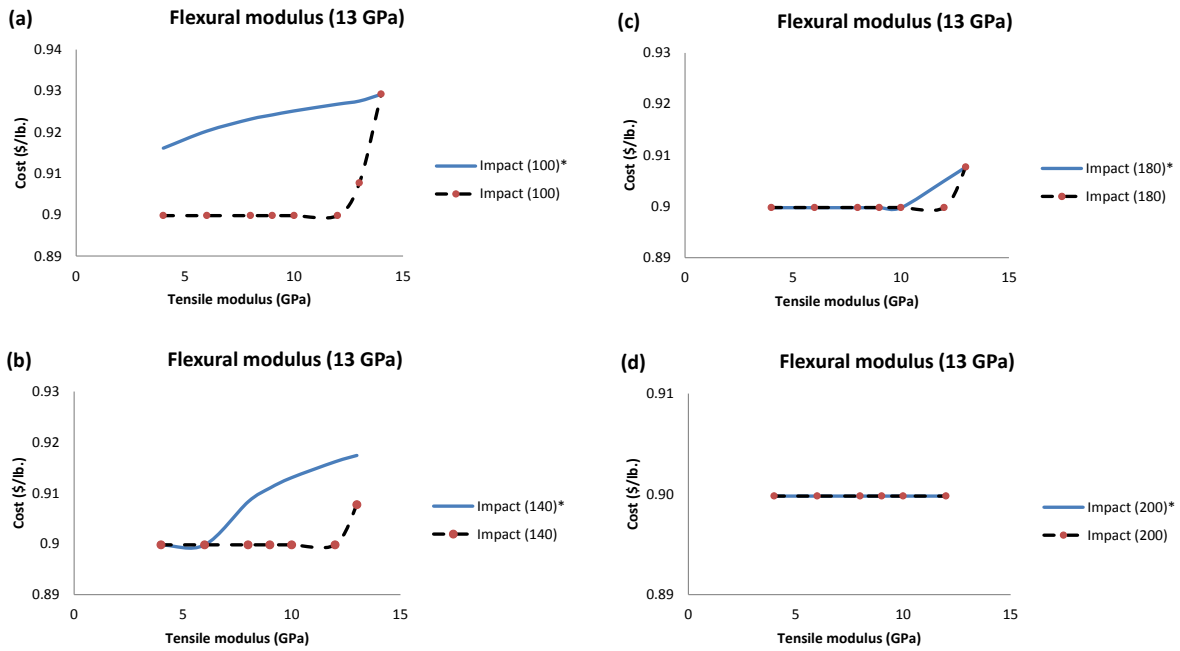

Figure B.8: The result of comparing the variance and cost function versus the tensile modulus at 13 GPa of flexural modulus. (a) I-zod impact 100, (b) I-zod impact 140, (c) I-zod impact 180, (d) I-zod impact 200.

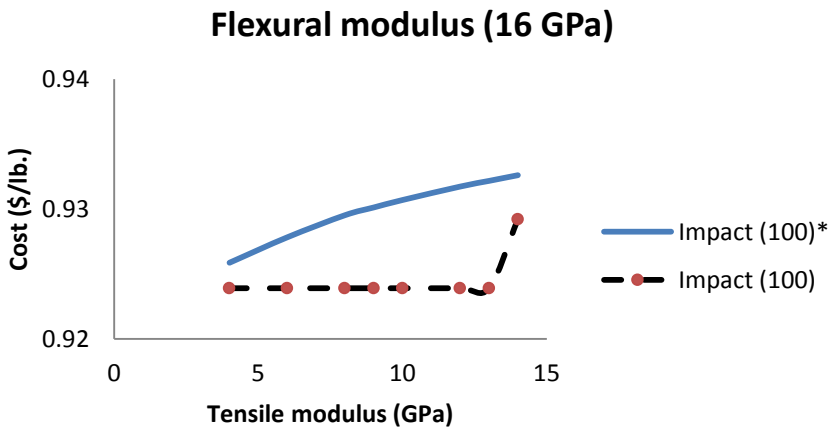

Figure B.9: The result of comparing the variance and cost function versus the tensile modulus at 100 J/m of I-zod impact, while flexural modulus was kept constant at 16 GPa.

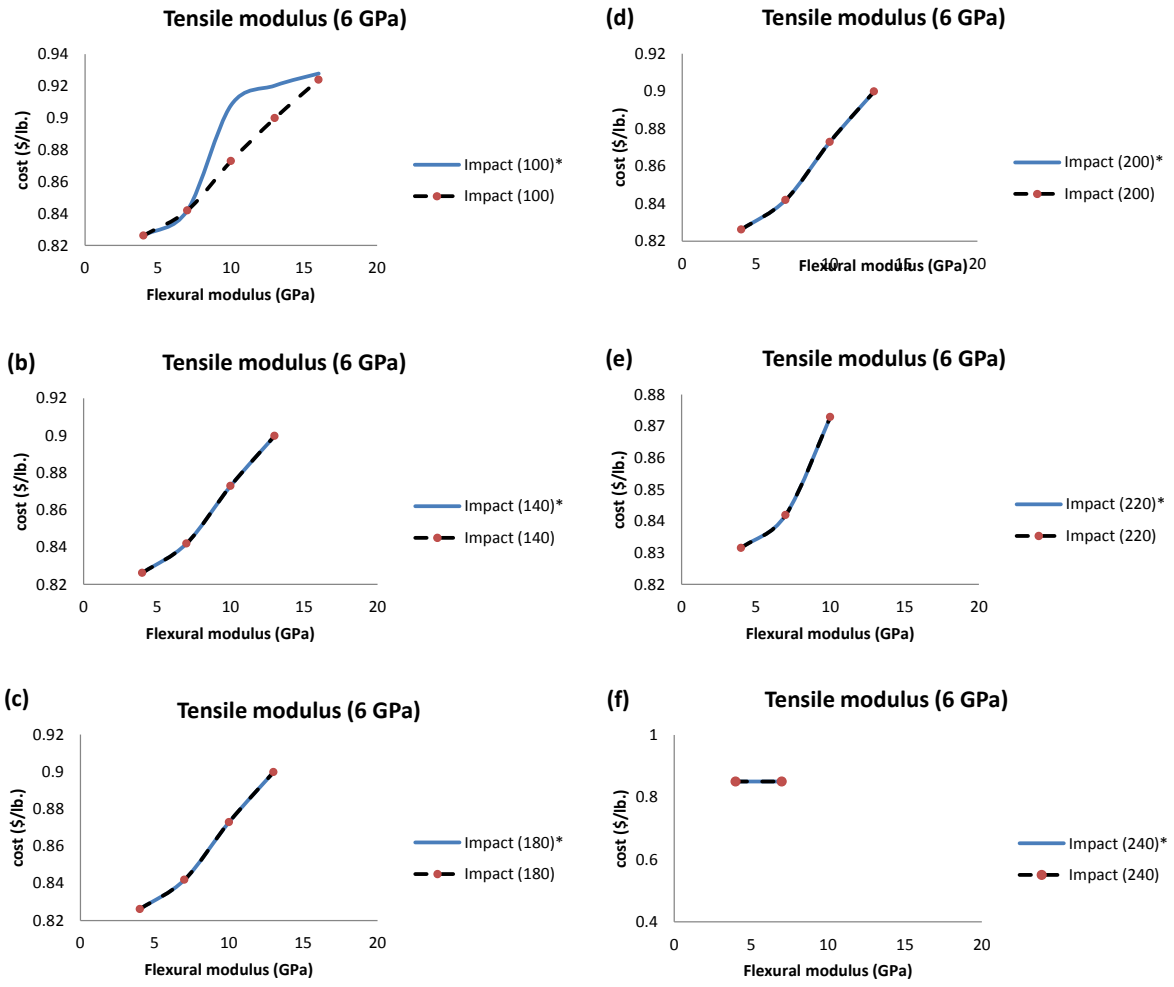

Figure B.10: The result of comparing the variance and cost function versus the flexural modulus at constant value of tensile modulus at 6 GPa. (a) I-zod impact 100 J/m, (b) I-zod impact 140 J/m, (c) I-zod impact 180 J/m, (d) I-zod impact 200 J/m, (e) I-zod impact 220 J/m, and (f) I-zod impact 240 J/m.

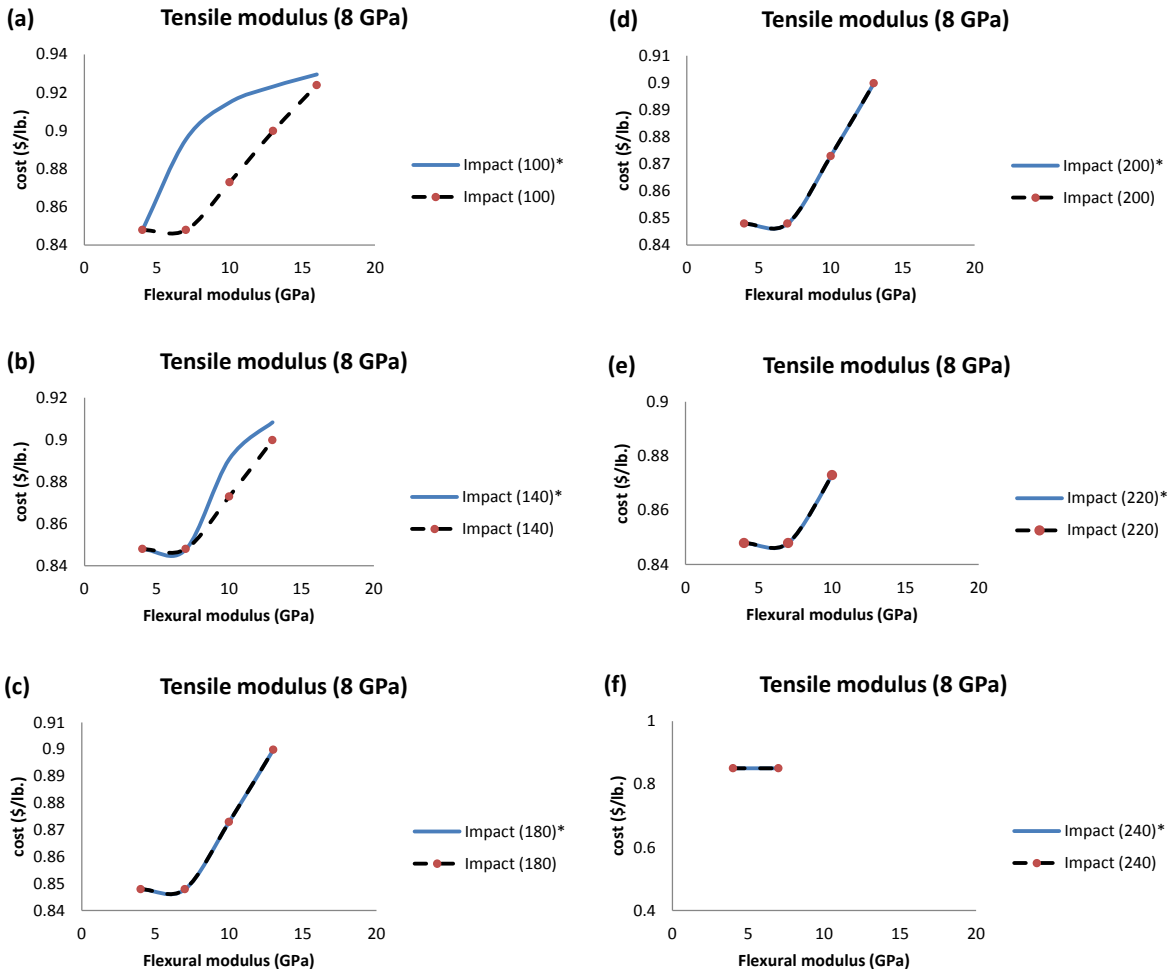

Figure B.11: The result of comparing the variance and cost function versus the flexural modulus at constant value of tensile modulus at 8 GPa. (a) I-zod impact 100 J/m, (b) I-zod impact 140 J/m, (c) I-zod impact 180 J/m, (d) I-zod impact 200 J/m, (e) I-zod impact 220 J/m, and (f) I-zod impact 240 J/m.

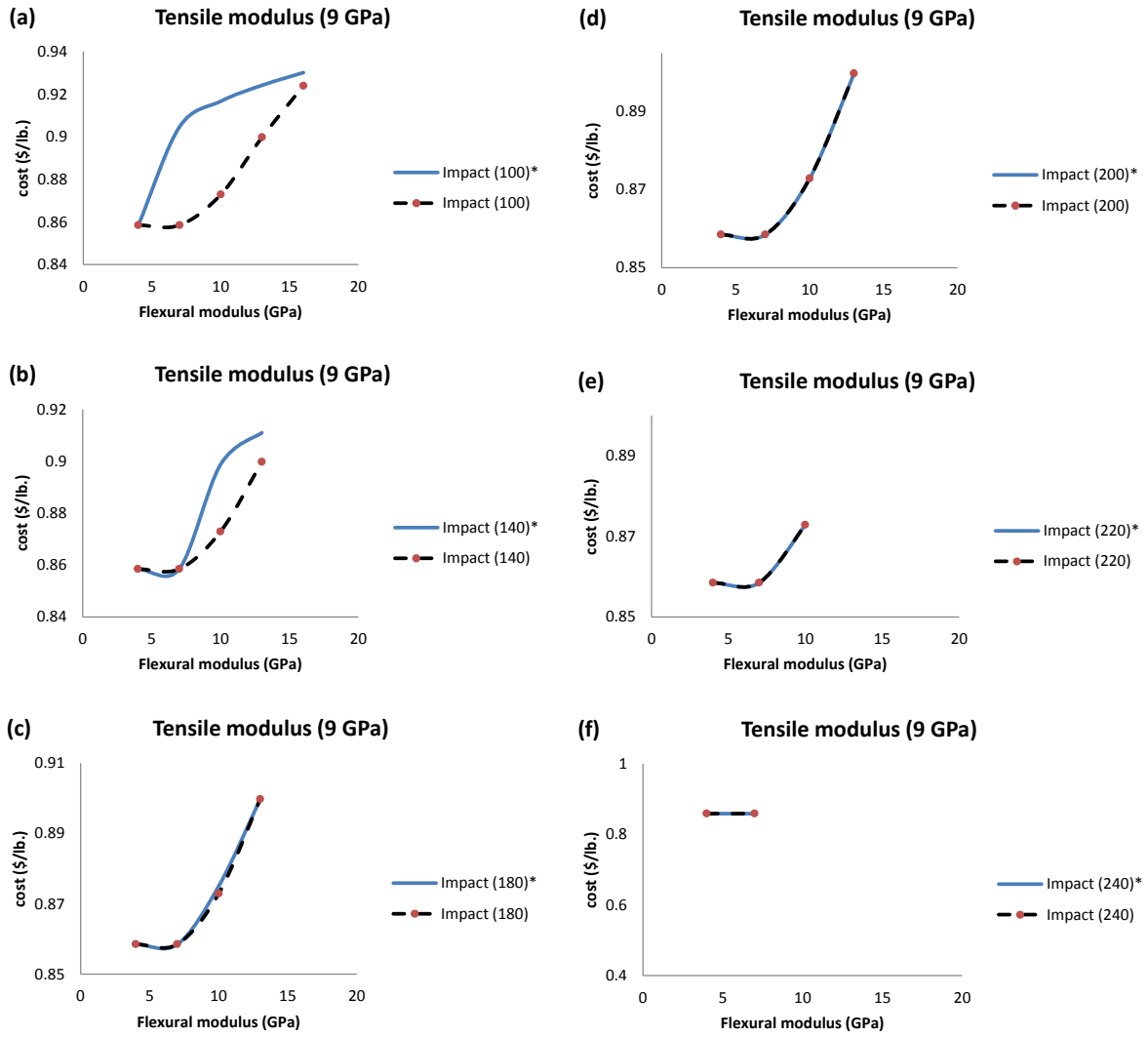

Figure B.12: The result of comparing the variance and cost function versus the flexural modulus at constant value of tensile modulus at 9 GPa. (a) I-zod impact 100 J/m, (b) I-zod impact 140 J/m, (c) I-zod impact 180 J/m, (d) I-zod impact 200 J/m, (e) I-zod impact 220 J/m, and (f) I-zod impact 240 J/m.

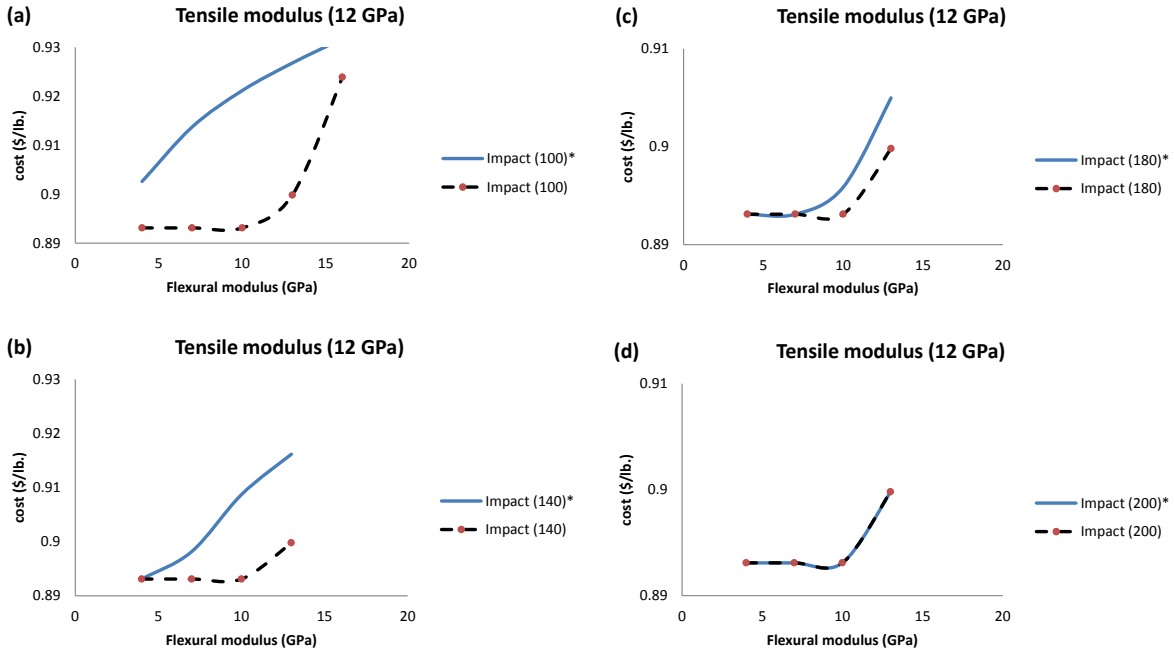

Figure B.13: The result of comparing the variance and cost function versus the flexural modulus at constant value of tensile modulus at 12 GPa. (a) I-zod impact 100 J/m, (b) I-zod impact 140 J/m, (c) I-zod impact 180 J/m, (d) I-zod impact 200 J/m.

Bibliography

Advani, S. G., and Tucker III, C. L. (1987). The use of tensors to describe and predict fiber orientation in short fiber composites. *Journal of Rheology, 31*(8), 751-784.

Al-Malaika, S., Golovoy, A., and Wilkie, C. A. (2001). *Specialty polymer additives : Principles and applications*. Malden, MA: Blackwell Science.

Askeland, D. R. (2011). In Wright W. J., Fulay P. P. and th ed. (Eds.), *The science and engineering of materials*. Stamford, CT: Cengage Learning.

Avriel, M. (2003). *Nonlinear programming : Analysis and methods*. Mineola, NY: Dover Publications.

Ba, N. N., Bapanapalli, S. K., Holbery, J. D., Smith, M. T., Kunc, V., Frame, B. J., . . . Tucker,C.L.,,III. (2008). Fiber length and orientation in long-fiber injection-molded thermoplastics. part I. modeling of microstructure and elastic properties. *Journal of Composite Materials, 42*(10), 1003-29.

Bader, M. G., and Bowyer, W. H. (1972). The mechanical properties of thermoplastics strengthened by short discontinuous fibres. *Journal of Physics D (Applied Physics), 5*(12), 2215-25.

Bader, M. G., and Bowyer, W. H. (1973). An improved method of production for high strength fibre-reinforced thermoplastics. *Composites, 4*(4), 150-6.

Benveniste, Y. (1987). A new approach to the application of mori-tanaka's theory in composite materials. *Mechanics of Materials, 6*(2), 147-57.

Brune, D. A., and Bicerano, J. (2002). Micromechanics of nanocomposites: Comparison of tensile and compressive elastic moduli, and prediction of effects of incomplete exfoliation and imperfect alignment on modulus. *Polymer, 43*(2), 369-87.

Camacho, C. W., Tucker,C.L.,,III, Yalvac, S., and McGee, R. L. (1990). Stiffness and thermal expansion predictions for hybrid short fiber composites. *Polymer Composites, 11*(4), 229-39.

Cooper, G. A. (1970). The fracture toughness of composites reinforced with weakened fibres. *Journal of Materials Science, 5*(8), 645-654.

Cottrell, A. H. (1964). Strong solids. *Royal Society -- Proceedings Series A, 282*(1388), 2-9.

Cox, H. L. (1952). The elasticity and strength of paper and other fibrous materials. *British Journal of Applied Physics, 3*, 72-79.

Cussler, E. L., and Moggridge, G. D.*Chemical product design (2nd edition)* Cambridge University Press.

Dong, Y., Bhattacharyya, D., and Hunter, P. J. (2008). Experimental characterisation and object-oriented finite element modelling of polypropylene/organoclay nanocomposites. *Composites Science and Technology, 68*(14), 2864-2875.

Driscoll, S. B., and ASTM International. (1998). *The basics of testing plastics mechanical properties, flame exposure, and general guidelines.* Retrieved

Eshelby, J. D. (1957). The determination of the elastic field of an ellipsoidal inclusion, and related problems. *Proceedings of the Royal Society of London.Series A, Mathematical and Physical Sciences, 241*(1226), pp. 376-396.

Fornes, T. D., and Paul, D. R. (2003). Modeling properties of nylon 6/clay nanocomposites using composite theories. *Polymer, 44*(17), 4993-5013.

Friedrich, K. (1985). Microstructural efficiency and fracture toughness of short fiber/thermoplastic matrix composites. *Composites Science and Technology, 22*(1), 43-74.

Gürdal, Z., Haftka, R. T., & Hajela, P.,. (1999). *Design and optimization of laminated composite materials*. New York: Wiley.

Halpin, J. C., and Kardos, J. L. (1976). HALPIN-TSAI EQUATIONS: A REVIEW. *Polymer Engineering and Science, 16*(5), 344-352.

Hbaieb, K., Wang, Q. X., Chia, Y. H. J., and Cotterell, B. (2007). Modelling stiffness of polymer/clay nanocomposites. *Polymer, 48*(3), 901-909.

Hine, P. J., Lusti, H. R., and Gusev, A. A. (2002). Numerical simulation of the effects of volume fraction, aspect ratio and fibre length distribution on the elastic and thermoelastic properties of short fibre composites. *Composites Science and Technology, 62*(10-11), 1445-53.

Hine, P. J., Lusti, H. R., and Gusev, A. A. (2004). On the possibility of reduced variable predictions for the thermoelastic properties of short fibre composites. *Composites Science and Technology, 64*(7-8), 1081-8.

Hu, H., Onyebueke, L., and Abatan, A. (2010). Characterizing and modeling mechanical properties of nanocomposites-review and evaluation. *Journal of Minerals & Materials Characterization & Engineering, 9*(4), 275-319.

Karger-Kocsis, J. (1995). *Polypropylene : Structure, blends and composites*. London; New York: Chapman & Hall.

Karian, H. G.,. (1999). *Handbook of polypropylene and polypropylene composites.* Retrieved

Kelly, A., and Tyson, W. R. (1965). Tensile properties of fibre-reinforced metals: Copper/tungsten and copper/molybdenum. *Journal of the Mechanics and Physics of Solids, 13*, 329-350.

Langer, S. A., Fuller E.R., J., and Carter, W. C. (2001). OOF: An image-based finite-element analysis of material microstructures. *Computing in Science & Engineering, 3*(3), 15-23.

Levenberg, K. (1944). A method for the solution of certain non-linear problems in least squares. *Quarterly of Applied Mathematics, 2*, 164-168.

Marquardt, D. W. (1963). An algorithm for least-squares estimation of nonlinear parameters. *Journal of the Society for Industrial and Applied Mathematics, 11*(2), pp. 431-441.

Mittal, V. (2008). Modeling the behavior of polymer-layered silicate nanocomposites using factorial and mixture designs. *Journal of Thermoplastic Composite Materials, 21*(1), 9-26.

Montgomery, D. C. (2011). In Runger G. C., th ed. (Eds.), *Applied statistics and probability for engineers*. Hoboken, NJ: Wiley.

Mori, T., and Tanaka, K. (1973). Average stress in matrix and average elastic energy of materials with misfitting inclusions. *Acta Metallurgica, 21*(5), 571-4.

Nielsen, L. E., Landel, R. F., and NetLibrary, I. (1994). *Mechanical properties of polymers and composites* (2 , rev a expa ed.). New York: M. Dekker.

Nocedal, J., and Wright, S. J.,. (1999). *Numerical optimization.* Retrieved

Peters, S. T. (1998). *Handbook of composites (2nd edition)* Springer - Verlag.

Phelps, J. H., and Tucker,C.L.,,III. (2009). An anisotropic rotary diffusion model for fiber orientation in short- and long-fiber thermoplastics. *Journal of Non-Newtonian Fluid Mechanics, 156*(3), 165-76.

Piggott, M. R. (1974). The effect of aspect ratio on toughness in composites. *Journal of Materials Science, 9*(3), 494-502.

Raghava, R. S. (1988). Thermal expansion of organic and inorganic matrix composites: A review of theoretical and experimental studies. *Polymer Composites, 9*(1), 1-11.

Rosato, D. V., Rosato, D. V., and Rosato, M. G. (2000). *Injection molding handbook (3rd edition)* Springer - Verlag.

Shi, D., Feng, X., Jiang, H., Huang, Y. Y., and Hwang, K. (2005). Multiscale analysis of fracture of carbon nanotubes embedded in composites. *International Journal of Fracture, 134*(3-4), 369-386.

Tandon, G. P., and Weng, G. J. (1984). The effect of aspect ratio of inclusions on the elastic properties of unidirectionally aligned composites. *Composites 83 Symposium, , 5*(4) 327-33.

Thomason, J. L. (2002a). Interfacial strength in thermoplastic composites - at last an industry friendly measurement method? *Composites Part A (Applied Science and Manufacturing), 33A*(10), 1283-8.

Thomason, J. L. (2002b). Micromechanical parameters from macromechanical measurements on glass reinforced polypropylene. *Composites Science and Technology, 62*(10-11), 1455-68.

Thomason, J. L. (2002c). Micromechanical parameters from macromechanical measurements on glass-reinforced polybutyleneterepthalate. *Composites - Part A: Applied Science and Manufacturing, 33*(3), 331-339.

Thomason, J. L. (2005). The influence of fibre length and concentration on the properties of glass fibre reinforced polypropylene. 6. the properties of injection moulded long fibre PP at high fibre content. *Composites Part A (Applied Science and Manufacturing), 36*(7), 995-1003.

Thomason, J. L. (2007). The influence of fibre length and concentration on the properties of glass fibre reinforced polypropylene: 7. interface strength and fibre strain in injection moulded long fibre PP at high fibre content. *Composites Part A (Applied Science and Manufacturing), 38*(1), 210-16.

Thomason, J. L., and Groenewoud, W. M. (1996). The influence of fibre length and concentration on the properties of glass fibre reinforced polypropylene: 2. thermal properties. *Composites Part A (Applied Science and Manufacturing), 27A*(7), 555-65.

Thomason, J. L., and Vlug, M. A. (1997). Influence of fibre length and concentration on the properties of glass fibre-reinforced polypropylene. 4. impact properties. *Composites Part A (Applied Science and Manufacturing), 28A*(3), 277-88.

Thomason, L., and Vlug, M. A. (1996). Influence of fibre length and concentration on the properties of glass fibre-reinforced polypropylene. I. tensile and flexural modulus. *Composites Part A (Applied Science and Manufacturing), 27A*(6), 477-84.

Tserpes, K. I., Papanikos, P., Labeas, G., and Pantelakis, S. G. (2008). Multi-scale modeling of tensile behavior of carbon nanotube-reinforced composites. *Theoretical and Applied Fracture Mechanics, 49*(1), 51-60.

Tsu-Wei Chou, and Li, C. (2006). Multiscale modeling of compressive behavior of carbon nanotube/polymer composites. *Composites Science and Technology, 66*(14), 2409-14.

Tucker III, C. L., and Liang, E. (1999). Stiffness predictions for unidirectional short-fiber composites: Review and evaluation. *Composites Science and Technology, 59*(5), 655-671.